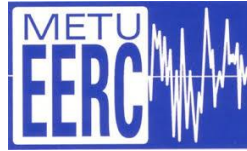




MIDDLE EAST TECHNICAL UNIVERSITY

**January 24, 2020 Elazığ-Sivrice Earthquake ($M_w=6.8$)
Reconnaissance Study Report**



**MIDDLE EAST TECHNICAL UNIVERSITY
EARTHQUAKE ENGINEERING RESEARCH CENTER**

REPORT NO: METU/EERC 2020-01

**FEBRUARY
2020**

ANKARA



CHAPTERS

CHAPTER 1 INTRODUCTION

CHAPTER 2 GEOLOGICAL SETTING OF THE REGION

CHAPTER 3 SEISMOLOGICAL SETTING AND STRONG GROUND MOTION

CHARACTERISTICS

CHAPTER 4 GEOTECHNICAL RECONNAISSANCE OBSERVATIONS



CHAPTER 1

Introduction

By:

Kemal Önder Çetin

Prof. Dr., Middle East Technical University, Civil Engineering Department.

Makbule İlgaç, Gizem Can, Elife Çakır, Berkan Söylemez,

Research Assistants, Middle East Technical University, Civil Engineering Department.



Table of Contents

1. Introduction	4
-----------------------	---

Table of Figures

Figure 1.1. Map of Turkey (Google Maps)	5
Figure 1.2. Different segments of the East Anatolia fault zone (Duman and Emre, 2013).....	6



1. Introduction

On January 24, 2020 20:55:11 (UTC), a moment magnitude M_w 6.8 (AFAD; Disaster and Emergency Management Presidency; www.afad.gov.tr) or 6.7 (USGS) earthquake occurred on the East Anatolian Fault zone, due to a NE-SW strike-slip fault rupture along the Sivrice-Pütürge Segment in Elazığ, Turkey. Within the confines of this report, the findings of geological, seismological and geotechnical and structural reconnaissance studies as well as preliminary field investigation studies will be presented. In addition to geological and geotechnical evaluations in the course of reconnaissance studies, some typical lifeline and superstructure damage examples are also given. Independent engineering groups composed of earth scientists, geological, geophysical, and civil engineers have compiled and documented perishable data immediate upon Elazığ-Sivrice earthquake. For the purpose of honoring collaborative research studies among different disciplines and universities, it was decided to present the findings in a co-authored report. We believe that this report and others will encourage and reinforce further interdisciplinary studies and culture of collaborative research.

The cities of Elazığ and Malatya are located in the eastern Turkey as shown in Figure 1.1. The epicenter is located at N38.3593°, E39.0630°, approximately 37 kms south-southwest of Elazığ, and 64 kms east of Malatya with a focal depth of 8.06 km (AFAD). Sivrice-Pütürge segment is located within the East Anatolian Fault system in association with the tectonic boundary of the Eurasian, Arabian and African plates and Anatolian Block, which accommodates approximately 5-10 mm annual slip (Gulerce et al. 2017). The effects of the Elazığ-Sivrice earthquake have been widely observed across Elazığ and Malatya regions, extending from Hazar Lake in the east to downtown Malatya in the west. The cities of Kahramanmaraş, Diyarbakır, Adıyaman, Şanlıurfa and Batman have also felt the earthquake shaking relatively strongly. Despite attempts to identify and map surface expressions of fault rupture, a clear evidence has not been reported (yet). However, in the literature and the press, there exist contradicting opinions.

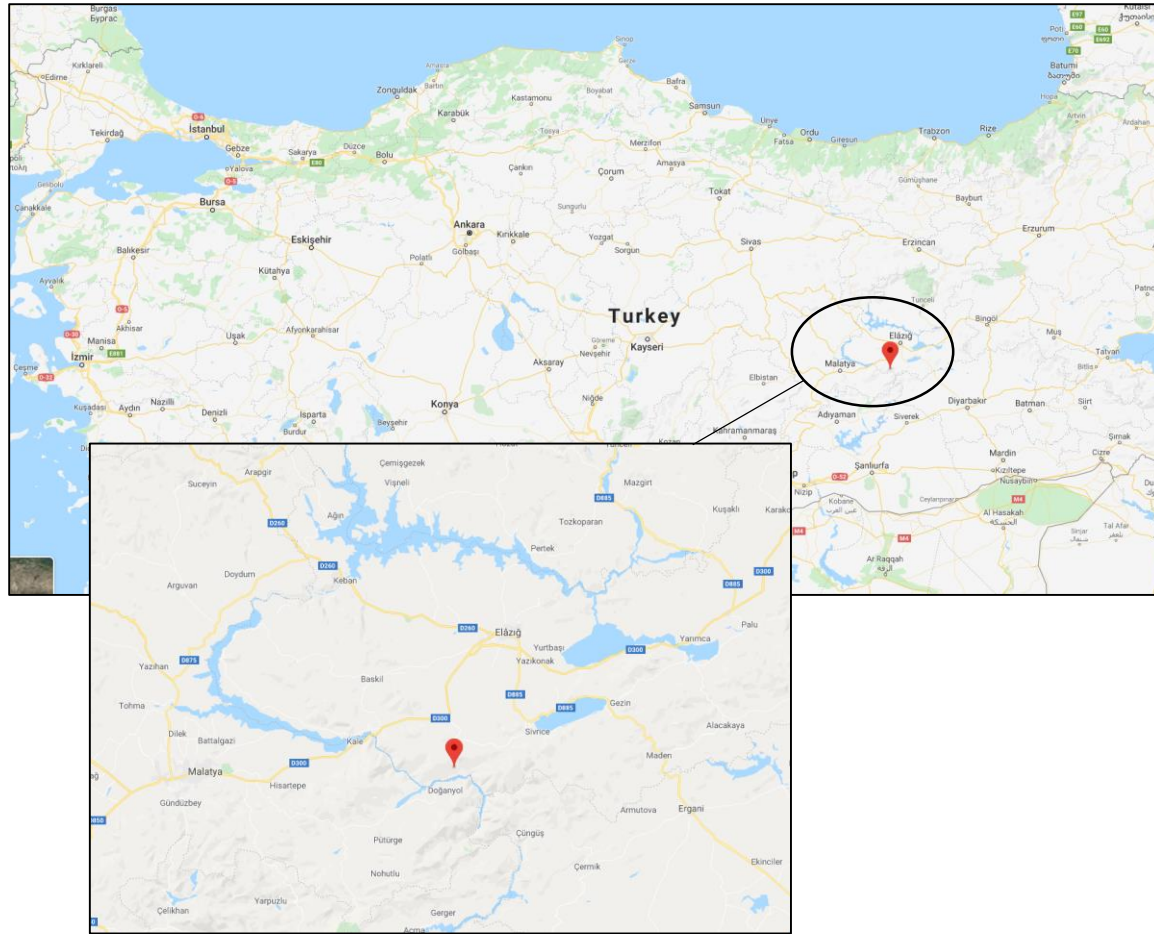


Figure 1.1. Map of Turkey (Google Maps)
The epicenter of the January 24, 2020 Earthquake is shown with a red pin.

Turkey is a tectonically active country, and regularly experiences damaging earthquakes. Within 250 km of January 24, 2020 earthquake event, on the EAFZ, seven other M_w 6 or larger events have been reported to occur since 1870's. Several of these events have been destructive:

In May 1971, M_w 6.9 Bingöl earthquake, 150 km to the northeast of this recent event killed 65 people and also caused significant damage.

In September 1975, M_w 6.7 Lice earthquake, about 140 km to the east of the recent event killed more than 2,000 people and caused significant local damage.

In May 1986, M_w 6.1 Sürgü earthquake, about 120 km to the west of this earthquake, killed 15 people and damaged over 4,000 houses.

In May 2003, M_w 6.4 Bingöl earthquake, 140 km to the northeast of the recent event's epicenter killed 177 people, injured hundreds, and destroyed over 700 buildings.



In March 2010, M_w 6.1 Elazığ-Kovancılar earthquake, 100 km to the northeast of 2020 event killed 42 people, injured 100 people, and destroyed close to 300 buildings.

On the basis of the events listed and the map shown in Figure 1.2, it can be concluded that January 24, 2020 event has occurred on a segment of the east Anatolian fault, which has been seismically quiet since the last earthquake in 1875.

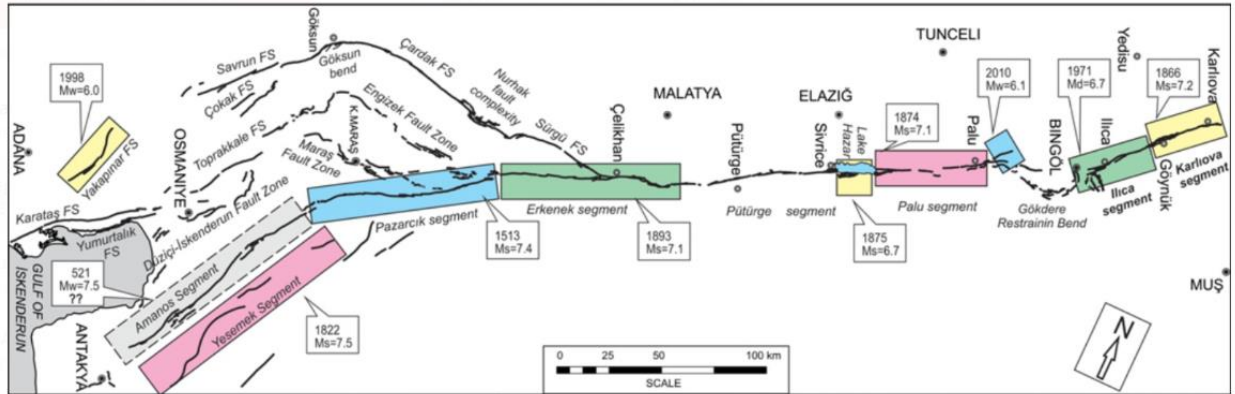


Figure 1.2. Different segments of the East Anatolia fault zone (Duman and Emre, 2013)

41 citizens lost their lives, and owing to successfully managed search and rescue operations, 45 citizens have been rescued from the heavily damaged and/or collapsed residential structures. 1,587 out of 1,631 injured citizens are soon discharged, 46 of citizens, 5 of whom are under intensive care, continue to be treated, as of February 3, 2020. Following the major shock of Elazığ-Sivrice earthquake, again as of February 3, 2020, a total number of 1,948 aftershocks occurred in the region. 23 of these aftershocks have magnitudes over 4.0.

In response to this event, several research teams have visited the region to investigate the effects of the earthquake. The preliminary objective of the reconnaissance efforts was to document the effects of strong shaking on buildings and ground failure such as the prevalence of liquefaction, landslides and surface fault rupture. Our research team has visited the area on the 31st of January to collect and document perishable data in the form of ground deformations, liquefaction, lateral spreading and slope instabilities, rock falls and retaining structures. Additionally, the performances of railway systems, hydraulic structures, highways and residential structures on the investigation route are also documented. As a result, the subsequent investigative efforts have been mostly focused on documenting the following topics:

- Background information related to the geology of the region,
- Seismology and ground motions of the event,
- Detailed mapping of ground deformations,
- Measuring ground deformation in the very near fault region,
- Assessing the performance of slope instabilities
- Assessing the performance of hydraulic structures and railways.

The findings regarding all these will be presented next.



References

Duman TY, Emre Ö. (2013). “The East Anatolian Fault: geometry segmentation and jog characteristics”. Geol Soc London Spec Publ 372: 495-529

Gülerce, Z., Soyman, K. B., Güner, B., & Kaymakci, N. (2017). “Planar seismic source characterization models developed for probabilistic seismic hazard assessment of Istanbul”. Natural Hazards and Earth System Sciences, 17(12), 2365

CHAPTER 2

Geological Setting of the Region

By:

Kemal Önder Çetin

Prof. Dr., Middle East Technical University, Civil Engineering Department.

Makbule İlgaç, Gizem Can, Elife Çakır, Berkan Söylemez,

Research Assistants, Middle East Technical University, Civil Engineering Department.



Table of Contents

2.# Geology of the Region.....	3#
2.1.# Tectonic Setting.....	3#
2.2.# Historical Earthquakes	5#
2.3.# Geological Setting of the Region	6#
2.3.1.#Keban Metamorphics	7#
2.3.2.#Elazığ Magmatites.....	7#
2.3.3.#Harami Formation	7#
2.3.4.#Kırkgeçit Formation	7#
2.3.5.#Karabakır Formation	8#
2.3.6.#Alluvium.....	8#

Table of Figures

Figure 2.1. Tectonic structure of Turkey (from Bozkurt 2001).....	3#
Figure 2.2. Active faults and fault segments in the vicinity of Elazığ and Malatya cities (MTA 2020)	4#
Figure 2.3. Seismicity of EAFZ during the last century (AFAD 2020)	5#
Figure 2.4. Geological map of Elazığ province (Palutoğlu, M., Tanyolu, E., 2006, in Turkish) ...	6#
Figure 2.5. Geological map of Elazığ City Center (Palutoğlu, M., Tanyolu, E., 2006)	9#
Figure 2.6. Generalized stratigraphic columnar section of Elazığ.....	10#



2. Geology of the Region

2.1. Tectonic Setting

January 24, 2020 Elazığ-Sivrice Earthquake occurred on Turkey's the second largest fault system: left lateral strike slip East Anatolian Fault Zone's (EAFZ) Sivrice-Pütürge segment. The EAFZ is defined by a zone of fault segments that joins the eastern end of the North Anatolian Fault Zone (NAFZ) to the Mediterranean Sea in the Gulf of Iskenderun (Taymaz et al 1991). NAFZ meets EAFZ at the Karlıova junction.

EAFZ exhibits translational characteristics, which is induced due to continent-continent collision of Arabian-African and the Eurasian plates. The interaction of four major tectonic plates of Arabian, Eurasian, Indian, and African with relatively smaller tectonic block of Anatolia is the source of high seismicity in the region, as shown in Figure 2.1 (USGS, Bozkurt 2001). Owing to more recent tectonic processes, EAFZ is under a tectonic compression regime in the N-S direction. The Anatolian block, squeezed between NAFZ and EAFZ, is moving towards the west. (Şengör et al., 1985, AFAD Report 2010). The EAFZ predominantly produces left-lateral strike-slip events with occasional normal segments, but its fault trace is less continuous and less localized than that of the NAFZ. Recent GPS data indicated that the slip rate in the EAFZ has an upper bound of 8 ± 1 mm/year (Ambraseys 2009).

Historically, the EAFZ has nucleated relatively small magnitude earthquakes in the twentieth century (www.koeri.boun.edu.tr) contrary to NAFZ, which characteristically generates M_w greater than 7 events. Figure 2.2 shows the active fault map of Turkey as provided by General Directorate of Mineral Research and Explorations (MTA).

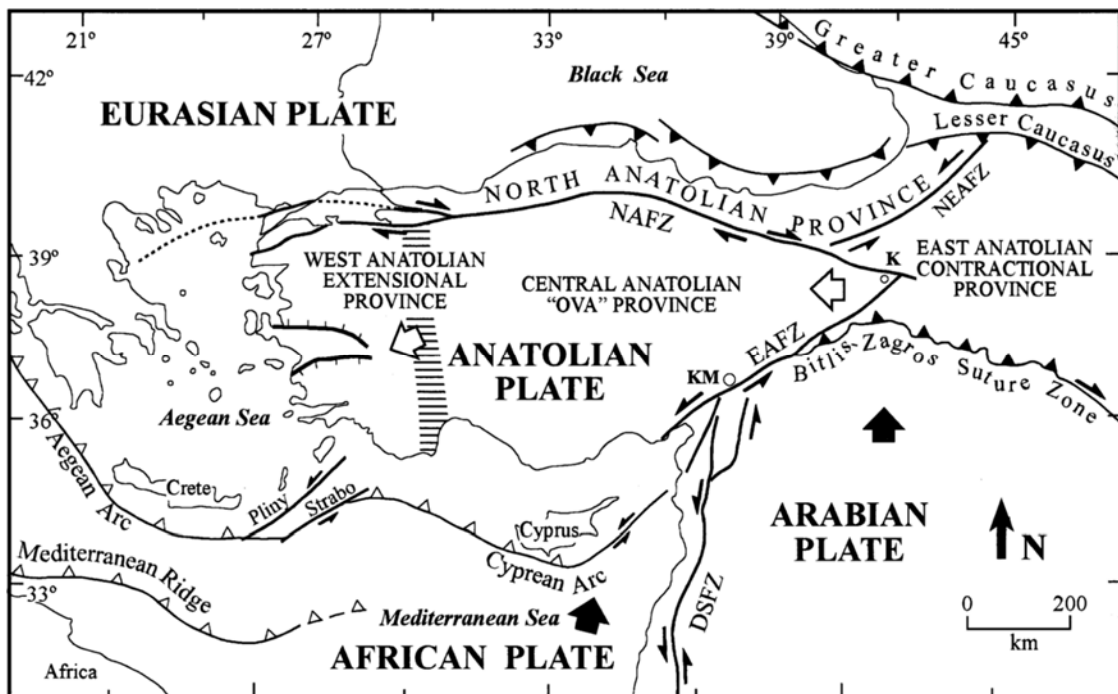
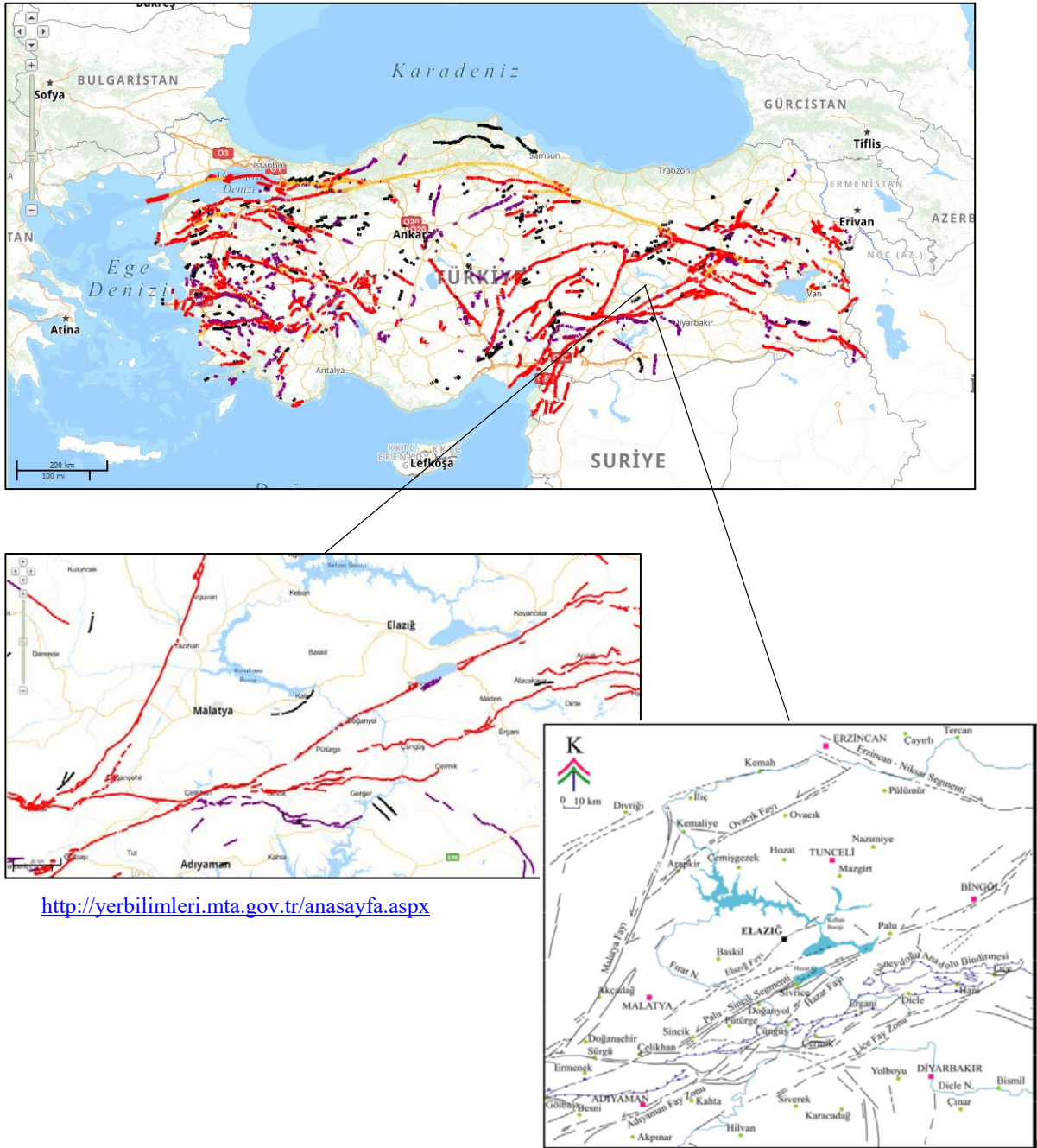


Figure 2.1. Tectonic structure of Turkey (from Bozkurt 2001).



<http://yerbilimleri.mta.gov.tr/anasayfa.aspx>

(from Palutoğlu, M. and Tanyolu, E., 2006)

Figure 2.2. Active faults and fault segments in the vicinity of Elazığ and Malatya cities (MTA 2020)



2.2. Historical Earthquakes

In the twentieth century, EAFZ produced several large earthquakes ($M_w > 7$) with surface rupturing exhibiting complex migration patterns, as shown in Figure 2.3 (Barka 1996; Utkucu et al. 2003). As reported by AFAD 2020, in the 20th century, on the EAFZ, 299 earthquakes occurred with M_w larger than 4.0, the largest of which was a 6.9 moment magnitude event. Also, before year 1900, 40 historical earthquakes have been reported in the region.

Several of these destructive earthquakes as summarized by USGS are briefly discussed below:

- M_w 6.9 Bingöl earthquake in May 1971, 150 km to the northeast of the killed 65 and also caused significant damage.
- M_w 6.7 Lice earthquake in September 1975, about 140 km to the east of today's earthquake killed more than 2,000 people and caused significant local damage.
- M_w 6.1 Sürgü earthquake in May 1986, about 120 km to the west of this earthquake, killed 15 and damaged over 4,000 houses.
- M_w 6.4 Bingöl earthquake in May 2003, 140 km to the northeast of today's event killed 177 people, injured hundreds, and destroyed over 700 buildings.
- M_w 6.1 Elazığ-Kovancılar earthquake in March 2010, a 100 km to the northeast killed 42, injured 100, and destroyed close to 300 buildings.

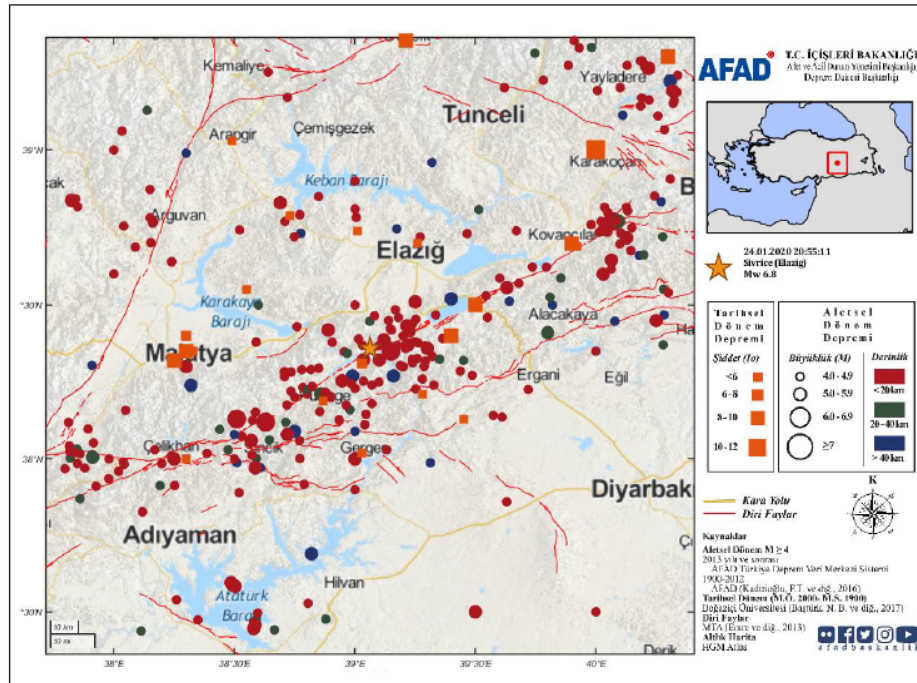


Figure 2.3. Seismicity of EAFZ during the last century (AFAD 2020)



2.3. Geological Setting of the Region

The geological units of Elazığ province, starting from the oldest to the youngest, are listed as:

- Keban metamorphites consisting of Permo Triassic aged crystallized limestones,
- Elazığ Magmatites consisting of senonian aged granite, granodiorite, basalt, basaltic pillow lava, andesite and dacite dykes and volcanosedimentary rocks,
- Harami Formation consisting of Upper Maestrichtian aged massive limestones,
- Kırkgeçit Formation consisting of Middle Eocene-Upper Oligocene aged conglomerate, sandstone, marl and limestones,
- Mine Complex consisting of sedimentary rocks such as mudstone, sandstone, claystone and magmatic rocks such as basalt, andesite and diabase,
- Karabakır Formation, consisting of upper Miocene-Lower Pliocene aged tuff, agglomerate, basaltic lava and lacustrine limestones with lateral transition.

Figure 2.4 shows the geological map of the province.

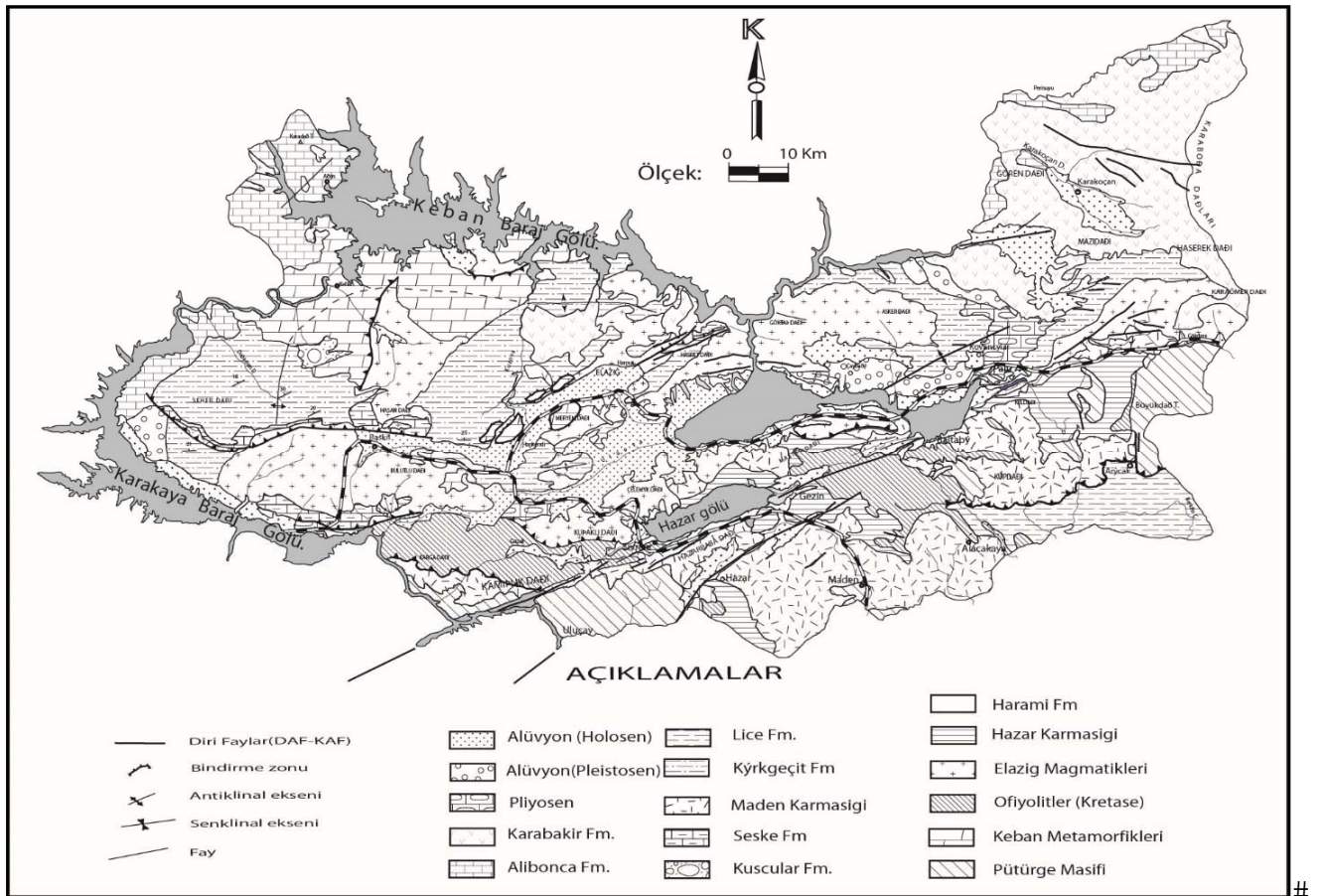


Figure 2.4. Geological map of Elazığ province (Palutoğlu, M., Tanyolu, E., 2006, in Turkish)



2.3.1. Keban Metamorphics

Keban metamorphics in Elazığ, is mostly located in the area between Abdullahpaşa-Sarıçubuk districts and Allahuekber Hill, and on the skirts of Mount Meryem southwest of Sürsürü district. It is covered by angular unconformities of Kırkgeçit Formation and exhibits unconformity with Karabakır Formation at the foot of Mount Meryem in the area between Abdullahpaşa, Cumhuriyet Sarıçubuk districts, and Allahuekber Hill.

Keban Metamorphics consist of recrystallized limestones-calcschist, marble, metaconglomerate-calcillites, but are mostly represented by recrystallized limestones in the study area.

2.3.2. Elazığ Magmatites

Elazığ Magmatites are sub-divided into magmatic rocks and Volcano-sedimentary rocks. Magmatic rocks are located in the west of Harput, north of Fevziçakmak, Esentepe and Safran districts, at the north of Fırat University, Cumhuriyet and Abdullahpaşa districts, about 1 km east of Şahinkaya Village, Yeniköy and Yedigâr districts, and in the vicinity of Keklik and Karataş hills. Volcano-sediments are usually located in between Eski Beyyurdu-Karşıyaka districts.

Keban Metamorphics tectonically overlie Elazığ Magmatites, whose base is not visible in the central settlement area of Elazığ province, and in accordance with Harami Formation, Kırkgeçit and Karabakır formations are angular unconformity. Elazığ Magmatites are lithologically composed of gabbro-diorites at the base, basaltic-andesitic volcanic rocks, and volcano-clastics overlying them, and granodiorite-tonalites and dacite dykes cutting them.

2.3.3. Harami Formation

Harami formation exists as a few hundred square-meters pockets in the north, south and east of Harput. The unit covering Elazığ Magmatites is covered by Kırkgeçit Formation generally represented by massive limestones. This unit consists of lenticular red conglomerate and sandstone at the bottom, sandy limestone and massive limestone at the lower levels. Formation environments are shallow, clear, not widespread, disconnected and exhibit reefal characteristics. Harami Formation was deposited in a narrow and shallow basin in Maastrichtian. Red conglomerates and sandstones at the base are terrestrial deposits with fan delta character. The sandy limestone and limestones overlying them are carbonate deposits, deposited in shallow sea. According to paleontological findings, it is Maastrichtian or older.

2.3.4. Kırkgeçit Formation

The Kırkgeçit Formation, which extends to the city of Van, is mapped in three different lithological columns. Sandstone-marl units outcrop in the north of Virane district, northeast and northwest. The conglomerate-sandstone is observed in the vicinity of Sarıçubuk and Şahinkaya Villages and Körpınar district, in the north of Cumhuriyet and Zafran districts, in the north and northeast of Harput, and the Marl units in the north of Akyazı and Virane districts, and about 1 km to the north. The sandstone-marl layers are interchangeable, and bear conglomerate levels.



2.3.5. Karabakır Formation

Karabakır formation is mapped in three geological units: volcanics, limestone and conglomerate-sandstone. Volcanic rocks are located about one km east of Yeniköy, and west of Yedigâr districts. Limestone member can be seen in the vicinity of Rızvan and Baz Hills and west of Doğukent, Salıbaba, Çatalçeşme districts. The conglomerate-sandstone lies in the north and northeast of Yeniköy District, around Yedigâr District. Karabakır Formation covers the Keban Metamorphics, Elazığ Magmatites and Kırkgeçit Formation unconformity. There are also unconformity. Pleistocene aged alluviums. The age of the Karabakır formation is the Upper Miocene according to its paleontological findings.

2.3.6. Alluvium

Alluvium sediments, which spread over large areas, are mapped in three separate units. Due to their different lithologies they are classified as silty clay, sandy gravelly-clay and sand-gravel.

Silty clay dominates the southeast of Sürsürü, Kültür, Olgunlar, Hicret, Akpınar, Sarayatık, Nailbey, University and Çarşı districts.

Sandy gravelly clays are mapped in the Sanayi district, south of Kırklar district, in the middle and north part of İzzetpaşa district, Yeni district, south and east of Fırat University campus, south, north and northwest of Sürsürü district, east of Abdullahpaşa district and in the south, near the north of Yedigâr district, in the direction of Aksaray district.

The sand-gravel layer is in the north and northwest of Abdullahpaşa district, south of Cumhuriyet district, in Ulukent, Yıldızbağları, Rızaiye, İcadiye, Mustafapaşa, Rüstempaşa, Aksaray, Kızılay, Gümüşkavak and north of Sanayi districts. It is also observed in Çatalçeşme, Doğukent districts between Salıbaba-Karşıyaka districts. The sand-gravel proportions vary from district to district with also variable clay layer thicknesses.

Figure 2.5 shows the geological units mapped in the vicinity of Elazığ city center, along with representative cross-sections, as explained in the preceding subsections. Also Figure 2.6 presents the generalized stratigraphic columnar section representing Elazığ geological setting.



Middle East Technical University
24 January 2020 Elazığ-Sivrice Earthquake ($M_w=6.8$)
Geological Setting of the Region

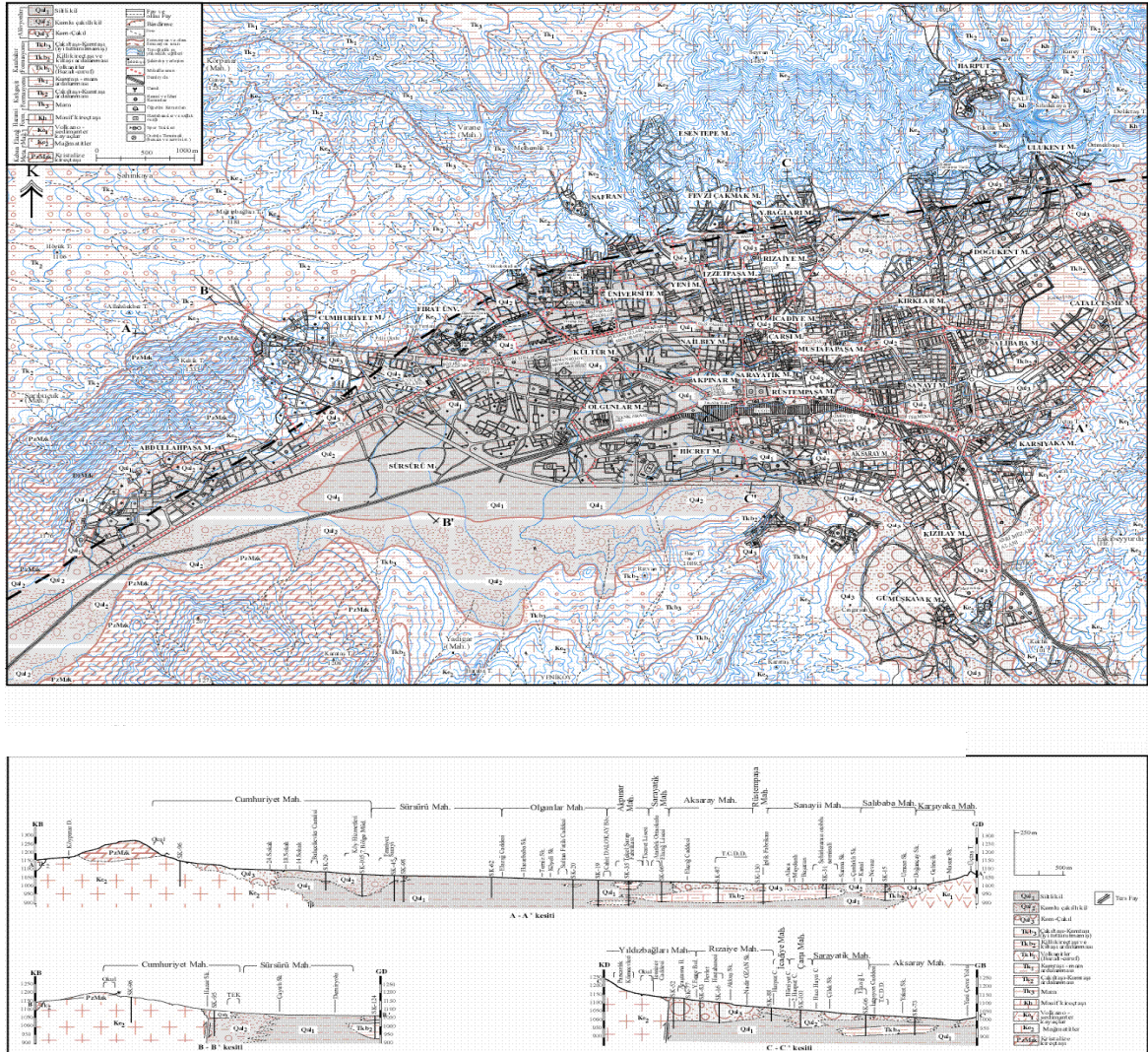


Figure 2.5. Geological map of Elazığ City Center (Palutoğlu, M., Tanyolu, E., 2006)



#

ÜS SİSTEM	SİSTEM	SERİ	KAT	LİTOLOJİ BİRİMLERİ	LİTOLOJİ	SİMGE	AÇIKLAMALAR
PALEOZOYİK	SENOZOYİK						
	NEOJEN	KUVATERNER					
		PLEYİSTOSEN					
		ÜST MİYOSEN - ALT PLİYOSEN					
	PALEOJEN	ORTA EOESEN - ÜST OLİGOSEN					
MESOZOYİK	KRETASE						
		ÜST KRETASE					
			ÜST MEASTRİTİYEN				
			HARAMİ FORMASYONU				
PALEOZOYİK	PERMO - TRIYAS						
			SENONİYEN				
			ELAZIĞ MAĞMATİTLERİ				
			KEBAN METAMORFİTLERİ				

Figure 2.6. Generalized stratigraphic columnar section of Elazığ
(Palutoğlu, M. and Tanyolu, E., 2006)



References

Barka, A. (1996). “Slip distribution along the North Anatolian Fault associated with the large earthquakes of the period 1939 to 1967”, *Bull. Seismol. Soc. Am.* 86, 1238-1254

Bozkurt E. (2001). “Neotectonics of Turkey—a synthesis”. *Geodinamica Acta* 14: 3-30.

N. Ambraseys, N.N. (2009). “Earthquakes in the Mediterranean and Middle East: a multidisciplinary study of seismicity up to 1900”. Cambridge University Press, Cambridge, UK 947pp.

Palutoğlu, M., Tanyolu E. (2006). “Seismicity of Elazığ Provincial Center Residential Area”, *Fırat University Journal of Science and Engineering*, 18 (4), 577-588. (in Turkish)

Sengör A. M. C., Gorur N., Saroglu F. (1985). “Strike-slip faulting and related basin formation in zones of tectonic escape: Turkey as a case study”. *Society of Economic Paleontologists and Mineralogists, Special Publication* 37: 227 – 264

Taymaz, T., Jackson, J. & McKenzie, D. P. (1991). “Active tectonics of the north and central Aegean Sea”, *Geophysical Journal International*, 106, 433–490.

USGS, United States Geological Survey

Utkucu, M., Nalbant, S., McClusky, J., Steacy, S., Alptekin, Ö., (2003). “Slip distribution and stress changes associated with the 1999 November 12, Düzce (Turkey) earthquake ($M_w = 7.1$).”, *Geophys. J. Int.* 153, 229–241.

CHAPTER 3

Seismological Setting and Strong Ground Motion Characteristics

By:

Kemal Önder Çetin, Ayşegül Askan Gündoğan, Zeynep Gülerce

Prof. Dr., Middle East Technical University, Civil Engineering Department.

Shaghayegh Karimzadeh

Instructor Dr., Middle East Technical University, Civil Engineering Department.

Makbule İlgaç, Gizem Can, Elife Çakır, Berkan Söylemez,

Research Assistants, Middle East Technical University, Civil Engineering Department.

Abdullah Altındal

Student, Middle East Technical University, Civil Engineering Department.



Table of Contents

3.1	Introduction	3
3.2	Seismological Characteristics of the Earthquake	3
3.3	Source Characteristics of the Event	4
3.4	Preliminary Analysis of Recorded Strong Ground Motions	6
3.5	Spatial Distribution of Macroseismic (Felt) Intensity in the Region	12

List of Figures

Figure 3. 1. Major tectonic structures and epicenters of the 2020 (red star) and 2010 (grey star) earthquakes along with seismicity within the last century.....	3
Figure 3. 2. Spatial distributions of the aftershocks between 24/01/2020-28/01/2020	4
Figure 3. 3. 24/01/2020 Malatya-Elazığ Earthquake $M_w=6.8$ and aftershock.....	5
Figure 3. 4. M_w vs. focal depth scatters recorded between January 24 to February 03, 2020 following the mainshock of 2020 Elazığ-Sivrice Earthquake (AFAD).....	6
Figure 3. 5. Locations of the five strong motion stations included in the AFAD's preliminary report. R_{JB} values are approximately estimated according to the surface rupture given in MTA report (blue dashed line). Blue and green lines are the Palu and Pütürge segments that are slightly modified for their termination points by Gülerce et al. (2017).....	7
Figure 3. 6. Comparison of the PGA values at different distances estimated by ASK08 to the recorded PGA values at the SGM Stations	8
Figure 3. 7. Comparison of the normalized geometric mean of recorded PGA values with the distance scaling of GMPEs for $M_w=6.8$, $VS_{30}=400$ m/s of a strike slip event (a) for TR-adjusted BA08, (b) for TR-adjusted CY08, (c) for BSSA14, (d) for CY14, (e) for Kale et al. (2015).	10
Figure 3. 8. The Updated Turkish Earthquake Hazard Map (from https://tdth.afad.gov.tr).....	11
Figure 3. 9. Preliminary Intensity Distribution given by AFAD	13
Figure 3. 10. Computed MMI distributions using MMI-PGA correlations (Bilal and Askan,2014)	13

List of Tables

Table 3. 1. Moment tensor solution by AFAD and USGS	5
Table 3. 2. Strong Ground Motion Stations and Recorded PGA values (after AFAD).....	7
Table 3. 3. Strong Ground Motion Characteristics and Recorded PGA values.....	12



3.1 Introduction

On January 24, 2020 20:55:11 (UTC), a destructive earthquake (moment magnitude, $M_w=6.8$ according to AFAD) had occurred on the left lateral strike slip East Anatolian Fault Zone (EAFZ), more specifically along the Pütürge segment extending in the NE-SW direction. The epicenter was located at N38.3593°, E39.0630°, approximately 37 km SSW of Elazığ and 64 km east of Malatya with the focal depth of 8.06 km according to AFAD.

3.2 Seismological Characteristics of the Earthquake

EAFZ is a NE-SW striking, left-lateral intra-continental strike slip fault system that extends between the Karlıova junction and Antakya at the NE corner of Mediterranean Sea (Şaroğlu et al., 1992). Duman and Emre (2013) proposed seven segments with segment lengths ranging between 31 and 113 km for the EAFZ master fault strand which is adopted in the Updated Active Fault Maps of MTA as well (Emre et al., 2013). Two separate segments are defined by Duman and Emre (2013): the Palu segment between Palu and Lake Hazar and the Pütürge segment between Lake Hazar and Sincik separated by the Lake Hazar releasing bend. The rupture zone of the 2010 Elazığ Kovancılar earthquake ($M_w=6.1$) coincided with the Palu segment; whereas, the rupture zone of this event is associated with the Pütürge segment (Figure 3.1). The causative fault of the 2020 event is considered to have increased stress levels due to the 2010 Kovancılar earthquake (Akkar et al., 2011).

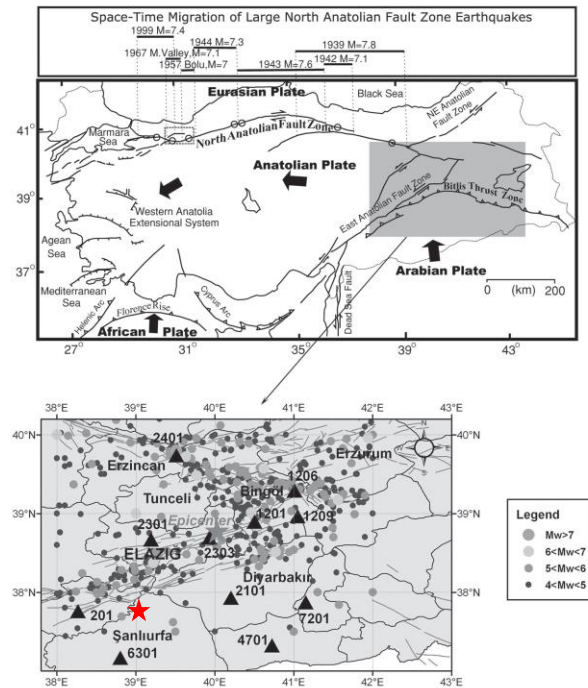


Figure 3. 1. Major tectonic structures and epicenters of the 2020 (red star) and 2010 (grey star) earthquakes along with seismicity within the last century.

Figure is modified from Akkar et al. (2011))



According to the preliminary report of field observations published by MTA, surface deformations related to this earthquake was observed for approximately 48 kilometers, starting from the Hazar Lake down to Pütürge (Malatya). These observations are consistent with the spatial distribution of the aftershocks shown in Figure 3.2; therefore, the approximate rupture plane defined by the surface deformations given in the preliminary MTA report is considered in this report to calculate the source-to-site distance metrics.

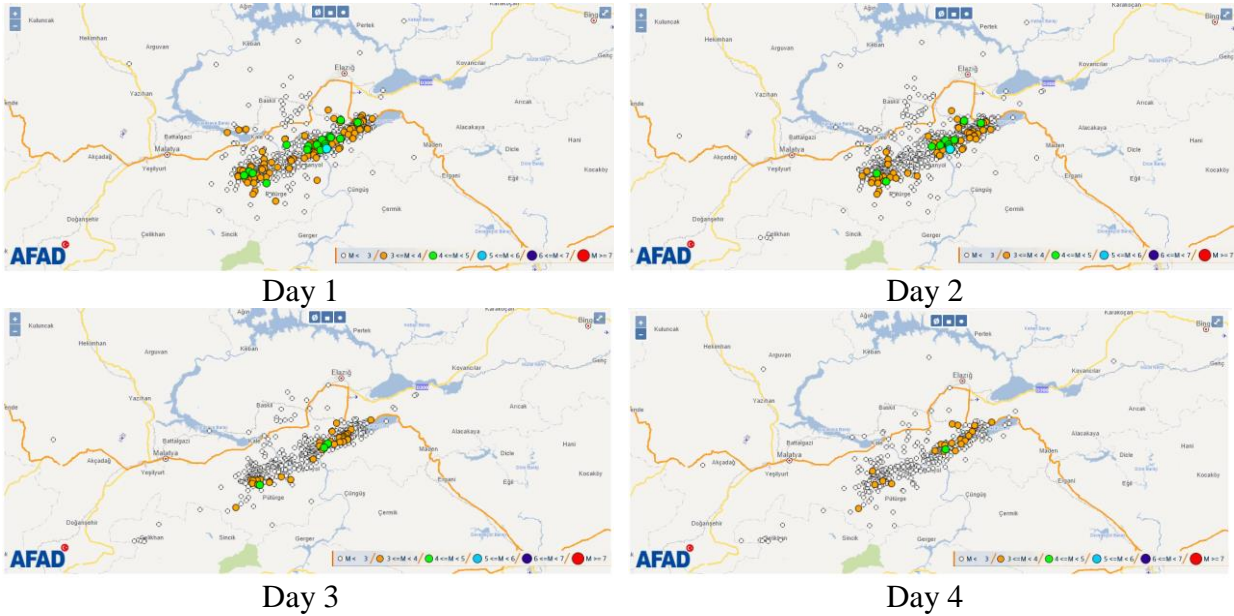



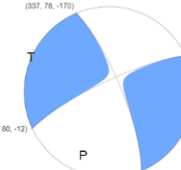
Figure 3. 2. Spatial distributions of the aftershocks between 24/01/2020-28/01/2020
(taken from <https://deprem.afad.gov.tr/ddakatalogu>)

3.3 Source Characteristics of the Event

The focal mechanism solutions for the mainshock, as provided by AFAD and USGS are shown in Table 3.1. They both provide planes that prove left lateral strike slip motions as dominant source mechanisms consistent with the regional tectonics and the properties of the causative fault. Additionally, geometric distribution and focal mechanism solutions of the aftershocks with moment magnitude values ranging between 4.0-5.1, are also shown in Figure 3.3.



Table 3. 1. Moment tensor solution by AFAD and USGS

AFAD	Strike 1	Dip 1	Rake 1	Strike 2	Dip 2	Rake 2
	248	76	1	158	89	166
USGS	Strike 1	Dip 1	Rake 1	Strike 2	Dip 2	Rake 2
	337	78	-170	245	80	-12

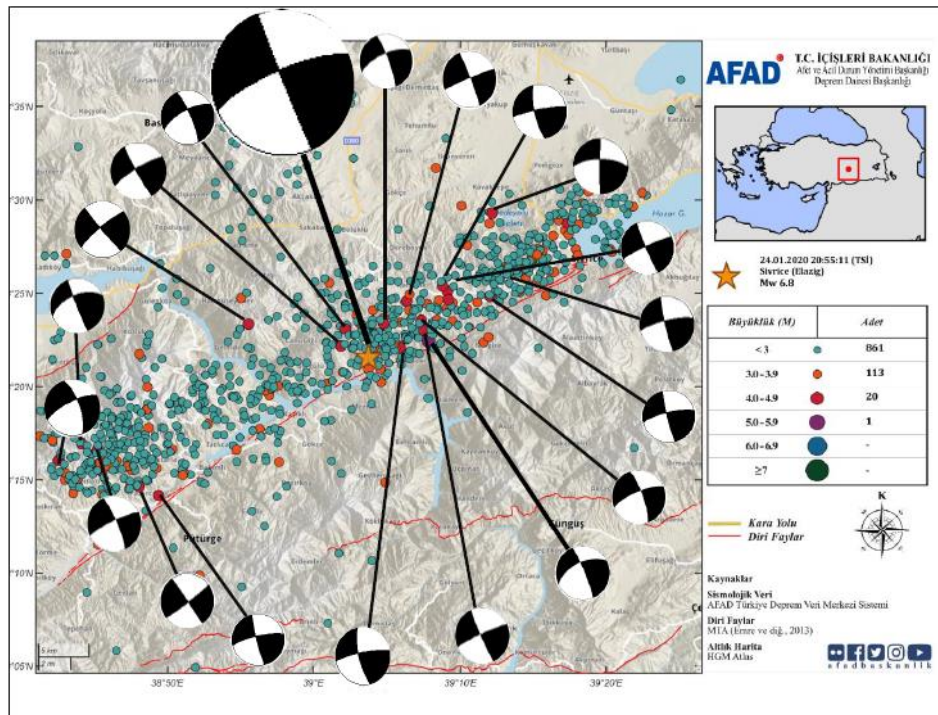


Figure 3. 3. 24/01/2020 Malatya-Elazığ Earthquake $M_w=6.8$ and aftershock distribution along with focal mechanism solutions given by AFAD.
(<https://deprem.afad.gov.tr/>)

The mainshock was followed by 1948 aftershocks with magnitudes ranging in between 0.8 and 5.1, within 10 days after the event. The focal depths of the aftershocks are mostly concentrated in between 5-20 kms from the ground surface consistent with the seismogenic depth of the region (Figure 3.4).

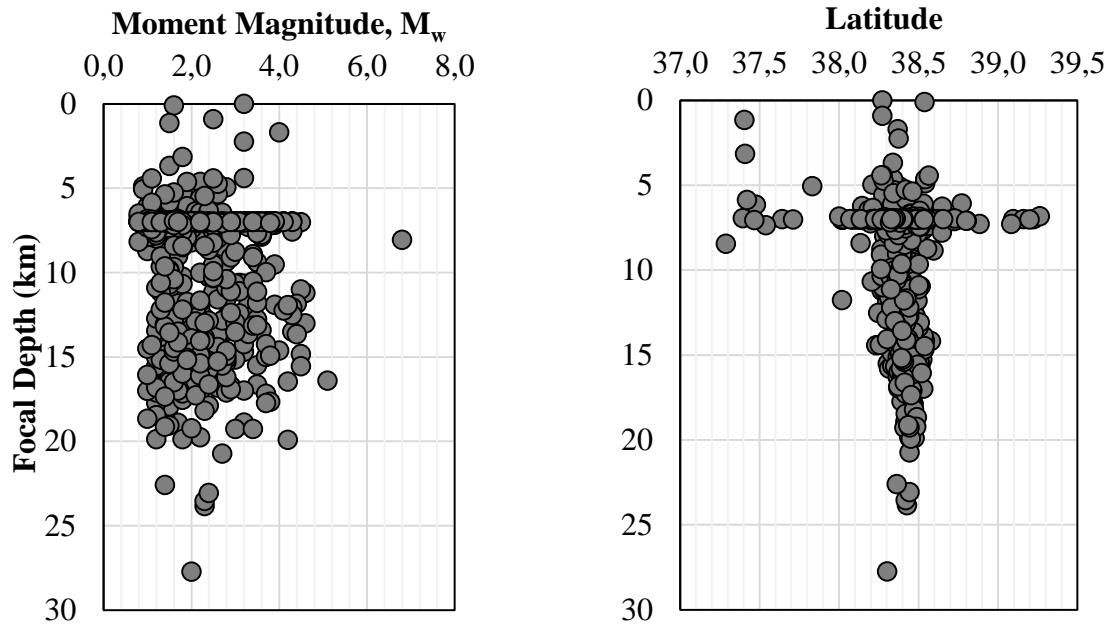


Figure 3. 4. M_w vs. focal depth scatters recorded between January 24 to February 03, 2020 following the mainshock of 2020 Elazığ-Sivrice Earthquake (AFAD)

3.4 Preliminary Analysis of Recorded Strong Ground Motions

The mainshock is recorded by 66 strong motion stations according to the preliminary report published immediately after the event by AFAD. In the preliminary report, only the largest three-component peak ground accelerations (PGA) recorded by five nearby stations were provided. Up to this date, the waveforms or the response spectra of the recordings were not disseminated to the public by AFAD; therefore, a detailed analysis of the strong motion characteristics is not included in this report. On the other hand, provided PGA values are useful for the preliminary and comparative analysis of recorded ground shaking levels with the current ground motion prediction equations (GMPEs) and the design PGA values provided in the recently-updated Turkish Seismic Hazard Map (2018).

Table 3.2 provides the geometric mean of the horizontal component PGA values recorded in this event that are gathered from AFAD's preliminary report. Fortunately, the shear wave velocity profiles for all stations are available: the time-averaged shear wave velocity at the first 30 meters (V_{S30}) for Pütürge (ID#4404), Center (ID#2301), and Maden (ID#2302) stations are measured by Sandıkkaya et al. (2010) and disseminated through <http://kyhdata.deprem.gov.tr> (last accessed January 31, 2020). The V_{S30} values of the other two stations, Sivrice (ID#2308) and Gerger (ID#0204), are taken from the final report of a recently finalized project funded by AFAD (Kurtuluş et al., 2019). These values are also provided in Table 3.2. To compare the distance attenuation of the recorded strong motions with the distance scaling of current GMPEs, the recorded values are normalized to $V_{S30} = 400$ m/s by using the site amplification scaling utilized in each model. Rupture (R_{RUP}) and Joyner-Boore (R_{JB}) distances given in Table 3.2 are calculated by using the fault plane shown in Figure 3.5. Because the termination points at both ends of the rupture plane



is still controversial, the source-to-site-distance metrics for Sivrice and Maden stations include a certain degree of uncertainty.

Table 3. 2. Strong Ground Motion Stations and Recorded PGA values (after AFAD)

Stations				Measured Acceleration Values (gals)			* R_{rup} (km)	* R_{jb} (km)	V_{s30}^{**} (m/s)
Station Code	Town	Latitude	Longitude	N-S	E-W	U			
2308	Sivrice	38.451	39.310	238	292.8	190.1	1.76	1.45	450
4404	Pütürge	38.196	38.874	207	239.2	153.9	5.49	5.4	1380
204	Gerger	38.029	39.035	94	110.1	60.8	28.62	28.6	555
2301	Center	38.670	39.193	119	140.7	66.3	27.87	27.85	407
2302	Maden	38.392	39.675	26.3	34	22.8	31.27	31.25	907

* Estimated based on the approximate location of the rupture plane based on the preliminary MTA report.

** Adapted from AFAD Ground Motion Station

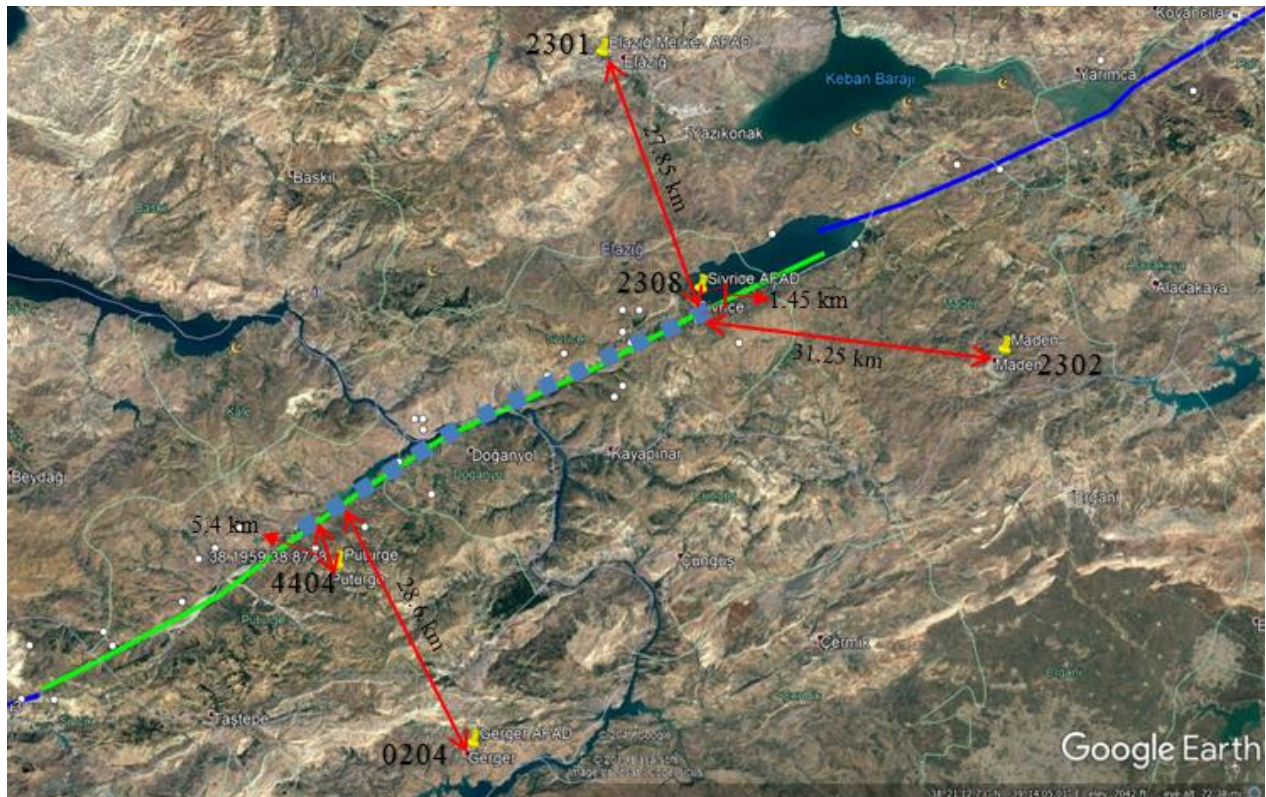


Figure 3. 5. Locations of the five strong motion stations included in the AFAD's preliminary report. R_{JB} values are approximately estimated according to the surface rupture given in MTA report (blue dashed line). Blue and green lines are the Palu and Pütürge segments that are slightly modified for their termination points by Gülerce et al. (2017)



Abrahamson et al. 2008 (ASK08) from NGA-West GMPE's is used along with the appropriate distance metrics and site conditions to predict the peak ground accelerations (PGA). Figure 3.6 shows the geometric mean of the PGA values as compared with the GMPE predictions for $V_{s,30}=200, 350, 500$ and 1100 m/s. Based on these comparisons, it is concluded that the recorded PGA values are in conformance with the predictions of Abrahamson et al GMPE. According to Wells and Coppersmith (1994) relationship, the length of the rupture is estimated as to vary in the range of 40-60 km consistent with the field and aftershock observations. This value is also compatible with the regional characteristics of the local tectonic environment, as stated in Gulerce et al. 2017.

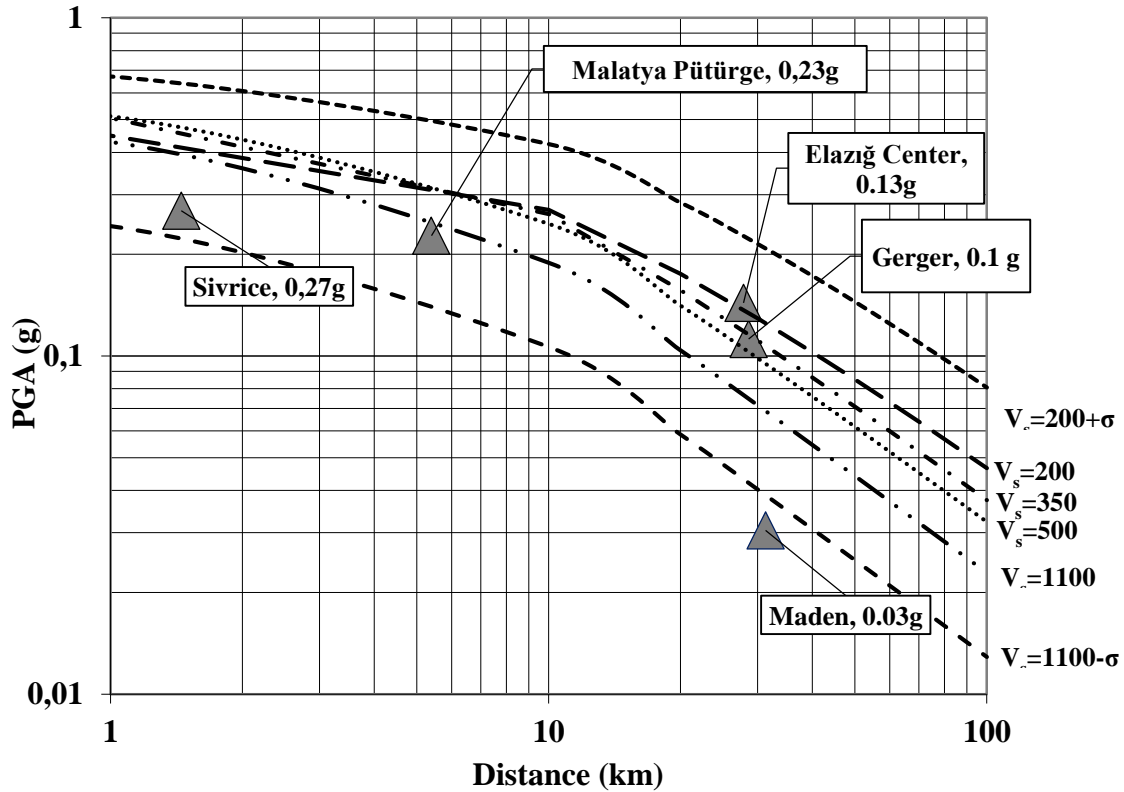


Figure 3. 6. Comparison of the PGA values at different distances estimated by ASK08 to the recorded PGA values at the SGM Stations

The geometric mean of the PGA values for the closest five stations to the zone of energy release are compared with the predicted median values obtained by ASK08. Figure 3.6 shows the comparisons of PGA response at different distances as compared to the values recorded at strong ground motion stations. Based on these comparisons, it is concluded that despite slightly lower values recorded at Sivrice and Maden stations, the PGA values are roughly in good agreement with the predictions of GMPE. The discussions and interpretations will be enriched when strong ground motion records and station data become publicly available.



A recent study by Kale (2019) has utilized several ranking methods for comparing the predictive performance of GMPEs for shallow crustal and active tectonic regions with the Turkish strong motion database. Analysis results indicated that the regional Kale et al. (2015) model, Turkey-adjusted version of the Boore and Atkinson (2008) model (Gülerce et al., 2016) and the global Chiou and Youngs (2014) model have better predictive performance among the other alternatives. Based on these findings, the normalized PGA values from this event are compared with the predictions lying in the $\text{median} \pm 1\sigma$ range given by TR-adjusted Boore and Atkinson (2008), TR-adjusted Chiou and Youngs (2008), Boore et al. (2014), Chiou and Youngs (2014) and Kale et al. (2015) in Figure 3.7. According to Figure 3.7, the PGAs recorded in Pütürge, Gerger and Elazığ Center stations are equal to or very close to the median estimations of the tested GMPEs. The PGA value recorded at the closest location to the epicenter, the Sivrice station is lower than the median estimations of Kale et al. (2015) and approximately one standard deviation lower than the median estimations of the other GMPEs. Similarly, the PGA value recorded at Maden station is significantly lower than the median estimations, lying outside the $\text{median} \pm 1\sigma$ range of each model. These findings are consistent with the distance attenuation plots given in Akkar et al. (2011): faster attenuation of waves due to low quality factor values in the region beyond 100 km was observed in the recorded ground motions of the 2010 Elazığ - Kovancılar Earthquake. The amount of data points beyond 30 km distance is currently very limited; therefore, the discussions and interpretations given here will be further elaborated when the strong ground motion records is publicly available.

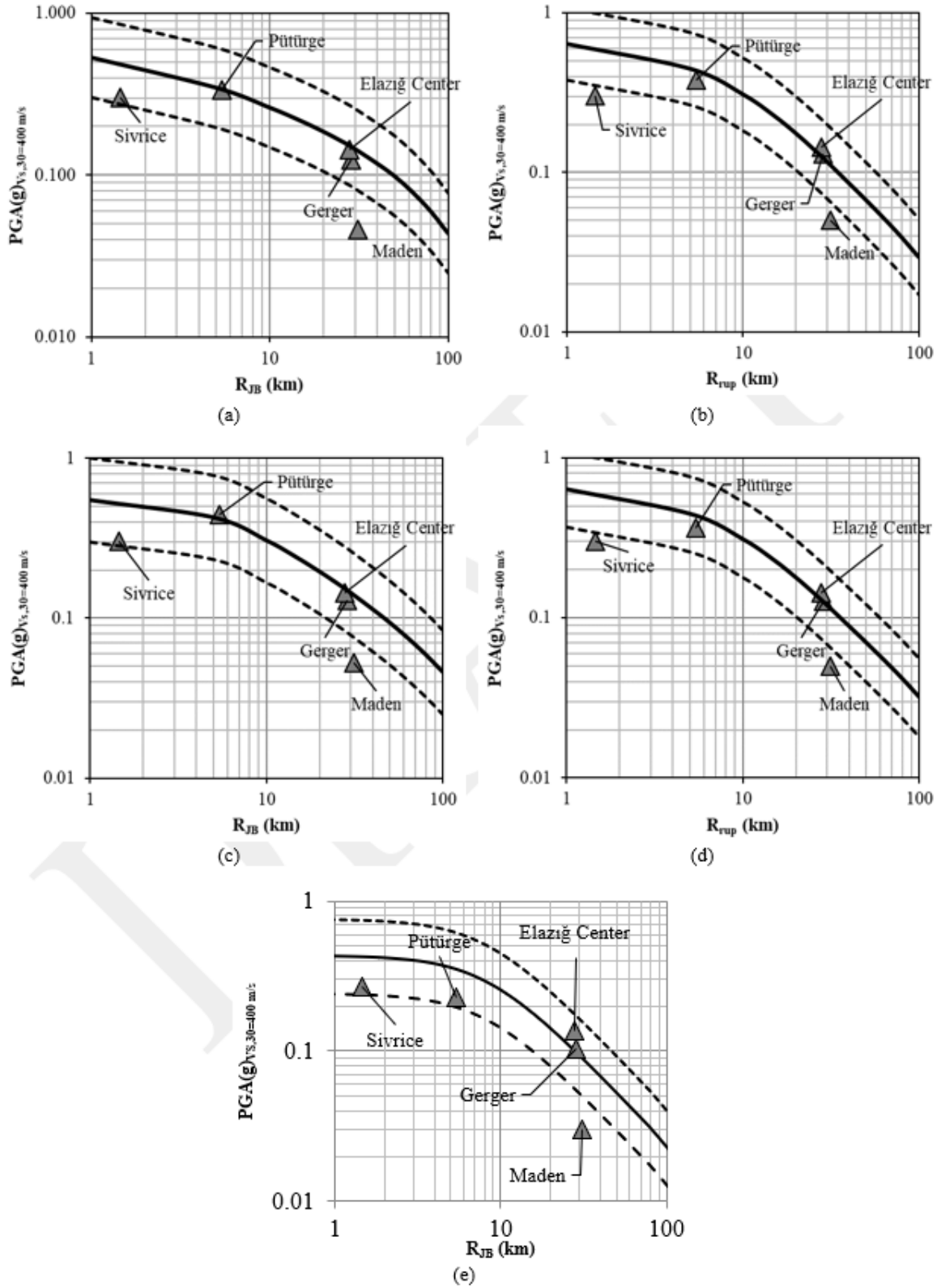


Figure 3. 7. Comparison of the normalized geometric mean of recorded PGA values with the distance scaling of GMPEs for $M_w=6.8$, $V_{S30}=400\text{m/s}$ of a strike slip event (a) for TR-adjusted BA08, (b) for TR-adjusted CY08, (c) for BSSA14, (d) for CY14, (e) for Kale et al. (2015).



The Turkish Seismic Hazard Map (TSHM) was updated in 2018 (Akkar et al., 2018) and is enforced by the updated Turkish Building Earthquake Code (TBDY, 2019) to obtain the design spectrum of regular buildings since the beginning of 2019. The short period ground motions (S_{DS}) with 20% and 10% chance of exceedance in 50 years (72 and 475 years return period, respectively) are downloaded from <https://tdth.afad.gov.tr> (last accessed in Feb 11, 2020) for each station as shown in Figure 3.8 and presented in Table 3.3. To calculate the S_{DS} values, the site classifications given in Table 3.2 are taken into account and the PGA values at the same hazard level are calculated by taking 40% of S_{DS} .

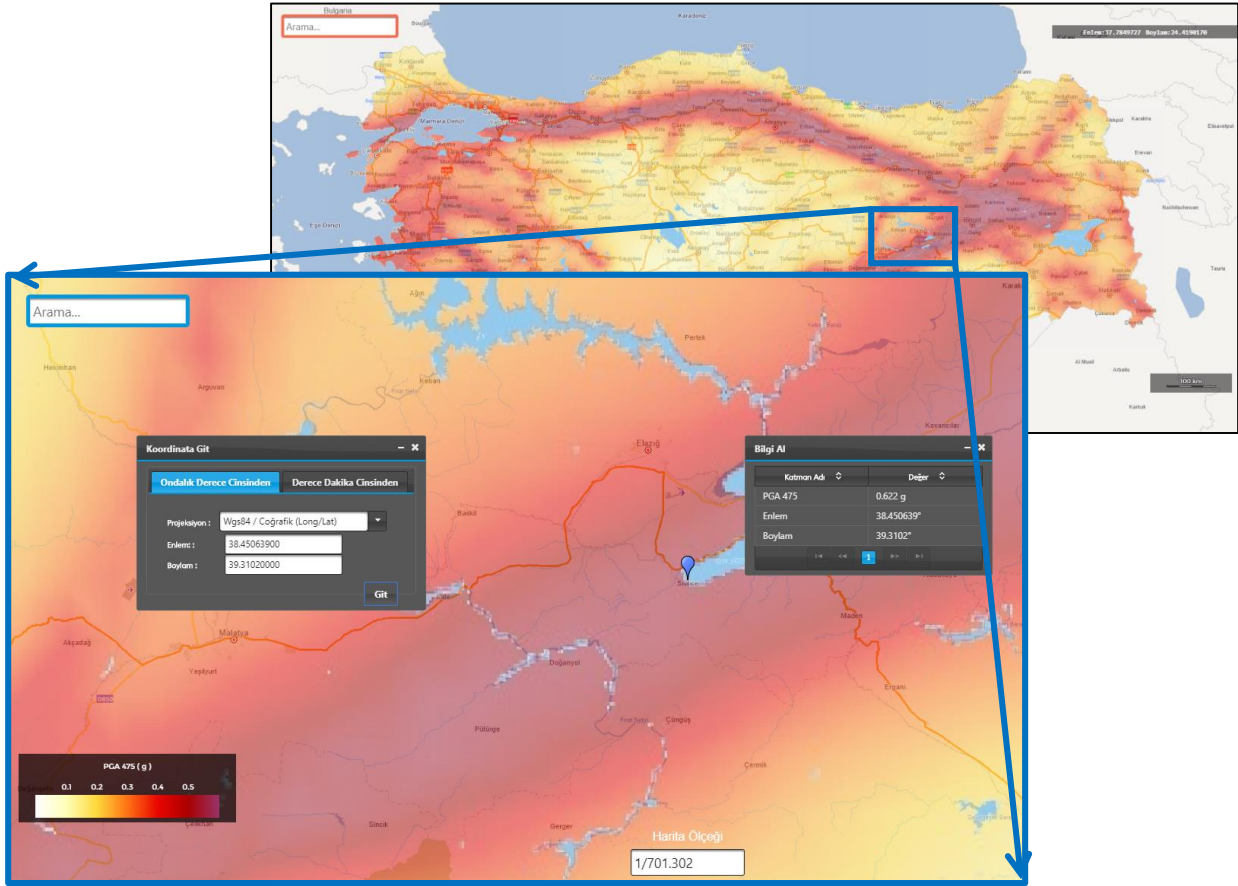


Figure 3. 8. The Updated Turkish Earthquake Hazard Map (from <https://tdth.afad.gov.tr>). Elazığ- Sivrice station (ID#2308) is pinned in blue color on the map and 475 years PGA value for that particular location is shown on the same figure.

TSHM suggests that the PGA values for 475-years and 72-years return periods are equal 0.722g and 0.277g for Sivrice station with the closest distance to the fault plane. Maximum accelerations recorded in this station (0.3g) is significantly lower than the PGA for 475-years return period and close to but slightly higher than the PGA for 72-years return period. A similar observation is valid for the Pütürge station as well. For the other stations with higher source to site distances, recorded maximum accelerations are smaller than the PGA suggested by TSHM for 72-years return period. On the basis of these, it is clearly seen that the Elazığ event is less severe than the design level earthquake.



It must be noted that, without full acceleration waveform data, it is not possible to compute and comment on the spectral accelerations which are critical on the evaluation of the seismic performance of the structures in the region.

Table 3. 3. Strong Ground Motion Characteristics and Recorded PGA values

Station Code	Site Class	$V_{s,30}$	E-W (g)	72-year return period					475-year return period				
				S_s	S_1	S_{DS}	S_{D1}	PGA	S_s	S_1	S_{DS}	S_{D1}	PGA
2308	ZC	450	0.30	0.539	0.126	0.692	0.189	0.277	1.504	0.396	1.805	0.594	0.722
4404	ZB	1380	0.24	0.548	0.122	0.493	0.098	0.197	1.578	0.403	1.42	0.322	0.568
204	ZC	555	0.11	0.344	0.085	0.447	0.127	0.179	0.883	0.233	1.06	0.35	0.424
2301	ZC	407	0.14	0.342	0.097	0.445	0.146	0.178	0.912	0.257	1.094	0.386	0.438
2302	ZB	907	0.04	0.428	0.107	0.385	0.086	0.154	1.148	0.306	1.033	0.245	0.413

3.5 Spatial Distribution of Macroseismic (Felt) Intensity in the Region

One way to measure the anticipated levels of ground shaking is to employ macroseismic intensity values. Particularly, a spatial distribution of such values is valuable immediately after an earthquake in order to evaluate the effects of the earthquake. Even though, the macroseismic intensity values have certain degrees of uncertainty when compared to instrumental measures of ground motions, they are employed all over the world for immediate assessment of earthquakes, particularly to see the effects on built environment and humans. It is possible to prepare empirical iso-seismal maps on the field by observations on human response and building damage. Another alternative is to use correlations between intensity and peak or spectral ground motion parameters.

The closest city center, Elazığ downtown, is approximately at 26.5 km from the zone of energy release, similarly Malatya and Adıyaman city centers are located 33.8 and 62.7 km from the epicenter. However, there are several smaller towns and villages in the fault vicinity likely experienced higher level of excitations. The preliminary intensity map in terms of Modified Mercalli Scale (MMI) by AFAD is shown in Figure 3.9. The values in this map are obtained by AFAD-RED system which employs correlations between MMI and strong ground motion parameters. The earthquake intensity map suggests that the maximum predicted MMI value is IX around the vicinity of the epicenter. Next, a computed MMI map is shown in Figure 3.10 where MMI distributions are computed from the following empirical correlation (Bilal and Askan, 2014):

$$MMI = 3.884 \times \log(PGA) + 0.132 \quad (1)$$

To compute the PGA values, Kale et al. (2015) is employed followed by calibrations at the 5 stations where PGA values are known. Then, conversion to MMI is performed through Equation (1). After the ground motion data is made public, these efforts will be repeated for the entire dataset.



It is observed that very similar MMI values are computed in the study area. The distribution of the intensity values is consistent with the fault plane as well as the spatial distribution of damage observations in the field, particularly around the rural area. In addition, through the team efforts, an observed MMI map is being prepared at the moment.

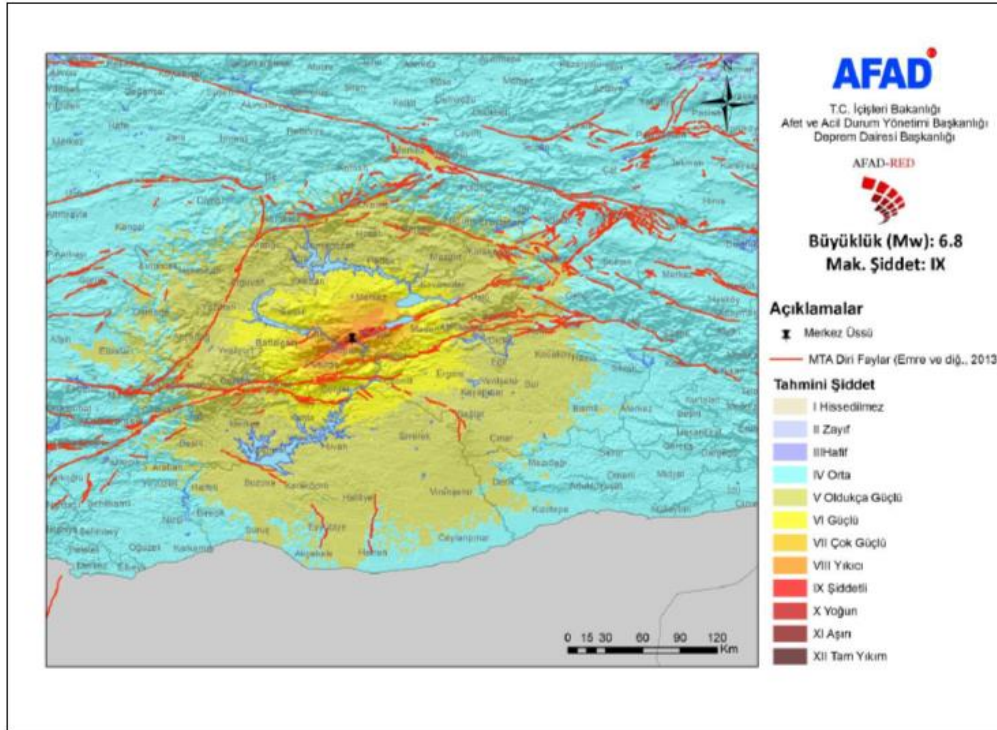


Figure 3. 9. Preliminary Intensity Distribution given by AFAD

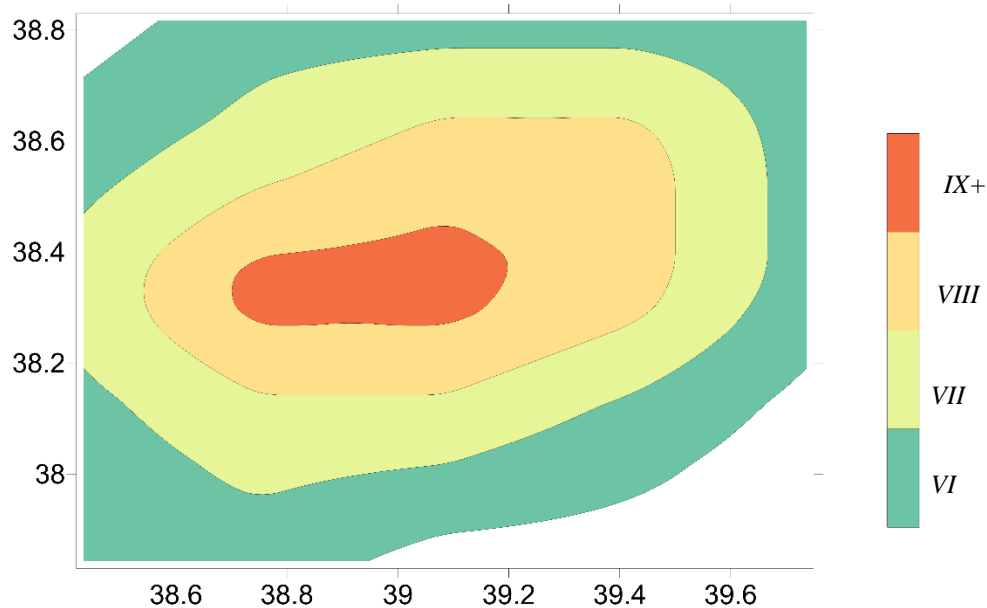


Figure 3. 10. Computed MMI distributions using MMI-PGA correlations (Bilal and Askan, 2014)



References

- Abrahamson, N., Atkinson, G., Boore, D., Bozorgnia, Y., Campbell, K., Chiou, B., Idriss, I. M., Silva, W., and Youngs, R., (2008). “Comparisons of the NGA ground-motion relations”, *Earthquake Spectra* 24, 45–66
- Akkar, S., Kale, Ö., Yenier, E., and Bommer, J. J. (2011) “The high-frequency limit of usable response spectral ordinates from filtered analogue and digital strong-motion accelerograms”, *Earthquake Engineering and Structural Dynamics* 40, 1387–1401.
- Akkar, S., A. Aldemir, A. Askan, S. Bakır, E. Canbay, I.O. Demirel, M.A. Erberik, Z. Gülerce, P. Gülkan, E. Kalkan, S. Prakash, M. A. Sandıkkaya, V. Sevilgen, B. Ugurhan, E. Yenier (2011). 8 March 2010 Elazığ-Kovancılar (Turkey) Earthquake: Observations on ground motions and building damage. *Seismological Research Letters*, 82, 42-58. (DOI: 10.1785/gssrl.82.1.42)
- Akkar, S., Azak T., Çan T., Çeken U., Demircioğlu Tümsa M. B., Duman, T. Y., Erdik, M., Ergintay, S., Kadirioğlu, F. T., Kalafat, D., Kale, Ö., Kartal R. F., Kekovalı K., Kılıç T. S., Zülfiyar Ö. (2018). “Evolution of seismic hazard maps in Turkey”, *Bulletin of Earthquake Engineering*, Vol.16, Issue 8, pp 3567-3570.
- Bilal, M. and A. Askan (2014). “Relationships between Felt Intensity and Recorded Ground-Motion Parameters for Turkey”, *Bulletin of the Seismological Society of America*, 104 (1), 484–496. (DOI: 10.1785/0120130093)
- Boore, D. M., and Atkinson, G. M., (2008). “Ground-motion prediction equations for the average horizontal component of PGA, PGV, and 5%-damped PSA at spectral periods between 0.0 1 s and 10.0 s”, *Earthquake Spectra* 24, 99–139
- Boore, D. M., Stewart, J. P., Seyhan, E., and Atkinson, G. A., (2014). “NGA-West 2 equations for predicting PGA, PGV, and 5%-damped PSA for shallow crustal earthquakes”, *Earthquake Spectra* 30, 1057–1087
- Chiou, B. S. J., and Youngs, R. R., (2008). “Chiou-Youngs NGA ground motion relations for the geometric mean horizontal component of peak and spectral ground motion parameters”, *Earthquake Spectra* 24, 173–217.
- Chiou, B. S. J., and Youngs, R. R., (2014). “Update of the Chiou and Youngs NGA model for the average horizontal component of peak ground motion and response spectra”, *Earthquake Spectra* 30, 1117–1155.
- Duman T. Y., Emre Ö. (2013). “The East Anatolian Fault: geometry segmentation and jog characteristics”. *Geol Soc London Spec Publ* 372: 495-529.



Emre Ö., Duman T. Y., Özalp S., Elmaci H., Olgun Ş., Şaroğlu F. (2013). “Active Fault Map of Turkey with an Explanatory Text”. Ankara, Turkey: General Directorate of Mineral Research and Exploration (MTA).

Gülerce, Z., Kargıoğlu, B., and Abrahamson, N. A. (2016) “Turkey-adjusted NGA-W1 horizontal ground motion prediction models,” *Earthquake Spectra* 32, 75–100.

Gülerce, Z., Soyman, K. B., Güner, B., & Kaymakci, N. (2017). “Planar seismic source characterization models developed for probabilistic seismic hazard assessment of Istanbul”. *Natural Hazards and Earth System Sciences*, 17(12), 2365.

Kale, Ö., Akkar, S., Ansari, A. and Hamzehloo, H. (2015). “A ground-motion predictive model for Iran and Turkey for horizontal PGA, PGV and 5%-damped response spectrum: Investigation of possible regional effects”, *Bulletin of the Seismological Society of America*, 105, 2A, 963-980

Kale, Ö. (2019). “Some Discussions on Data-Driven Testing of Ground-Motion Prediction Equations under the Turkish Ground-Motion Database”, *Journal of Earthquake Engineering*, 23(1), 160–181

Kurtuluş, C., Sertçelik, F., Sertçelik, İ., Kuru, T., Tekin, K., Ateş, E., Apak, A., Kökbudak, D., Sezer, S., & Yalçın, D. (2019). “Determination of the national strong ground motion recording stations’ soil parameters”, *National Earthquake Research Program (UDAP), AFAD* (in Turkish)

Sandıkçaya, M. A., Yılmaz, M. T., Bakır, B. S., & Yılmaz, Ö. (2010). “Site classification of Turkish national strong-motion stations”. *Journal of Seismology*, 14(3), 543–563.

Şaroğlu, F., Emre, Ö. & Kuşçu, İ. (1992). “Active Fault Map of Turkey at Scale 1:1 000 000”, *Mineral Research and Explorations Institute of Turkey Publication*, Ankara, 3 sheets.

Turkish Building Earthquake Code TBDY, 2019

Wells D. L., Coppersmith K. J. (1994) “New empirical relationships among magnitude, rupture length, rupture width, rupture area, and surface displacement”. *Bulletin of the Seismological Society of America*; 84 (4): 974–1002



CHAPTER 4

Geotechnical Reconnaissance Observations

Kemal Önder Çetin

Prof. Dr., Middle East Technical University, Civil Engineering Department.

Mesut Gör,

Assist. Prof. Dr., Fırat University, Civil Engineering Department

Makbule İlgaç, Gizem Can, Elife Çakır, Berkan Söylemez,

Research Assistants, Middle East Technical University, Civil Engineering Department.

Faik Cüceoğlu, DSİ, Graduate Student, Middle East Technical University, Civil Engineering



Table of Contents

4. Geotechnical Observations.....	6
4.1. Downtown Elazığ Soil Site Conditions.....	6
4.1.1. Downtown Elazığ	6
4.2. Ground Deformations in the Very Near Fault Region	12
4.2.1. Day 1: Hazar Lake Coast.....	14
4.2.2. Day 2: Kamışlık, Fırat River, Malatya and Elazığ, Kapıkaya Dam Sites	62
4.3. Rockfalls.....	101
4.4. Earth Structures	103
4.4.1. Hydraulic Dams	103
4.5. Railways	110
4.6. Seismic Soil Liquefaction and Lateral Spreading Cases Observed in Hazar Lake and Karakaya Dam Reservoir Shores.....	111

Table of Figures

Figure 4.1. Typical Borelog for Elazığ-Mustafapaşa District.....	7
Figure 4.2. Typical Borelog for Elazığ-Şahinkaya District	8
Figure 4.3. Typical Borelog for Elazığ-Sürsürü	9
Figure 4.4. Typical Borelog for Elazığ-Sürsürü District	10
Figure 4.5. Typical Borelog for Elazığ-Zafran District	11
Figure 4.6. Site Visits-Day 1.....	12
Figure 4.7. Site Visits-Day 2.....	13
Figure 4.8. A view of the site taken by Sivrice road.....	14
Figure 4.9. A small crack observed near the highway embankment	15
Figure 4.10. Clayey site and no signs of ground failure	16
Figure 4.11. Clayey site, no signs of failure	17
Figure 4.12. Seismically-induced volumetric settlement in the dock of Hazar Lake	18
Figure 4.13. Measurements of seismically-induced volumetric settlement in the dock of.....	19
Figure 4.14. Displacements observed on reinforced concrete dock blocks	20
Figure 4.15. Seismically-induced lateral spreading on the beach of Hazar Lake	21
Figure 4.16. Seismically-induced lateral spreading ground deformations mapped on the	22
Figure 4.17. Seismically-induced lateral spreading on the beach of Hazar Lake	23
Figure 4.18. Another view of seismically-induced lateral spreading cracks	24
Figure 4.19. Mapping efforts of seismically-induced lateral spreading on the	25
Figure 4.20. No ground failure on a neighboring beach of Hazar Lake	26
Figure 4.21. No ground failure on a neighboring beach of Hazar Lake	26
Figure 4.22. A view of a damaged Mosque at Sivrice (Merkez Camii)	27
Figure 4.23. A view of railway tracks without any damage at Sivrice	28
Figure 4.24. Toppled chimneys in Sivrice	29
Figure 4.25. Toppled chimney in Sivrice.....	30



Figure 4.26. No signs of ground failure	31
Figure 4.27. A view of the tunnel in Stop 5	32
Figure 4.28. Guney Kurtalan Express Train passing by	33
Figure 4.29. No failure on the road embankment	34
Figure 4.30. No ground failure at the 6 th stop	35
Figure 4.31. No ground failure was observed at the shores of 7 th stop	36
Figure 4.32. Sand boil observed in Stop 8	37
Figure 4.33. Sand boils observed in Stop 8	38
Figure 4.34. Sand boils observed in Stop 8	39
Figure 4.35. Sandy soil layers observed in Stop 8	40
Figure 4.36. A line of sand boils observed in Stop 8	41
Figure 4.37. Sand boil observed in Stop 8	42
Figure 4.38. Sand boil observed in Stop 8	43
Figure 4.39. No ground failure was observed at shore of 9 th stop	44
Figure 4.40. A railway tunnel and rails exhibiting no damage	45
Figure 4.41. A view of tunnel body at Stop 10	46
Figure 4.42. Side view of tunnel wall at Stop 10	47
Figure 4.43. Interbeddings observed in volcanic rocks	47
Figure 4.44. No ground failure was observed at shore of 10 th stop	48
Figure 4.45. No ground failure was observed at shore of 11 th stop	49
Figure 4.46. Sand boils observed	50
Figure 4.47. Rockfall at 13 th stop (general view)	51
Figure 4.48. Rockfall at 13 th stop (upper bench)	52
Figure 4.49. Rockfalls at 13 th stop	53
Figure 4.50. Measurement of rockfalls' dimensions at 13 th stop	54
Figure 4.51. Rockfalls at 13 th stop (Slope angle determination)	55
Figure 4.52. Side view of the slope	56
Figure 4.53. Side view of the slope	57
Figure 4.54. Rockfalls at 14 th stop	58
Figure 4.55: Seismic soil liquefaction-induced sand boils at Stop 15	59
Figure 4.56. Seismic soil liquefaction-induced sand boils	60
Figure 4.57. Seismic soil liquefaction-induced sand boils	61
Figure 4.58. Doğanyol Port Failure adapted from IHA report	62
Figure 4.59. Fallen rocks on the highway	63
Figure 4.60. New Kömürhan Bridge under construction on Fırat River	64
Figure 4.61. Road to Doğanyol	65
Figure 4.62. Cracks on the wall of a residential building in Battalgazi Village	66
Figure 4.63. Minaret's of village Mosque	67
Figure 4.64. Separation of two adjacent buildings in Battalgazi Village	67
Figure 4.65. No foundation displacements observed at a residential building in Battalgazi Village	68
Figure 4.66. Historical monument in the Battalgazi Village	68
Figure 4.67. Railway and bridge at 20 th stop	69
Figure 4.68. Residential buildings in the Bahçelievler district of Battalgazi Village	70
Figure 4.69. Cracks on the wall of a residential building in the Bahçelievler district of Battalgazi Village	71



Figure 4.70. Views of frozen soil in Toygar district of Battalgazi Village	72
Figure 4.71. Views of frozen clayey soils in Toygar district of Battalgazi Village	73
Figure 4.72. Water trench in Dolamantepe district of Battalgazi Village	74
Figure 4.73. Dolamantepe district of Battalgazi Village	74
Figure 4.74. Minaret's of a Mosque in the Hanımınçiftliği district of Battalgazi Village	75
Figure 4.75. Side views of Kapıkaya Dam	76
Figure 4.76. Side view of Kapıkaya Dam downstream face.....	77
Figure 4.77. Crest view of Kapıkaya Dam	78
Figure 4.78. Water in-take structure of Kapıkaya Dam.....	79
Figure 4.79. Spillway of Kapıkaya Dam	80
Figure 4.80. Spillway of Kapıkaya Dam	81
Figure 4.81. Abutment slopes of Kapıkaya Dam.....	82
Figure 4.82. Right abutment natural slopes	82
Figure 4.83. Settlement Plate, piezometer, data acquisition house and inclinometer borehole located at Kapıkaya Dam	83
Figure 4.84. View of Kale shore	84
Figure 4.85. Another view of Kale shore.....	84
Figure 4.86. Kale shore	85
Figure 4.87. Seismic soil liquefaction-induced sand boils at Kale shore	85
Figure 4.88. Seismic soil liquefaction-induced sand boils at Kale shore	86
Figure 4.89. Seismic soil liquefaction-induced sand boils at Kale shore	87
Figure 4.90. Seismic soil liquefaction-induced sand boils at Kale shore	87
Figure 4.91. Seismic soil liquefaction-induced sand boils at Kale shore	88
Figure 4.92. Snow-covered road on our way to Çevrimtaş	88
Figure 4.93. Tents for the people suffering from the earthquake	89
Figure 4.94. Volumetric settlement at the foundation of a residential building	89
Figure 4.95. Residential buildings located at the Abdullah Paşa district of Elazığ city center	90
Figure 4.96. Cracks observed at the entrance of Eğitim Apartment.	90
Figure 4.97. A residential building located in the Abdullah Paşa district of Elazığ city center ..	91
Figure 4.98. Cracking observed at the entrance of the of a residential building	91
Figure 4.99. Cracks at the first floor, and fallen bricks	92
Figure 4.100. View of the basement of a residential building, rusty reinforcement bars, poor detailing and construction	92
Figure 4.101. Elazığ ground motion station.....	93
Figure 4.102. A crack on a concrete fence in Sürsürü district of Elazığ city center.....	94
Figure 4.103. Settlement mapped at the entrance of some buildings	95
Figure 4.104. Settlements observed.....	96
Figure 4.105. Settlement observed.....	96
Figure 4.106. Cracks on partition walls	97
Figure 4.107. Drilling efforts	97
Figure 4.108. Damaged Minaret of Rüstem Paşa Yol Üstü Mosque.....	98
Figure 4.109. Longitudinal cracks observed on a building located in the Mustafa Paşa district..	99
Figure 4.110. Demolishment of a heavily-damaged building in the Mustafa Paşa district of Elazığ city center.....	100
Figure 4.111. Rock falls observed at the shores of Hazar Lake at 13 th stop.....	101
Figure 4.112. Cross section of the rockfall at 13 th stop	101



Figure 4.113. Back analysis of rockfall	102
Figure 4.114. Karakaya Dam (DSİ)	104
Figure 4.115. Cip Dam (DSİ)	105
Figure 4.116. Kapıkaya Dam (DSİ)	106
Figure 4.117. Keban Dam (DSİ)	107
Figure 4.118. Boztepe (Recai Kutan) Dam (DSİ)	108
Figure 4.119. Longitudinal cracks on Dedeyolu Dam crest (DSİ)	109
Figure 4.120. Turkish railway route map and the routes of Van Gölü and Güney Kurtalan Express Trains	110
Figure 4.121. A summary of ground failure observations along the shores of Hazar Lake	111
Figure 4.122. A summary of ground failure observations along the shores of Fırat River and Malatya-Elazığ Route	112
Figure 4.123. A sketch of lateral spread deformations at 2 nd stop	113
Figure 4.124. Deformations and cracks due to lateral spreading observed along	114
Figure 4.125. Deformations and cracks due to lateral spreading observed along	114
Figure 4.126. No ground failure at the natural beach neighboring the lateral spreading	115
Figure 4.127. Surface manifestations of soil liquefaction in Hazar Lake (8 th stop)	115
Figure 4.128. Surface manifestations of soil liquefaction in Hazar Lake (15 th stop)	116
Figure 4.129. Surface manifestation of soil liquefaction at Kale Village shores (26 th stop)	116
Figure 4.130. Surface manifestation of soil liquefaction at Kale Village shores	117
Figure 4.131. Location of sand boil samples taken from Hazar Lake shores	117
Figure 4.132. Location of sand boil samples taken from Kale Village shores	118
Figure 4.133. Location of the samples taken during site investigation (general view)	118
Figure 4.134. Particles size distribution curves of the sand ejecta taken from liquefied sites....	119

Table of Tables

Table 4-1. Fallen rock blocks measurements recorded at 13 th stop	102
Table 4-2. Inspected dams by DSİ reconnaissance team after Sivrice Earthquake	103
Table 4-3. Grain size distribution of sand ejecta	118



4. Geotechnical Observations

This chapter discusses the preliminary geotechnical field observations made during and after the reconnaissance studies performed during the period of January 26-February 1st. After a brief introduction of the geotechnical conditions in Elazığ Province, the field observations in the form of pictures and maps along with simple interpretations will be presented. On the path during reconnaissance studies, some structural performance observations were also made, which will be presented for documentation purposes. Detailed geotechnical discussion and interpretations including in-depth analyses will be the scope of future studies.

4.1. Downtown Elazığ Soil Site Conditions

On the basis of available local geotechnical data, the geotechnical setting of downtown Elazığ's most affected four districts namely, i) Mustafapaşa, ii) Şahinkaya, iii) Sürsürü, iv) Zafran will be discussed next. The available shear wave velocity measurements by Multi-Channel Surface Wave Analysis Method (MASW) along with Standard Penetration Test results establish the basis of these assessments. A generalized representative borehole is constructed for these districts as discussed in the following sections.

4.1.1. Downtown Elazığ

4.1.1.1. Elazığ-Mustafapaşa District

Several structurally damaged residential buildings were mapped in Elazığ-Mustafapaşa district, which is located in the city center of Elazığ city. Mustafapaşa district consists of Plio-Quaternary aged young sediments. Typical soil type observed in the district is classified as brown gravelly sandy clay. Groundwater table is typically observed at 15 meters. A representative lithology is presented in Figure 4.1. Shear wave velocity of the upper 30 m ($V_{s,30}$) for the region is estimated as 300-350 m/s by Multi-Channel Surface Wave Analysis Method (MASW). Note that the borelog given in Figure 4.1 reflects idealized soil conditions, which may not representative for the whole district.

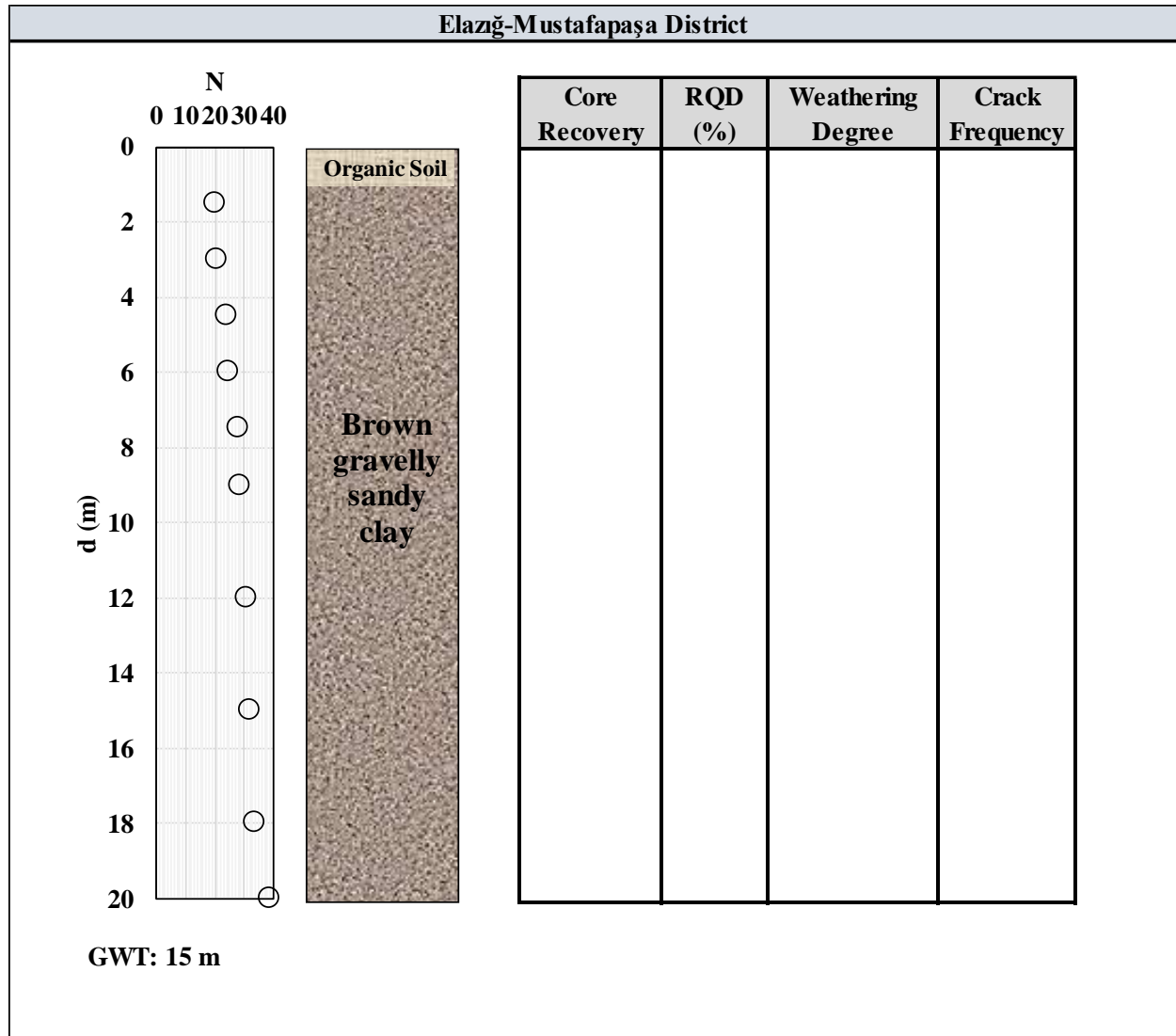


Figure 4.1. Typical Borelog for Elazığ-Mustafapaşa District



4.1.1.2. Elazığ-Şahinkaya District

In Şahinkaya district, again a concentration of structural damage has been observed. The district foundation soil/rock profile is composed of mostly weathered sandstone. The weathering and fracturing decreases with depth. Groundwater table is located at 6 meters. A representative soil/rock profile is presented in Figure 4.2. Shear wave velocity of the upper 30 m ($V_{s,30}$) for the district is estimated as 400-500 m/s by Multi-Channel Surface Wave Analysis Method (MASW).

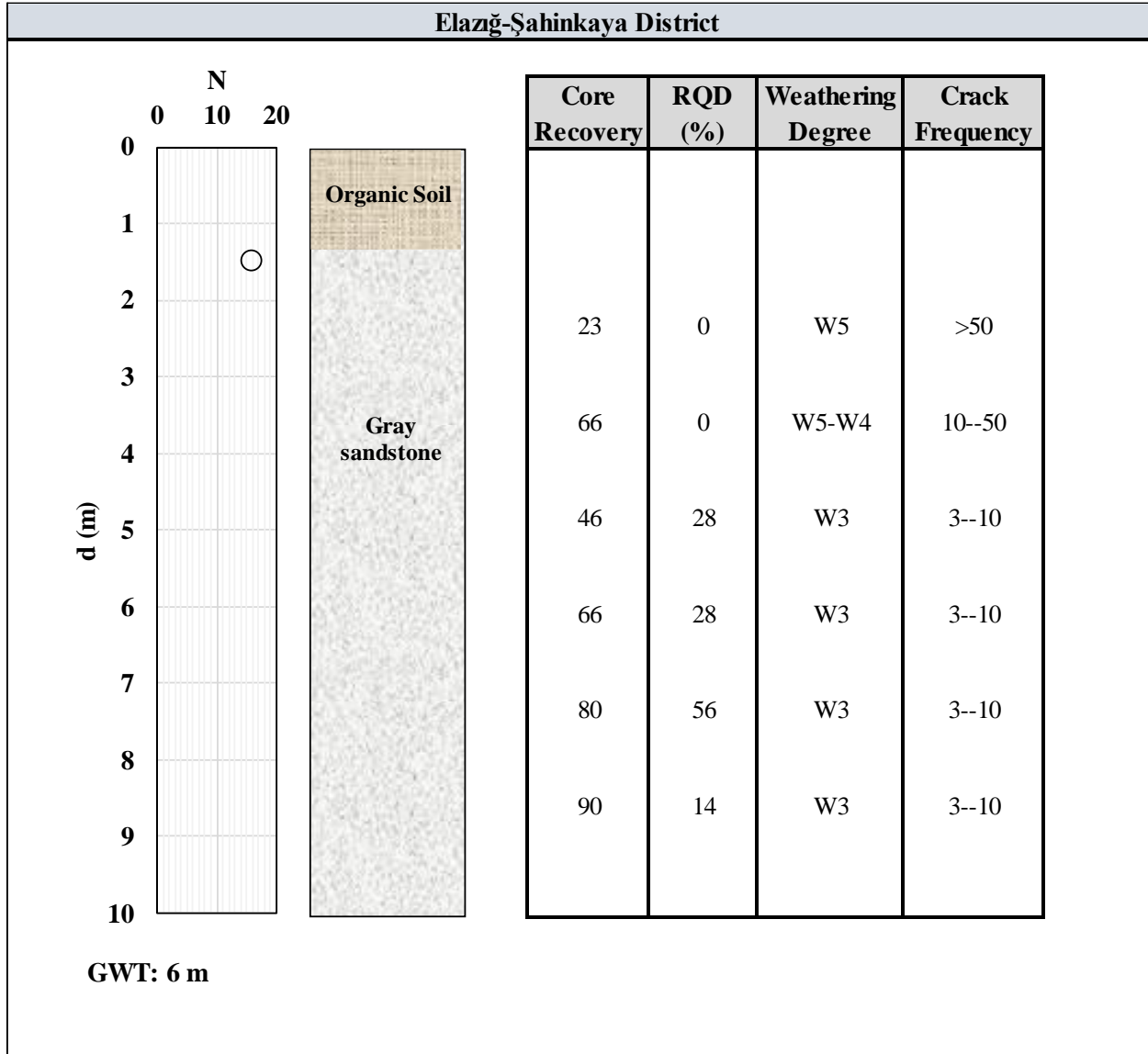


Figure 4.2. Typical Borelog for Elazığ-Şahinkaya District



4.1.1.3. Elazığ-Sürsürü District

The most of the structural damage had been concentrated in Elazığ-Sürsürü district, where Plio-Quaternary aged young sediments dominate foundation profiles. The upper surficial layers are classified as brown gravelly sandy clay. Groundwater table is located below 15 m depth. Two representative lithology are presented in Figure 4.3. Shear wave velocity of the upper 30 m ($V_{s,30}$) for the region is estimated as 350-400 m/s by Multi-Channel Surface Wave Analysis Method (MASW).

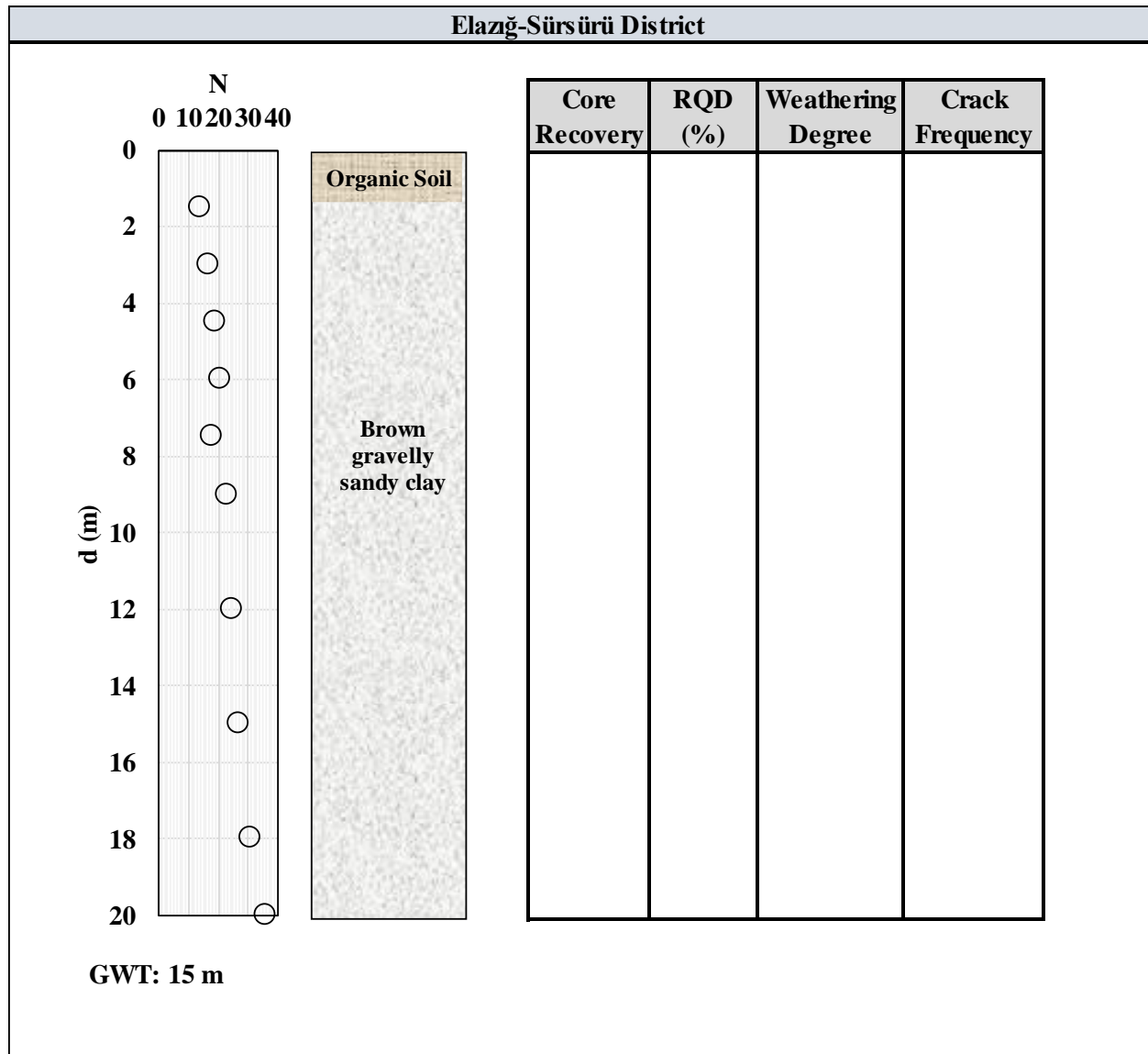


Figure 4.3. Typical Borelog for Elazığ-Sürsürü



During the site visit, a field investigations study including borehole drilling, undisturbed and disturbed soil sampling with SPT measurements, was witnessed. The borelog of this study is retrieved by personal communication and is presented in Figure 4.4.

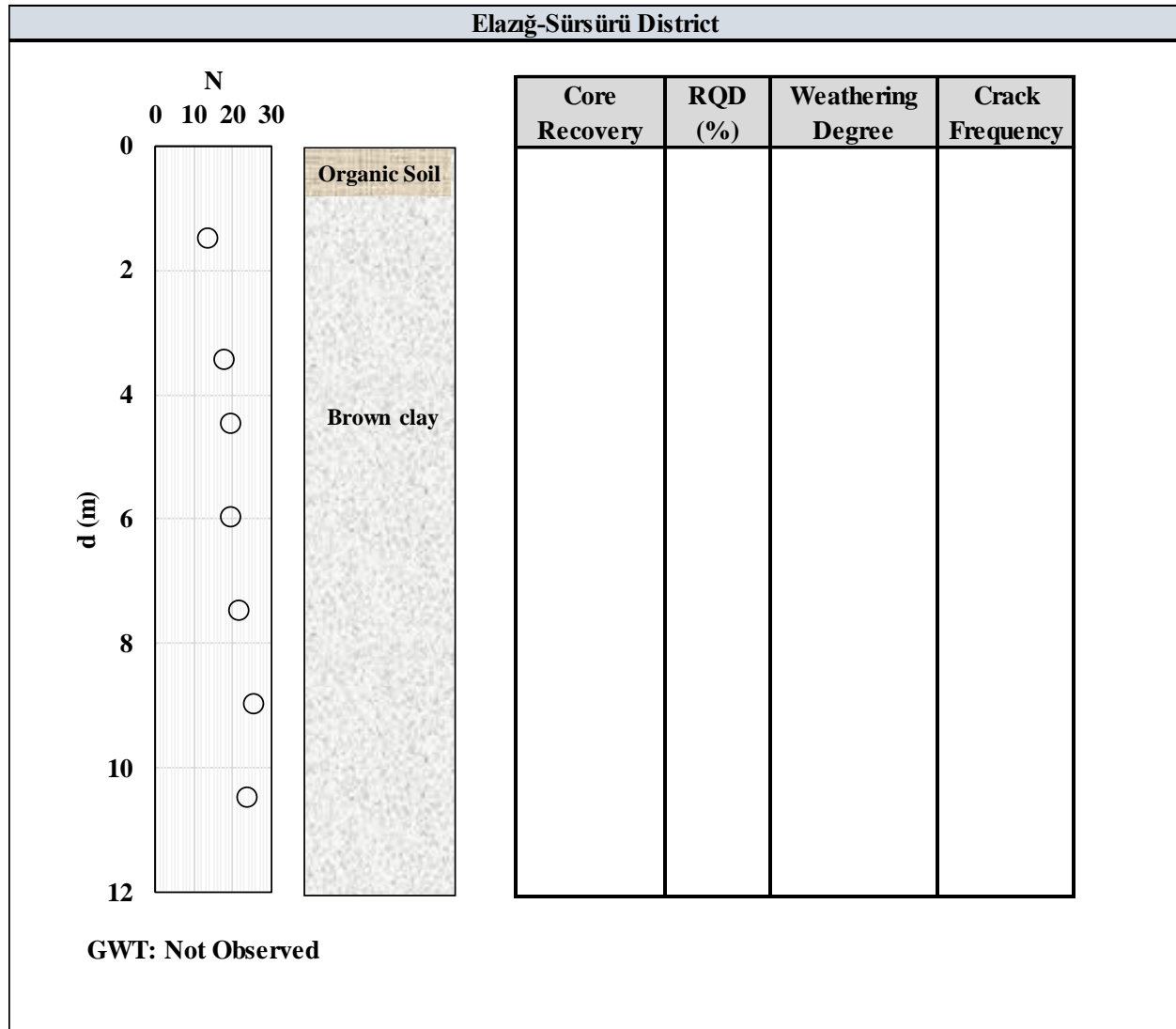


Figure 4.4. Typical Borelog for Elazığ-Sürsürü District



4.1.1.4. Elazığ-Zafran District

Mainly weathered and fractured gray-beige sandstone is observed in Elazığ-Zafran District. The rock becomes relatively intact with depth. Groundwater table is observed to be deeper than 10 meters. A representative soil/rock profile is presented in Figure 4.5. Shear wave velocity for the upper 30 m ($V_{s,30}$) is estimated as 650-700 m/s by Multi-Channel Surface Wave Analysis Method (MASW). The structural damage patterns specific for the district are not available yet, and will be the scope of future studies.

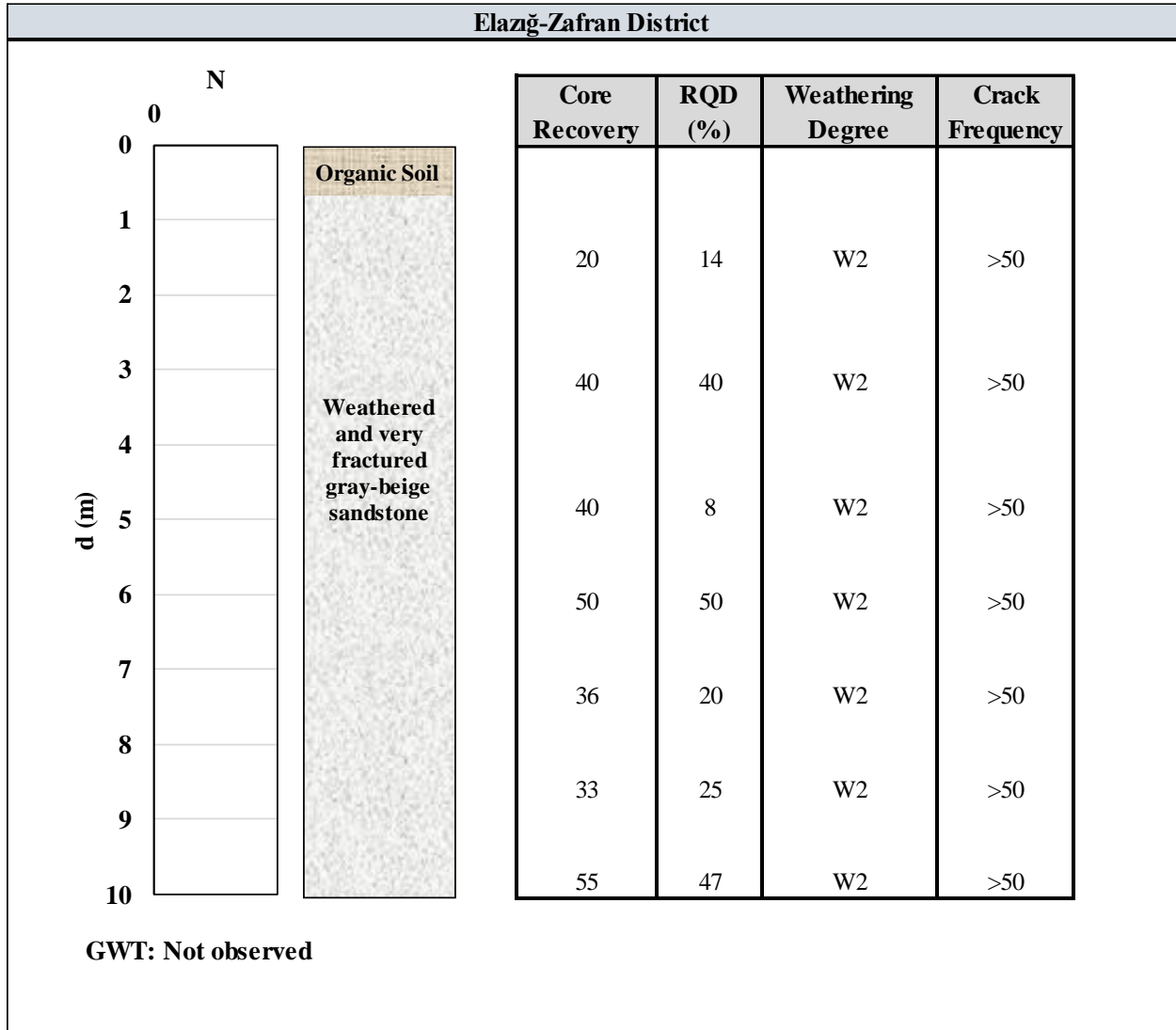


Figure 4.5. Typical Borelog for Elazığ-Zafran District



4.2. Ground Deformations in the Very Near Fault Region

The reconnaissance team visited Elazığ and Malatya regions on the days of 31.01.2020 – 01.02.2020. Hazar Lake is visited on the first day, the route of which is shown in Figure 4.6. The team stopped at 16 locations around Hazar Lake. The detailed observations are discussed in Section 4.2.1.



Figure 4.6. Site Visits-Day 1



Kamışlık, Fırat River, Malatya and Elazığ, Kapıkaya Dam sites are visited in the second day, as shown in Figure 4.7. The team stopped again at 16 locations. The detailed observations from day two are discussed in Section 4.2.2.

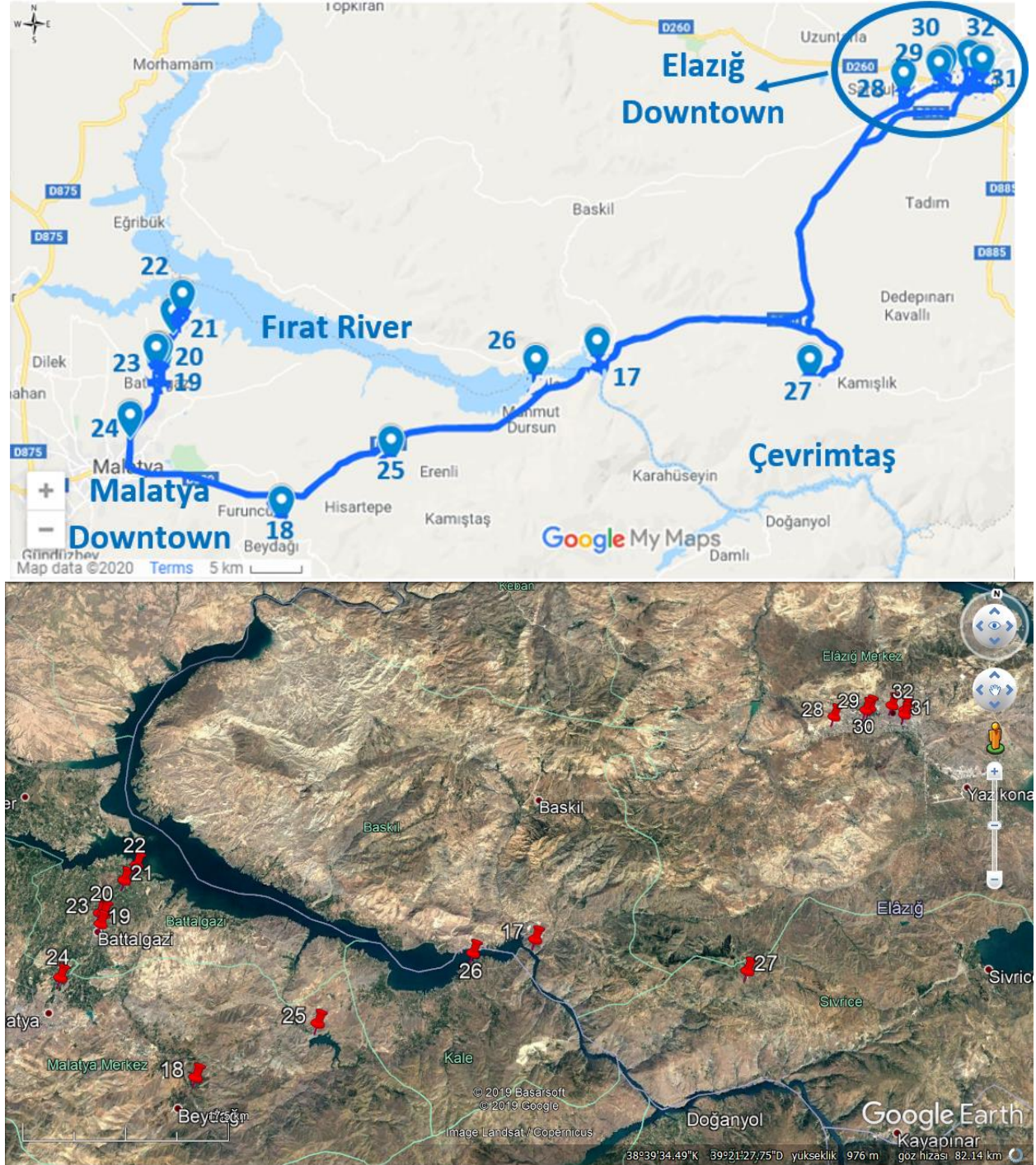


Figure 4.7. Site Visits-Day 2



4.2.1. Day 1: Hazar Lake Coast

1st stop - Sivrice Road

The surficial soils and the alluvial geological setting are concluded to be suitable for liquefaction triggering. However, no signs of liquefaction in the form of sand boils, lateral spread, excessive settlements, etc. were observed at the first stop, as shown in Figure 4.8.



Figure 4.8. A view of the site taken by Sivrice road
(38°28'08.6"N 39°16'40.2"E / 31.01.2020 / 11:47)

A small crack indicating a local bench failure was observed near the Sivrice road embankment, as shown in Figure 4.9. The crack is examined and presumed as a sign of a local small-scale slope instability problem.



Figure 4.9. A small crack observed near the highway embankment
(38°28'08.0"N 39°16'38.7"E / 31.01.2020 / 11:50)



On the first stop just down the road embankment, a neighboring site was also visited, as shown in Figure 4.10. The site is composed of surficial clayey soils based on field observations. No damage and surface manifestation of ground deformations were observed.



Figure 4.10. Clayey site and no signs of ground failure
(38°28'09.0"N 39°16'46.8"E / 31.01.2020 / 11:51)



A crack was observed on the sidewalk near to Sivrice road as presented in Figure 4.11. The orientation of the cracking does not support a slope instability problem, which may be interpreted as an old crack existing before the earthquake.

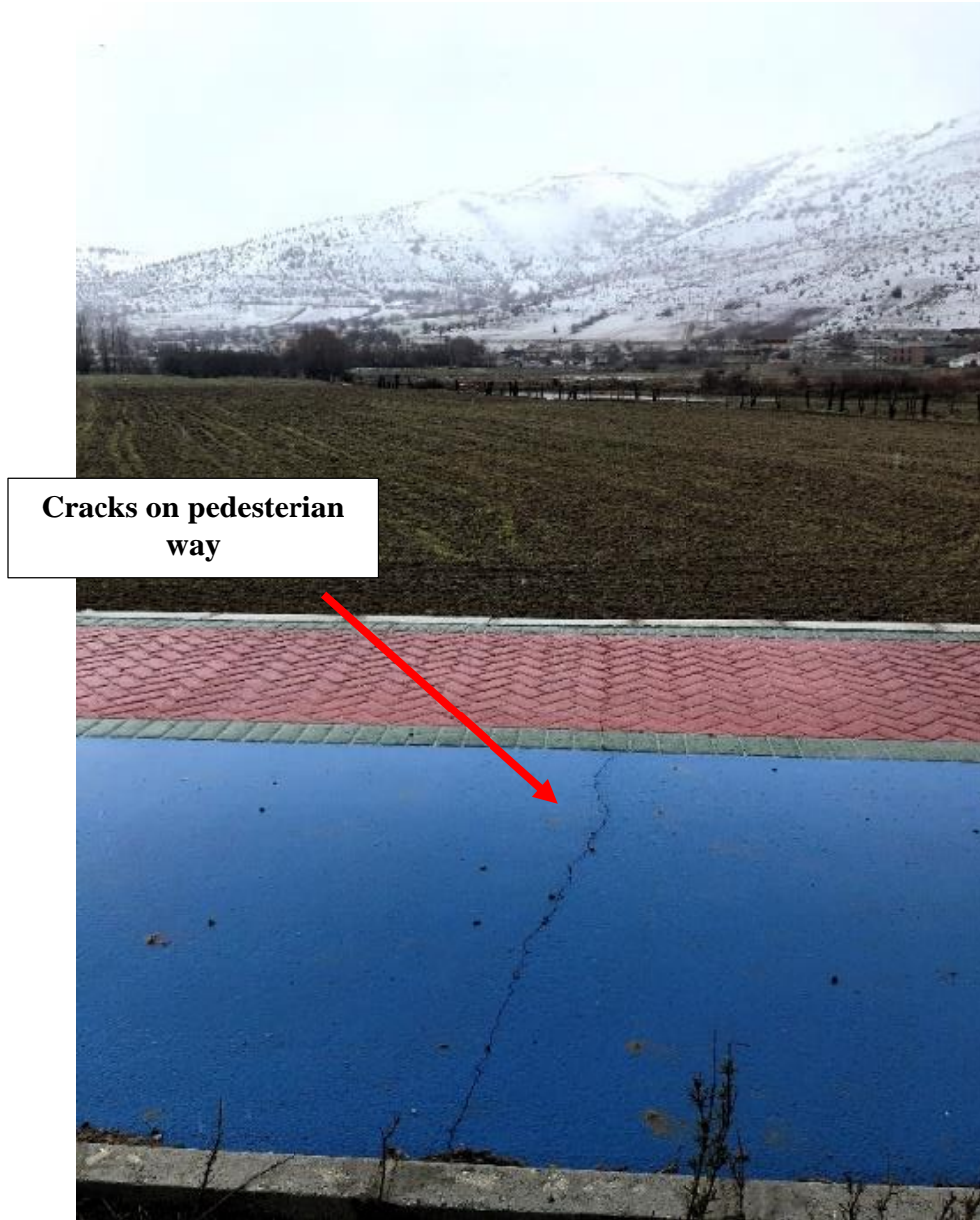


Figure 4.11. Clayey site, no signs of failure
(38°28'10.0"N 39°17'03.6"E / 31.01.2020 / 11:56)



2nd stop - Sivrice Dock

Seismically-induced lateral spreading and volumetric settlements were observed on the natural beach of Hazar Lake shoreline and Sivrice dock. Observed ground failure was mapped and discussed in a detailed manner in Section 4.7. Distribution of volumetric settlement and lateral displacements are mapped as shown in Figures 4.12 to 4.19, respectively. Next to the lake beach, where liquefaction manifestation is observed, a neighboring beach has exhibited no signs of ground failure, as given in Figure 4.20 and 4.21.

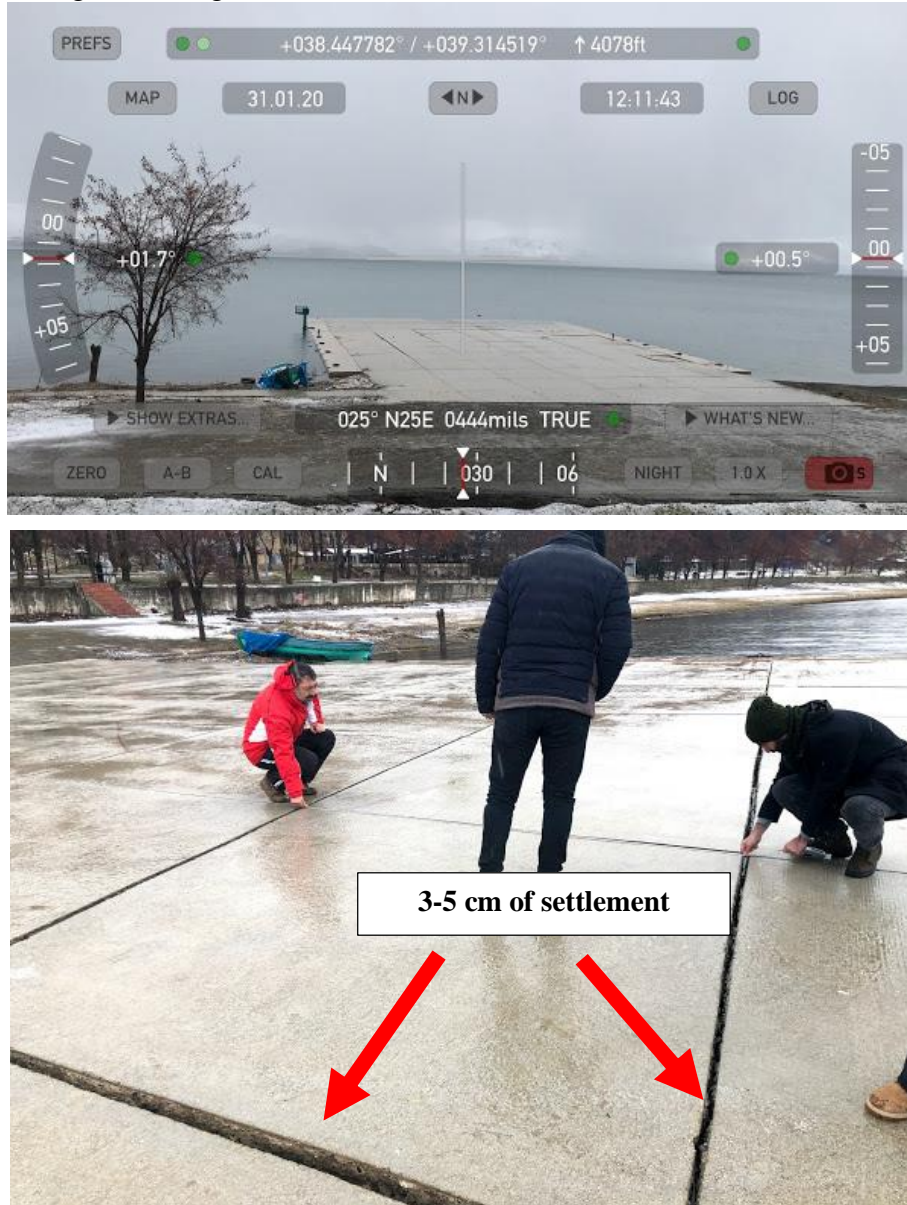


Figure 4.12. Seismically-induced volumetric settlement in the dock of Hazar Lake
(38°28'10.0"N 39°17'03.6"E / 31.01.2020 / 12:11 & 38°26'53.2"N 39°18'53.4"E / 31.01.2020 / 12:14)



Figure 4.13. Measurements of seismically-induced volumetric settlement in the dock of
Hazar Lake
($38^{\circ}26'53.1''N$ $39^{\circ}18'53.6''E$ / 31.01.2020 / 12:16 & $38^{\circ}26'53.2''N$ $39^{\circ}18'52.9''E$ / 31.01.2020 / 12:13)

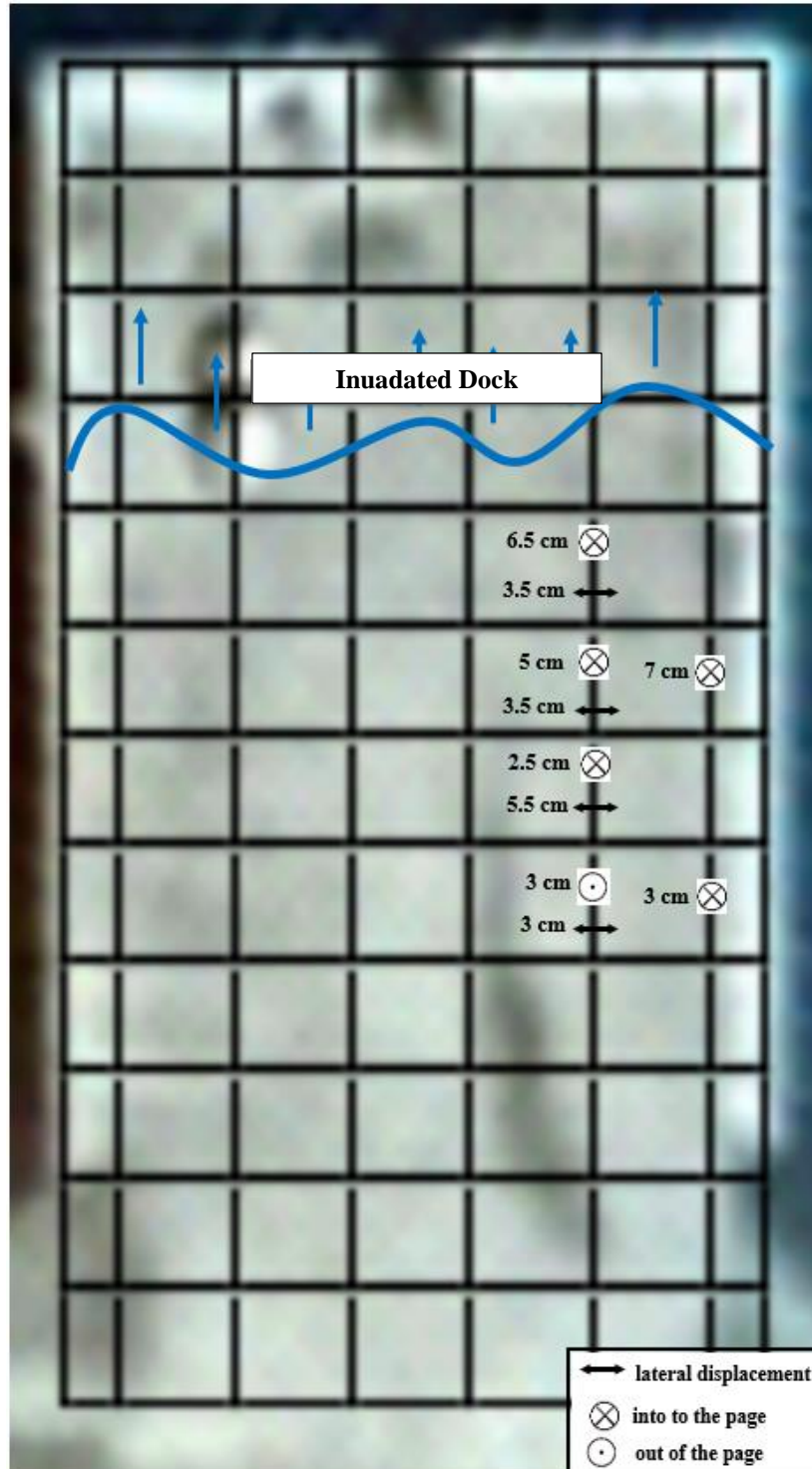


Figure 4.14. Displacements observed on reinforced concrete dock blocks



Figure 4.15. Seismically-induced lateral spreading on the beach of Hazar Lake
($38^{\circ}26'53.7''N$ $39^{\circ}18'54.2''E$ / 31.01.2020 / 12:21 & $38^{\circ}26'50.7''N$ $39^{\circ}18'56.9''E$ / 31.01.2020 / 12:21)



Figure 4.16. Seismically-induced lateral spreading ground deformations mapped on the beach of Hazar Lake
(38°26'50.7"N 39°18'56.7"E / 31.01.2020 / 12:28)



Figure 4.17. Seismically-induced lateral spreading on the beach of Hazar Lake
($38^{\circ}26'48.4''N$ $39^{\circ}18'57.4''E$ / 31.01.2020 / 12:31 & $38^{\circ}26'50.1''N$ $39^{\circ}18'57.2''E$ / 31.01.2020 / 12:54)



Figure 4.18. Another view of seismically-induced lateral spreading cracks
(38°26'50.7"N 39°18'55.4"E / 31.01.2020 / 12:36)



Figure 4.19. Mapping efforts of seismically-induced lateral spreading on the beach of Hazar Lake
($38^{\circ}26'50.0''N$ $39^{\circ}18'57.2''E$ / 31.01.2020 / 13:14)



Figure 4.20. No ground failure on a neighboring beach of Hazar Lake
($38^{\circ}26'48.9''N$ $39^{\circ}18'59.4''E$ / 31.01.2020 / 13:08)



Figure 4.21. No ground failure on a neighboring beach of Hazar Lake
($38^{\circ}26'48.9''N$ $39^{\circ}18'59.4''E$ / 31.01.2020 / 13:08)



3rd stop

A structurally damaged Mosque located in Sivrice is shown in Figure 4.22.

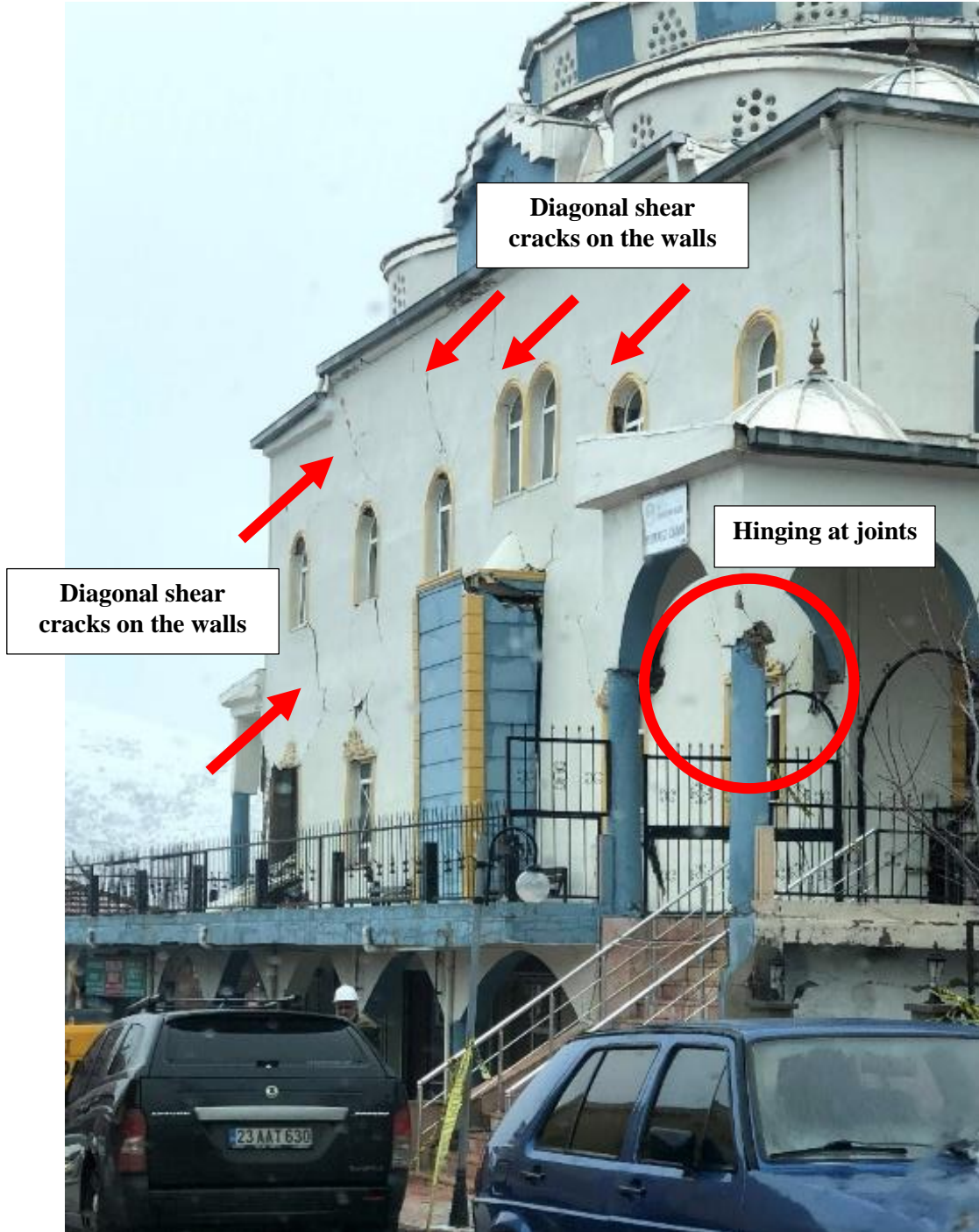


Figure 4.22. A view of a damaged Mosque at Sivrice (Merkez Camii)
($38^{\circ}26'54.2''N$ $39^{\circ}18'34.6''E$ / 31.01.2020 / 13:25)



Moreover, the railway tracks were observed to experience no damage, as shown in Figure 4.23.



Figure 4.23. A view of railway tracks without any damage at Sivrice
(38°26'49.5"N 39°18'33.4"E / 31.01.2020 / 13:29)



Toppled chimneys were observed as presented in Figure 4.24 and Figure 4.25. These failures show the intensity of shaking observed at the site, indicating a Mercalli intensity scale of VIII.



Figure 4.24. Toppled chimneys in Sivrice
(38°26'49.6"N 39°18'32.9"E / 31.01.2020 / 13:29)



Figure 4.25. Topped chimney in Sivrice
(38°26'49.7"N 39°18'33.0"E / 31.01.2020 / 13:30)



4th stop

In the fourth stop, surface geology has changed to volcanic rocks, as shown in Figure 4.26. No ground failure was observed due to earthquake.



Figure 4.26. No signs of ground failure
(38°26'32.0"N 39°19'11.4"E / 31.01.2020 / 13:42 & 38°26'33.2"N 39°19'10.0"E / 31.01.2020 / 13:42 &
38°26'31.9"N 39°19'04.4"E / 31.01.2020 / 13:34)



5th stop

No damage was observed on the railway tunnel. Railway tunnel is open to service and Guney Kurtalan Express Train was serving, as documented in Figures 4.27 and 4.28 along with the coordinates of the pictures taken.



Figure 4.27. A view of the tunnel in Stop 5
(38°26'43.7"N 39°20'40.8"E / 31.01.2020 / 13:54)



Figure 4.28. Guney Kurtalan Express Train passing by
($38^{\circ}26'56.9''N$ $39^{\circ}21'16.7''E$ / 31.01.2020 / 13:59)



The shoreline by the railway tunnel was also visited. The road embankment has relatively steep slopes (nearly 45°); however, no ground failure was observed along this shoreline (Figure 4.29).



Figure 4.29. No failure on the road embankment
($38^\circ 26' 43.7''$ N $39^\circ 20' 40.7''$ E / 31.01.2020 / 13:54)



6th stop

The surficial soil layers are composed of low plasticity clays as shown in Figure 4.30. No signs of ground failure were observed.



Figure 4.30. No ground failure at the 6th stop
(38°27'17.1"N 39°21'49.3"E / 31.01.2020 / 14:03)



7th stop

No ground failure was observed at steep slopes of the 7th stop, as shown in Figure 4.31.



Figure 4.31. No ground failure was observed at the shores of 7th stop
(38°27'31.0"N 39°22'55.9"E / 31.01.2020 / 14:08)



8th stop

Seismically-induced liquefaction failure was observed in the form of sand boils as shown in Figures from 4.32 to 4.38.



Figure 4.32. Sand boil observed in Stop 8
(38°27'49.7"N 39°24'01.1"E / 31.01.2020 / 14:38)



Figure 4.33. Sand boils observed in Stop 8
(38°27'49.8"N 39°24'03.0"E / 31.01.2020 / 14:14)

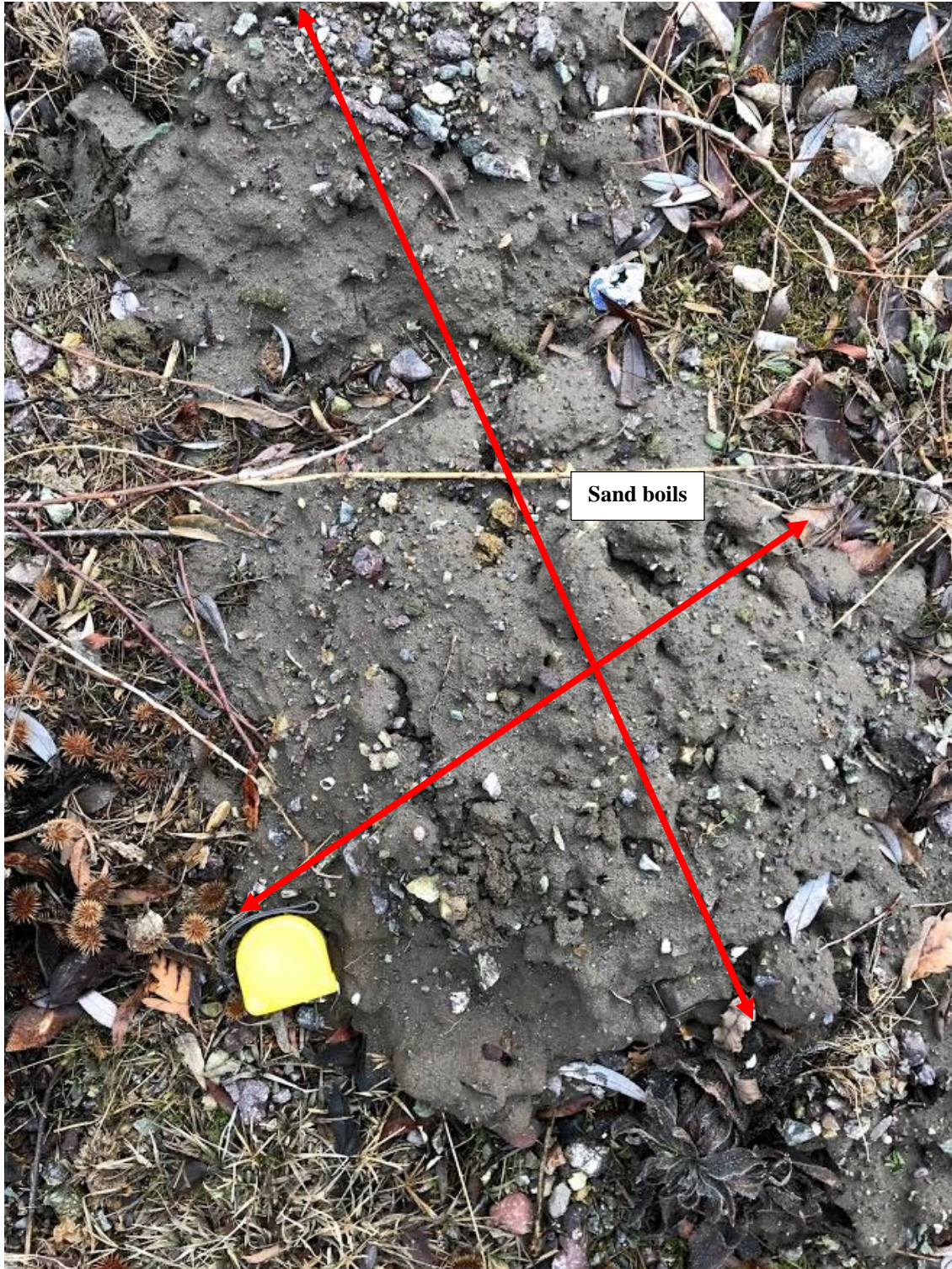


Figure 4.34. Sand boils observed in Stop 8
(38°27'49.9"N 39°24'02.8"E / 31.01.2020 / 14:17)



Figure 4.35. Sandy soil layers observed in Stop 8
(38°27'50.3"N 39°24'02.1"E / 31.01.2020 / 14:21)



Figure 4.36. A line of sand boils observed in Stop 8
($38^{\circ}27'49.7''N$ $39^{\circ}24'03.3''E$ / 31.01.2020 / 14:16)



Figure 4.37. Sand boil observed in Stop 8
(38°27'49.6"N 39°24'01.7"E / 31.01.2020 / 14:38)



Sand boil
Samples were retrieved
from the ejecta

Figure 4.38. Sand boil observed in Stop 8
(38°27'50.1"N 39°24'01.3"E / 31.01.2020 / 14:43)



9th stop

No ground failure was observed at this site, as presented in Figure 4.39.



Figure 4.39. No ground failure was observed at shore of 9th stop
(38°28'22.2"N 39°25'24.9"E / 31.01.2020 / 14:53)



10th stop

A relatively very short (~15 m long) railway tunnel was constructed at the toe of a highly weathered rock steep slope. Tunnel has been possibly designed to eliminate toe excavations, which may trigger slope instability problems. No damage was observed, as also presented in Figures 4.40 to 4.43. Additionally, no slope failure was observed near Hazar Lake, as presented in Figure 4.44.



Figure 4.40. A railway tunnel and rails exhibiting no damage
(38°28'52.8"N 39°27'18.2"E / 31.01.2020 / 15:08)



Figure 4.41. A view of tunnel body at Stop 10
(38°28'53.2"N 39°27'18.4"E / 31.01.2020 / 15:09)



Figure 4.42. Side view of tunnel wall at Stop 10
(38°28'53.2"N 39°27'18.4"E / 31.01.2020 / 15:09)



Figure 4.43. Interbeddings observed in volcanic rocks
(38°28'53.2"N 39°27'17.9"E / 31.01.2020 / 15:08)



Figure 4.44. No ground failure was observed at shore of 10th stop
(38°28'52.6"N 39°27'16.9"E / 31.01.2020 / 15:04)



11th stop

At 11th stop, no ground failure was observed as shown in Figure 4.45.



Figure 4.45. No ground failure was observed at shore of 11th stop
(38°29'37.1"N 39°29'02.3"E / 31.01.2020 / 15:18)



12th stop

Sand boils were observed at 12th stop. These surface manifestations are shown in Figure 4.46.



Figure 4.46. Sand boils observed
(38°29'58.5"N 39°30'24.6"E / 31.01.2020 / 15:29 & 38°29'57.6"N 39°30'23.9"E / 31.01.2020 / 15:30
& 38°29'57.7"N 39°30'24.0"E / 31.01.2020 / 15:30)

13th stop

Rock falls were mapped at 13th stop as shown in Figures 4.47 to 4.51. Approximate dimensions (length, width, height) of the rocks are measured in the field. A simulation of the rock fall mechanism suggested a peak ground velocity of 4-6 m/s at the region as will be discussed later in the report. Fallen rock blocks horizontal distances from the toe of the first bench were measured as 3-5 m. The details of rockfall assessments will be presented later in the report.



Figure 4.47. Rockfall at 13th stop (general view)
(38°31'40.3"N 39°28'02.9"E / 31.01.2020 / 16:20)



Figure 4.48. Rockfall at 13th stop (upper bench)
(38°31'41.5"N 39°27'60.0"E / 31.01.2020 / 16:10)



Figure 4.49. Rockfalls at 13th stop
(38°31'41.0"N 39°27'59.6"E / 31.01.2020 / 16:13)



Figure 4.50. Measurement of rockfalls' dimensions at 13th stop.
(38°31'41.3"N 39°27'59.5"E / 31.01.2020 / 16:15 & 38°31'41.5"N 39°27'59.0"E / 31.01.2020 / 16:16)



Figure 4.51. Rockfalls at 13th stop (Slope angle determination)
(38°31'40.8"N 39°28'00.8"E / 31.01.2020 / 16:20 & 38°31'41.3"N 39°27'59.5"E / 31.01.2020 / 16:17)



14th stop

A 65° slope was documented to be stable as shown in Figures 4.52 and 4.53.



Figure 4.52. Side view of the slope
(38°30'11.7"N 39°23'33.4"E / 31.01.2020 / 16:34 & 38°30'11.8"N 39°23'33.3"E / 31.01.2020 / 16:34)



Figure 4.53. Side view of the slope
($38^{\circ}30'11.6''N$ $39^{\circ}23'33.7''E$ / 31.01.2020 / 16:34)



Fallen rock blocks were also observed and mapped at the 14th stop. Approximate diameter of the rocks varies from 80 cm to 120 cm, and the slope angle was measured as 39° . Figure 4.54 shows the slope and fallen rocks.



Figure 4.54. Rockfalls at 14th stop
($38^\circ30'11.4''N$ $39^\circ23'34.9''E$ / 31.01.2020 / 16:37 & $38^\circ30'11.3''N$ $39^\circ23'34.7''E$ / 31.01.2020 / 16:37)



15th stop

Seismically-induced liquefaction failure was observed in the form of sand boils at the 15th stop. Examples of sand boils in different forms are presented in Figures 4.55 to 4.57. Note that the plane tree leaves were covered by the sand boils in Figure 4.55.



Figure 4.55: Seismic soil liquefaction-induced sand boils at Stop 15
(38°29'32.3"N 39°21'03.8"E / 31.01.2020 / 16:57 & 38°29'34.5"N 39°21'03.6"E / 31.01.2020 / 17:11)



Figure 4.56. Seismic soil liquefaction-induced sand boils
(38°29'32.1"N 39°21'02.0"E / 31.01.2020 / 16:58)



Figure 4.57. Seismic soil liquefaction-induced sand boils
(38°29'34.5"N 39°21'03.7"E / 31.01.2020 / 17:12)



16th stop

At the 16th stop, a complete tour around the lake was completed. We felt lucky to complete our field studies before the start of heavy snow, which covered the surface manifestations immediately.

4.2.2. Day 2: Kamışlık, Fırat River, Malatya and Elazığ, Kapıkaya Dam Sites

In the second day, our plan was to start the reconnaissance studies at Doganyol, where a port failure was observed. Unfortunately, due to heavy snow, the highway to Doğanyol was closed. However, the port failure was documented based on a video shared by Ihlas Press Agency (IHA). Figure 4.58 shows the port failure, which was adapted from the IHA video shared in Youtube.



Figure 4.58. Doğanyol Port Failure adapted from IHA report
(38°33'34.6"N 39°04'10.6"E)



17th stop

2-3 m diameter rocks were fallen freshly on the shoulders of the highway, as shown in Figure 4.59.



Figure 4.59. Fallen rocks on the highway
(38°26'19.8"N 38°49'38.8"E / 01.02.2020 / 7:23)



New Kömürhan Bridge under construction on Fırat River was visited, which experienced no damage as shown in Figure 4.60.



Figure 4.60. New Kömürhan Bridge under construction on Fırat River
(38°26'29.6"N 38°49'10.3"E / 01.02.2020 / 7:25)



18th stop

As stated earlier, in the second day's morning the plan was to go to the Doğanyol village; however, the road accessing to Doğanyol was closed at the hills due to heavy snow storm, as shown in Figure 4.61. The Gendarme prohibited cars traveling beyond this point.



Figure 4.61. Road to Doğanyol
(38°18'39.9"N 38°29'41.7"E / 01.02.2020 / 7:52)



19th stop – Battalgazi Village / Malatya

Damages on a number of non-engineered masonry, and reinforced concrete structures were observed in the Battalgazi village, as shown in Figures 4.62- 4.66. Some of these structures suffered from intensive cracking, partial collapse, whereas some others experienced no evident damage. The minarets of village Mosques were not damaged. Historical monument (Ulu Cami) was also documented to be not damaged. No signs of ground deformation-induced structural failures.



Figure 4.62. Cracks on the wall of a residential building in Battalgazi Village
(38°25'21.7"N 38°21'56.9"E / 01.02.2020 / 8:30 & 38°25'24.4"N 38°21'53.6"E / 01.02.2020 / 8:28)



Figure 4.63. Minaret's of village Mosque
($38^{\circ}25'28.6''N$ $38^{\circ}21'55.5''E$ / 01.02.2020 / 8:41)



Figure 4.64. Separation of two adjacent buildings in Battalgazi Village
($38^{\circ}25'40.4''N$ $38^{\circ}22'02.8''E$ / 01.02.2020 / 8:44 & $38^{\circ}25'35.4''N$ $38^{\circ}22'00.4''E$ / 01.02.2020 / 8:43)



Figure 4.65. No foundation displacements observed at a residential building in Battalgazi Village
(38°25'20.7"N 38°21'59.3"E / 01.02.2020 / 8:31)



Figure 4.66. Historical monument in the Battalgazi Village
(38°25'15.5"N 38°21'59.7"E / 01.02.2020 / 8:32)



20th stop

Railway tracks were observed to be not damaged at the 29th stop. The railway was under service as presented in Figure 4.67. In the same figure a small bridge is shown again with no signs of damage.



Figure 4.67. Railway and bridge at 20th stop
(38°26'00.1"N 38°21'59.1"E / 01.02.2020 / 8:49 & 38°26'00.2"N 38°22'01.3"E / 01.02.2020 / 8:50)



21st stop - Battalgazi Village Bahçelievler District / Malatya

A number of structural damages were observed, mostly concentrating on masonry buildings in Bahçelievler district of Battalgazi village, as shown in Figure 4.68 and 4.69.



Figure 4.68. Residential buildings in the Bahçelievler district of Battalgazi Village
(38°26'51.2"N 38°22'19.2"E / 01.02.2020 / 8:52 & 38°26'51.1"N 38°22'19.2"E / 01.02.2020 / 8:53)



Figure 4.69. Cracks on the wall of a residential building in the Bahçelievler district of Battalgazi Village
(38°27'48.5"N 38°22'50.6"E / 01.02.2020 / 8:56 & 38°27'49.0"N 38°22'51.7"E / 01.02.2020 / 8:56)



22nd stop - Battalgazi Village, Toygar District/ Malatya

Although it is composed of alluvial deposits with potential for ground failure, no signs of it were observed. Surficial soils, observed to be of high plasticity clays, and frozen ground were listed as two factors, which might have impeded possible ground failure, as shown in Figures 4.70 and 4.71.



Figure 4.70. Views of frozen soil in Toygar district of Battalgazi Village
(38°28'38.6"N 38°23'26.4"E / 01.02.2020 / 9:02 & 38°28'38.6"N 38°23'27.1"E / 01.02.2020 / 9:03)



Figure 4.71. Views of frozen clayey soils in Toygar district of Battalgazi Village
($38^{\circ}28'38.9''N$ $38^{\circ}23'27.3''E$ / 01.02.2020 / 9:03 & $38^{\circ}28'39.8''N$ $38^{\circ}23'29.3''E$ / 01.02.2020 / 9:05)



23rd stop

A water canal and the highway bridge were documented with no signs of damage, as shown in Figure 4.72 and Figure 4.73. Note that the observed cracks were dated older, and are not associated with the recent earthquake event.



Figure 4.72. Water trench in Dolamantepe district of Battalgazi Village
(38°26'00.4"N 38°21'44.1"E / 01.02.2020 / 9:25)



Figure 4.73. Dolamantepe district of Battalgazi Village
(38°25'59.9"N 38°21'41.5"E / 01.02.2020 / 9:26)



24th stop

The minaret of village Mosque was not damaged, as shown in Figure 4.74.

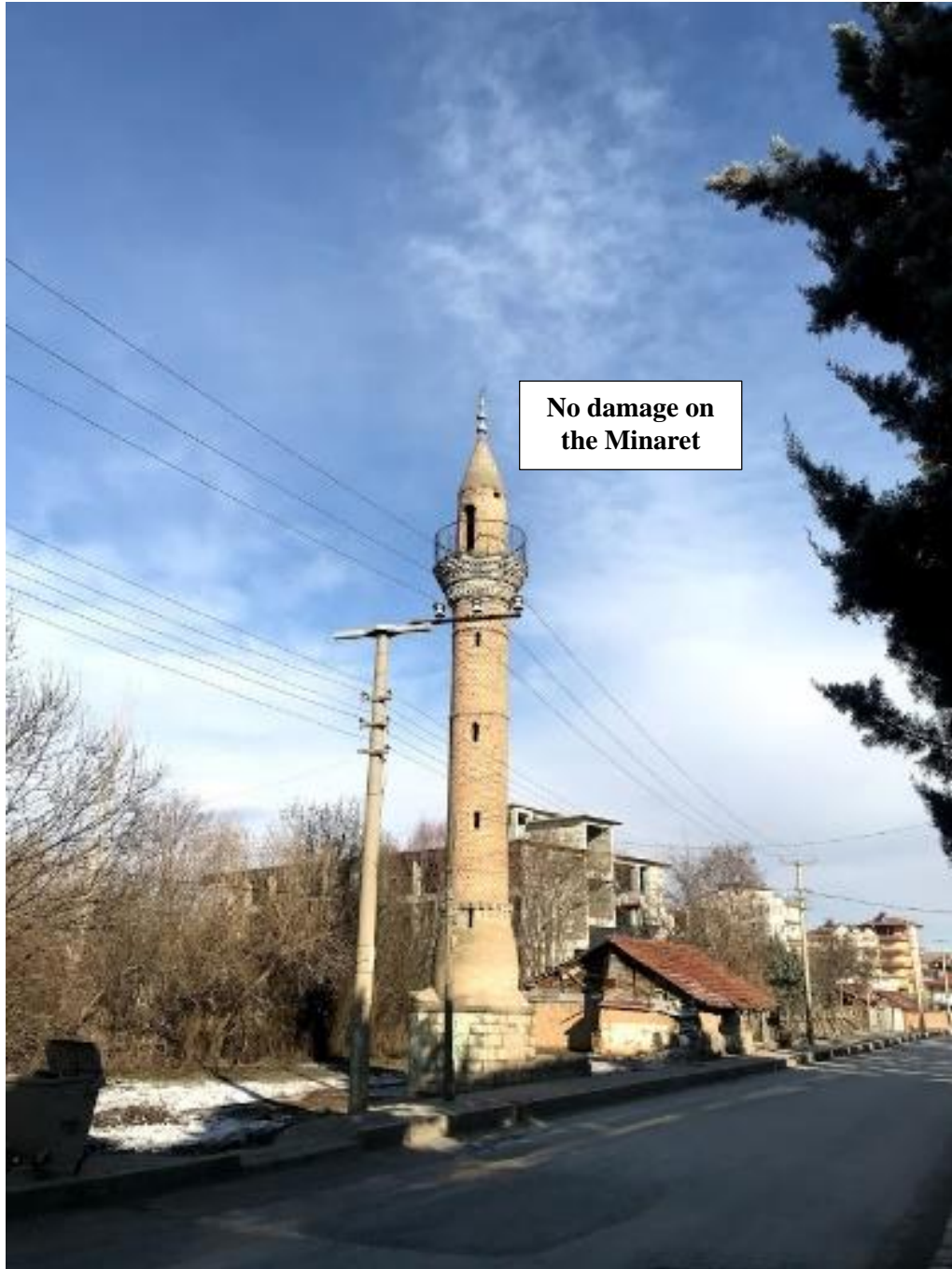


Figure 4.74. Minaret's of a Mosque in the Hanımınçiftliği district of Battalgazi Village
(38°22'39.4"N 38°20'08.7"E / 01.02.2020 / 9:44)



25th stop – Kapıkaya Dam / Malatya

The dam was built on Memikhan River for irrigation purposes. It is an 89.5 m high clay core rockfill dam. The crest and normal water elevations were 868 m and 864.9, respectively. During our visit the water level was measured as 854.70 m. The right and left abutments along with the dam body itself were documented to be not affected from the shaking. Also, no damage to water in-take and spillways were observed. Pictures taken at the dam site can be seen in Figures 4.75 to 4.83.



Figure 4.75. Side views of Kapıkaya Dam
(38°21'19.1"N 38°36'33.9"E / 01.02.2020 / 10:21 & 38°21'16.3"N 38°36'35.0"E / 01.02.2020 / 10:38)



Figure 4.76. Side view of Kapıkaya Dam downstream face
($38^{\circ}21'16.3''N$ $38^{\circ}36'33.2''E$ / 01.02.2020 / 10:40 & $38^{\circ}21'13.1''N$ $38^{\circ}36'26.7''E$ / 01.02.2020 / 10:46)

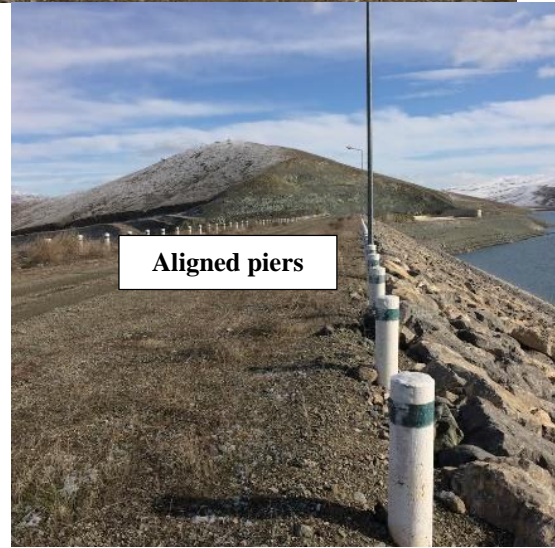


Figure 4.77. Crest view of Kapıkaya Dam
($38^{\circ}21'15.9''N$ $38^{\circ}36'32.8''E$ / 01.02.2020 / 10:40 & $38^{\circ}21'12.6''N$ $38^{\circ}36'26.9''E$ / 01.02.2020 / 10:46 &
 $38^{\circ}21'16.9''N$ $38^{\circ}36'36.0''E$ / 01.02.2020 / 11:13)



Figure 4.78. Water in-take structure of Kapıkaya Dam
(38°21'16.9"N 38°36'36.0"E / 01.02.2020 / 11:13)



Figure 4.79. Spillway of Kapıkaya Dam
(38°21'17.2"N 38°36'36.7"E / 01.02.2020 / 11:14)



Figure 4.80. Spillway of Kapıkaya Dam
(38°21'19.1"N 38°36'33.9"E / 01.02.2020 / 10:22 & 38°21'19.2"N 38°36'34.1"E / 01.02.2020 / 10:22)



Figure 4.81. Abutment slopes of Kapıkaya Dam
($38^{\circ}21'07.1''N$ $38^{\circ}36'22.0''E$ / 01.02.2020 / 10:51)



Figure 4.82. Right abutment natural slopes
($38^{\circ}21'18.7''N$ $38^{\circ}36'36.0''E$ / 01.02.2020 / 10:25)



Figure 4.83. Settlement Plate, piezometer, data acquisition house and inclinometer borehole located at Kapıkaya Dam
(not available / 01.02.2020 / 10:50 & 38°21'11.7"N 38°36'23.5"E / 01.02.2020 / 10:48
38°21'11.1"N 38°36'23.7"E / 01.02.2020 / 10:48 & 38°21'10.2"N 38°36'23.0"E / 01.02.2020 / 11:06)



26th stop - Kale Village / Malatya

Seismically-induced liquefaction failure was observed in the Kale shores (Figure 4.84 and 4.85) in the form of sand boiling at 15th stop. A site view is shown in Figure 4.86. Pictures documenting sand boils are presented in Figures 4.87 to 4.91.



Figure 4.84. View of Kale shore
($38^{\circ}25'25.1''N$ $38^{\circ}45'46.1''E$ / 01.02.2020 / 12:12)



Figure 4.85. Another view of Kale shore
($38^{\circ}25'22.2''N$ $38^{\circ}45'40.9''E$ / 01.02.2020 / 12:17)



Figure 4.86. Kale shore
($38^{\circ}25'15.9''N$ $38^{\circ}45'28.8''E$ / 01.02.2020 / 12:39)

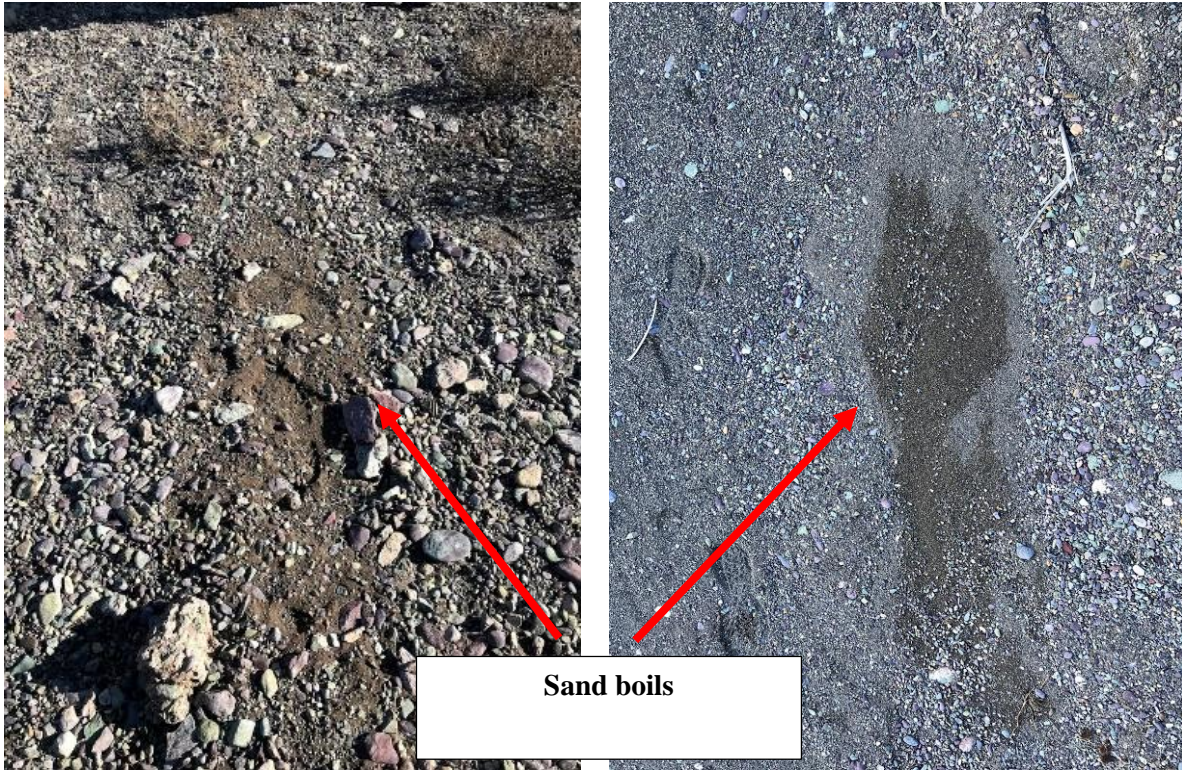


Figure 4.87. Seismic soil liquefaction-induced sand boils at Kale shore
($38^{\circ}25'19.9''N$ $38^{\circ}45'33.2''E$ / 01.02.2020 / 12:25 & $38^{\circ}25'14.6''N$ $38^{\circ}45'24.7''E$ / 01.02.2020 / 12:45)



Figure 4.88. Seismic soil liquefaction-induced sand boils at Kale shore
(38°25'15.2"N 38°45'24.1"E / 01.02.2020 / 12:45)



Figure 4.89. Seismic soil liquefaction-induced sand boils at Kale shore
($38^{\circ}25'22.8''N$ $38^{\circ}45'38.4''E$ / 01.02.2020 / 12:21)



Figure 4.90. Seismic soil liquefaction-induced sand boils at Kale shore
($38^{\circ}25'19.9''N$ $38^{\circ}45'32.1''E$ / 01.02.2020 / 12:27)



Figure 4.91. Seismic soil liquefaction-induced sand boils at Kale shore
($38^{\circ}25'15.2''N$ $38^{\circ}45'32.2''E$ / 01.02.2020 / 12:32 & $38^{\circ}25'15.2''N$ $38^{\circ}45'23.9''E$ / 01.02.2020 / 12:45)

27th stop

Our intent was to access to Çevrimtaş, the epicentral district. However, the road was closed to traffic due to heavy snow. (Figure 4.92). It was decided to spend the rest of the reconnaissance time in Elazığ downtown.



Figure 4.92. Snow-covered road on our way to Çevrimtaş
($38^{\circ}25'26.3''N$ $39^{\circ}03'01.3''E$ / 01.02.2020 / 13:52)



28th stop – Abdullah Paşa District / Elazığ

A number of structurally damaged residential buildings were documented in Abdullah Paşa district of Elazığ city center, as shown in Figures 4.93 to 4.100. The level of damage varies in a large scale, from no damage to heavy damage. No signs of foundation failures were observed except a few rare cases of volumetric settlements of foundation backfill soils.



Figure 4.93. Tents for the people suffering from the earthquake
(38°39'30.0"N 39°08'59.5"E / 01.02.2020 / 14:28)



Figure 4.94. Volumetric settlement at the foundation of a residential building
(38°39'29.8"N 39°08'58.4"E / 01.02.2020 / 14:29 & 38°39'28.9"N 39°09'01.9"E / 01.02.2020 / 14:30)

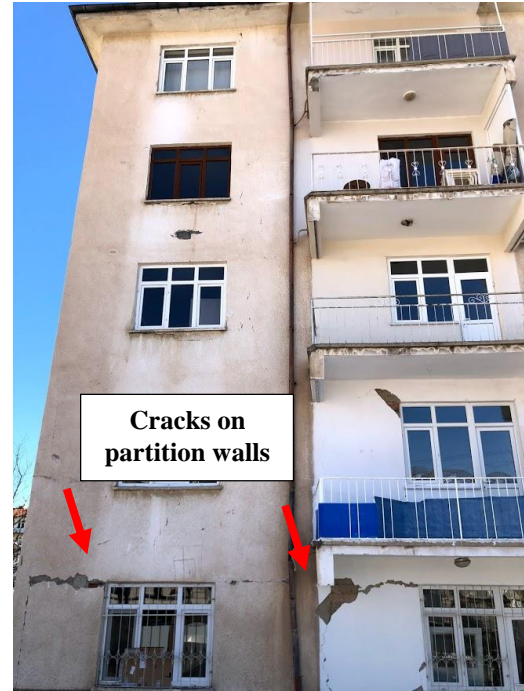


Figure 4.95. Residential buildings located at the Abdullah Paşa district of Elazığ city center ($38^{\circ}39'29.3''N$ $39^{\circ}09'02.6''E$ / 01.02.2020 / 14:32 & $38^{\circ}39'29.6''N$ $39^{\circ}08'59.0''E$ / 01.02.2020 / 14:28)



Figure 4.96. Cracks observed at the entrance of Eğitim Apartment. ($38^{\circ}39'29.2''N$ $39^{\circ}09'01.6''E$ / 01.02.2020 / 14:31 & $38^{\circ}39'32.0''N$ $39^{\circ}09'00.8''E$ / 01.02.2020 / 14:36)



Figure 4.97. A residential building located in the Abdullah Paşa district of Elazığ city center ($38^{\circ}39'25.2''N$ $39^{\circ}09'10.3''E$ / 01.02.2020 / 14:45)



Figure 4.98. Cracking observed at the entrance of the of a residential building ($38^{\circ}39'21.9''N$ $39^{\circ}09'10.4''E$ / 01.02.2020 / 14:50)



Figure 4.99. Cracks at the first floor, and fallen bricks
($38^{\circ}39'31.9''N$ $39^{\circ}08'57.9''E$ / 01.02.2020 / 14:38 & $38^{\circ}39'32.0''N$ $39^{\circ}09'01.3''E$ / 01.02.2020 / 14:39)

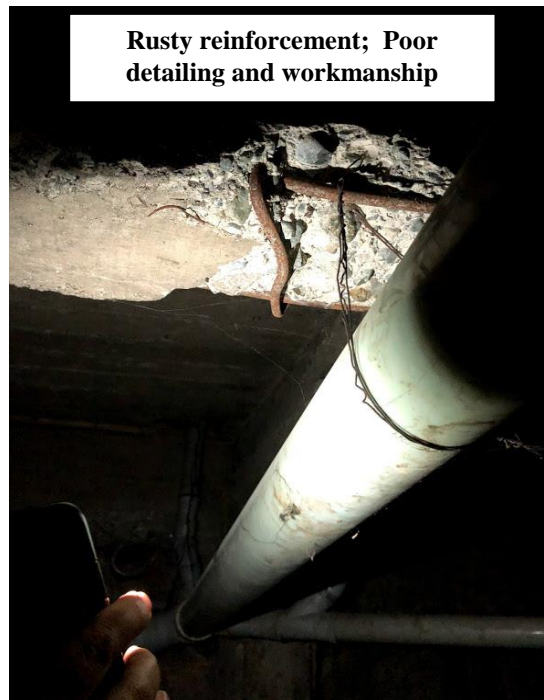


Figure 4.100. View of the basement of a residential building, rusty reinforcement bars, poor detailing and construction
($38^{\circ}39'24.8''N$ $39^{\circ}09'10.7''E$ / 01.02.2020 / 14:48)



29th stop

Elazığ ground motion station located at the Ministry of Environment and Urban Planning was visited (Figure 4.101).

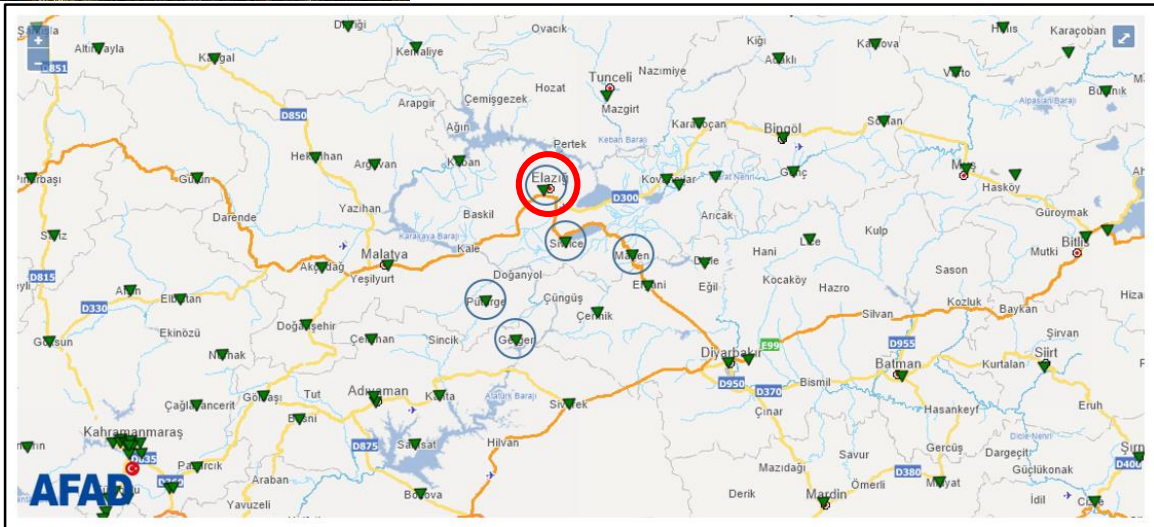


Figure 4.101. Elazığ ground motion station

($38^{\circ}40'13.2''N$ $39^{\circ}11'31.3''E$ / 01.02.2020 / 15:08 & $38^{\circ}40'13.5''N$ $39^{\circ}11'31.6''E$ / 01.02.2020 / 15:09)

30th stop - Sürsürü District / Elazığ

The most of the structural damage was concentrated in Elazığ-Sürsürü district. Several structurally damaged residential buildings were documented, as shown in Figures 4.102 to 4.106. The level of damage varies in a large scale, from no damage to heavy damage. Cracks at the pavements, walls and foundations, due to cyclic and residual lateral and volumetric deformations were observed.

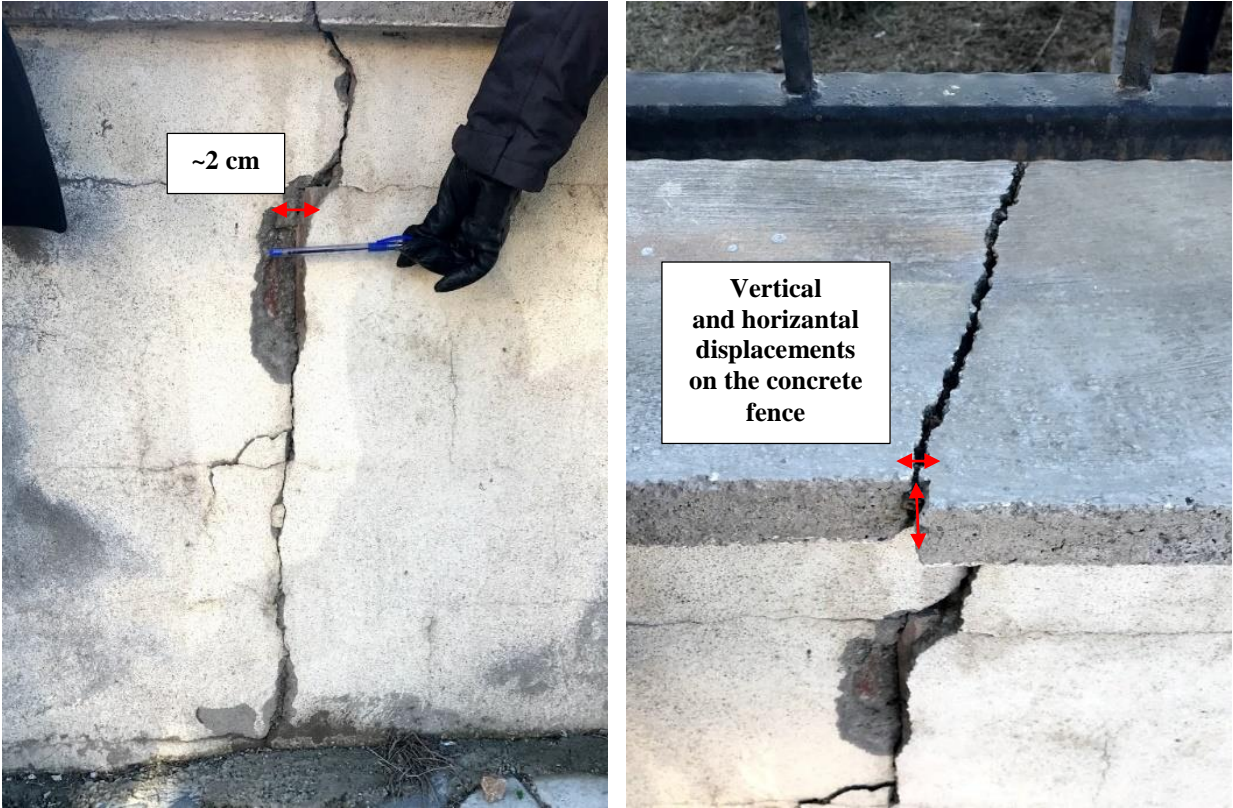


Figure 4.102. A crack on a concrete fence in Sürsürü district of Elazığ city center
(38°40'05.5"N 39°11'12.4"E / 01.02.2020 / 15:28 & 38°40'05.5"N 39°11'12.4"E / 01.02.2020 / 15:28)



Figure 4.103. Settlement mapped at the entrance of some buildings
($38^{\circ}40'04.7''N$ $39^{\circ}11'12.4''E$ / 01.02.2020 / 15:31 & $38^{\circ}40'05.9''N$ $39^{\circ}11'08.2''E$ / 01.02.2020 / 15:41
 $38^{\circ}40'05.9''N$ $39^{\circ}11'08.1''E$ / 01.02.2020 / 15:41 & $38^{\circ}40'04.7''N$ $39^{\circ}11'09.7''E$ / 01.02.2020 / 15:40)



Figure 4.104. Settlements observed
($38^{\circ}40'05.7''N$ $39^{\circ}11'09.6''E$ / 01.02.2020 / 15:57 & $38^{\circ}40'05.1''N$ $39^{\circ}11'10.0''E$ / 01.02.2020 / 15:57)



Figure 4.105. Settlement observed.
($38^{\circ}40'07.0''N$ $39^{\circ}11'04.8''E$ / 01.02.2020 / 15:47)

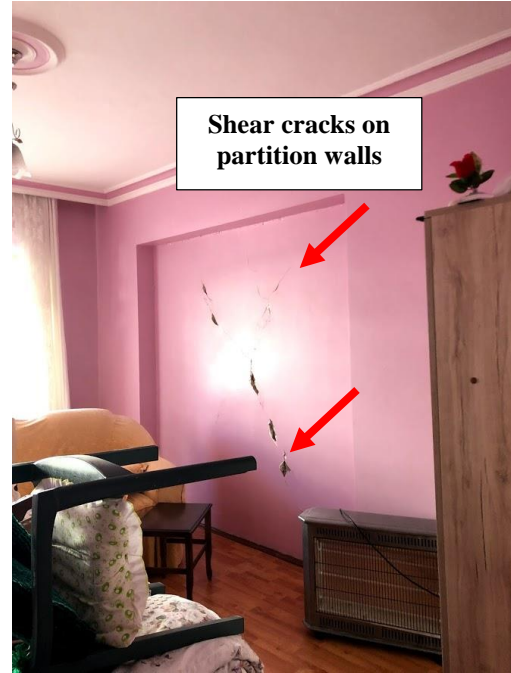
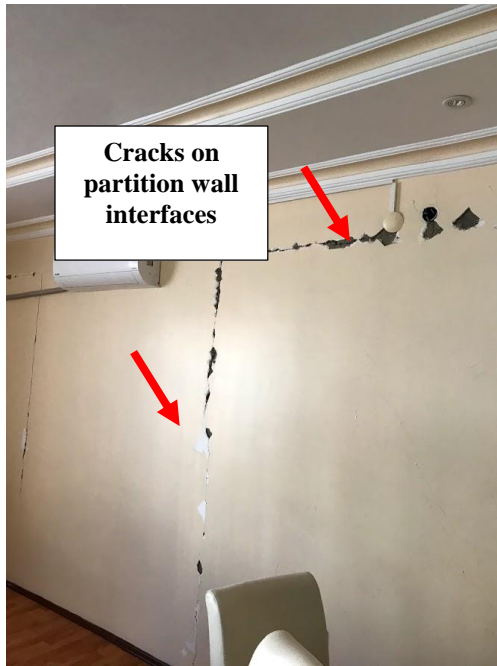


Figure 4.106. Cracks on partition walls

($38^{\circ}40'03.9''N$ $39^{\circ}11'13.5''E$ / 01.02.2020 / 15:35 & $38^{\circ}40'04.2''N$ $39^{\circ}11'14.2''E$ / 01.02.2020 / 15:36)

During the site visit, a site investigation study was witnessed. A soil sample was taken from the borehole for laboratory testing. An automatic SPT trip hammer was used as shown Figure 4.107. The available borelog up to the depth of 12 m was retrieved.



Figure 4.107. Drilling efforts

($38^{\circ}40'03.9''N$ $39^{\circ}11'14.8''E$ / 01.02.2020 / 15:18 & $38^{\circ}40'03.1''N$ $39^{\circ}11'16.1''E$ / 01.02.2020 / 15:18)



31st stop

The minaret of Rüstem Paşa Yol Üstü Mosque was damaged after the earthquake, as shown in Figure 4.108.

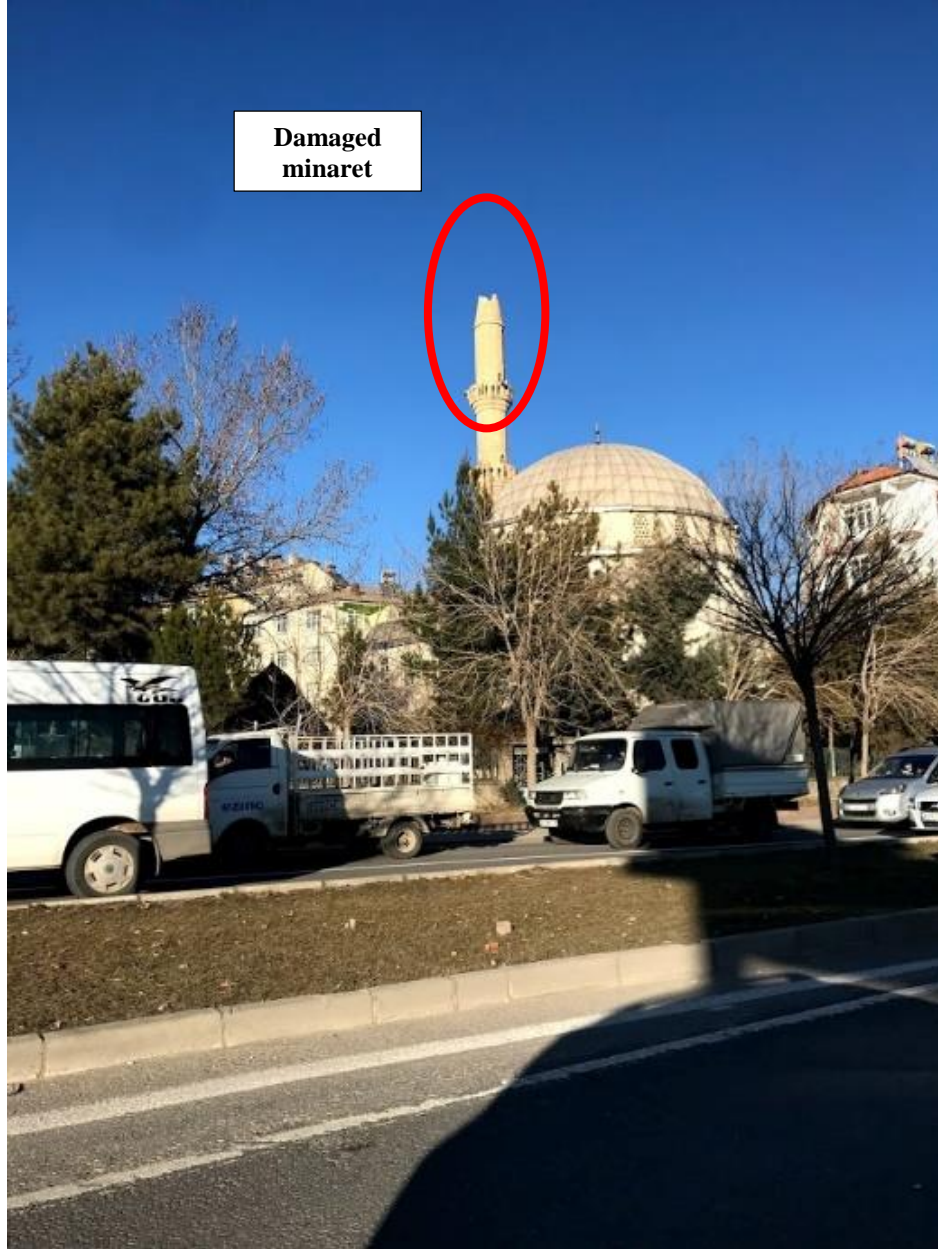


Figure 4.108. Damaged Minaret of Rüstem Paşa Yol Üstü Mosque
in Rüstem Paşa district of Elazığ city center
(38°39'58.4"N 39°13'54.7"E / 01.02.2020 / 16:22)



32nd stop - Mustafa Paşa District / Elazığ

A few structurally damaged residential buildings were documented in Mustafa Paşa district of Elazığ city center, as shown in Figure 4.109. Some of the structures had suffered from intensive cracking (Figure 4.109), partial collapse, whereas some others experienced no evident damage. A highly damaged building was demolished on February 1st 2020, as shown in Figure 4.110.

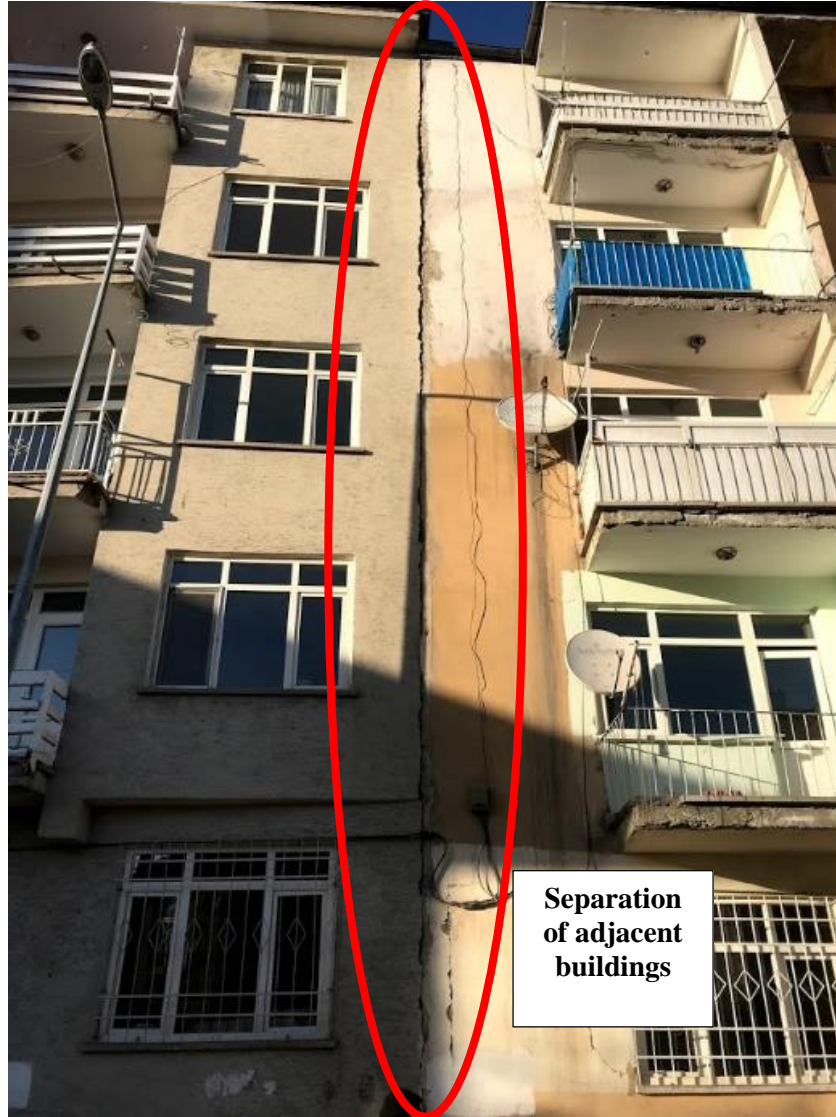


Figure 4.109. Longitudinal cracks observed on a building located in the Mustafa Paşa district ($38^{\circ}40'15.9''N$ $39^{\circ}13'59.9''E$ / 01.02.2020 / 16:34)



Figure 4.110. Demolishment of a heavily-damaged building in the Mustafa Paşa district of
Elazığ city center
(38°40'15.2"N 39°13'57.5"E / 01.02.2020 / 16:31)

4.3. Rockfalls

Field reconnaissance team observed rockfalls during their visit to the coast of Hazar Lake as shown in Figure 4.111 and 4.112. In this section, a more detailed discussion of these rockfalls will be presented.

At the first rockfall site, the surface geology reveals phyllyites with schistosity texture. The cross section is 15 m high with a slope of 50° . The dimensions of the fallen rocks and the distance from the edge of the benches are mapped in the field. No fallen rocks were observed on the lower, second bench of the highway cut. Slope angle, length and height of different sections of the upper and lower benches, and possible height that rock falls were initiated were also mapped in the field. RocFall 2019 software program is used to guesstimate the initial velocity of the rock.



Figure 4.111. Rock falls observed at the shores of Hazar Lake at 13th stop
($38^\circ 31' 40.0''\text{N}$ $39^\circ 28' 01.5''\text{E}$ / 31.01. 2020 / 16:08)



Figure 4.112. Cross section of the rockfall at 13th stop
($38^\circ 31' 40.3''\text{N}$ $39^\circ 28' 02.9''\text{E}$ / 31.01.2020 / 16:20)



The dimensions of the some fallen rock blocks and the distance of these rocks to the toe of the upper bench are recorded in the field as also summarized in Table 4-1.

Table 4-1. Fallen rock blocks measurements recorded at 13th stop
(38.528061, 39.466550)

Length (cm)	Height (cm)	Width (cm)	Distance of the rock blocks to the toe of the slope (m)
60	30	35	3.9
32	15	30	5
55	30	28	3.2

As seen in Figure 4.113, back analysis is performed to guess the initial velocity of the rock blocks to reach their final positions observed in the field. RocFall 2019 by RocScience is used for the purpose. Based on these very preliminary assessments, velocity range to trigger the fall and match with observed travel distances is calculated as 4 to 6 m/s.

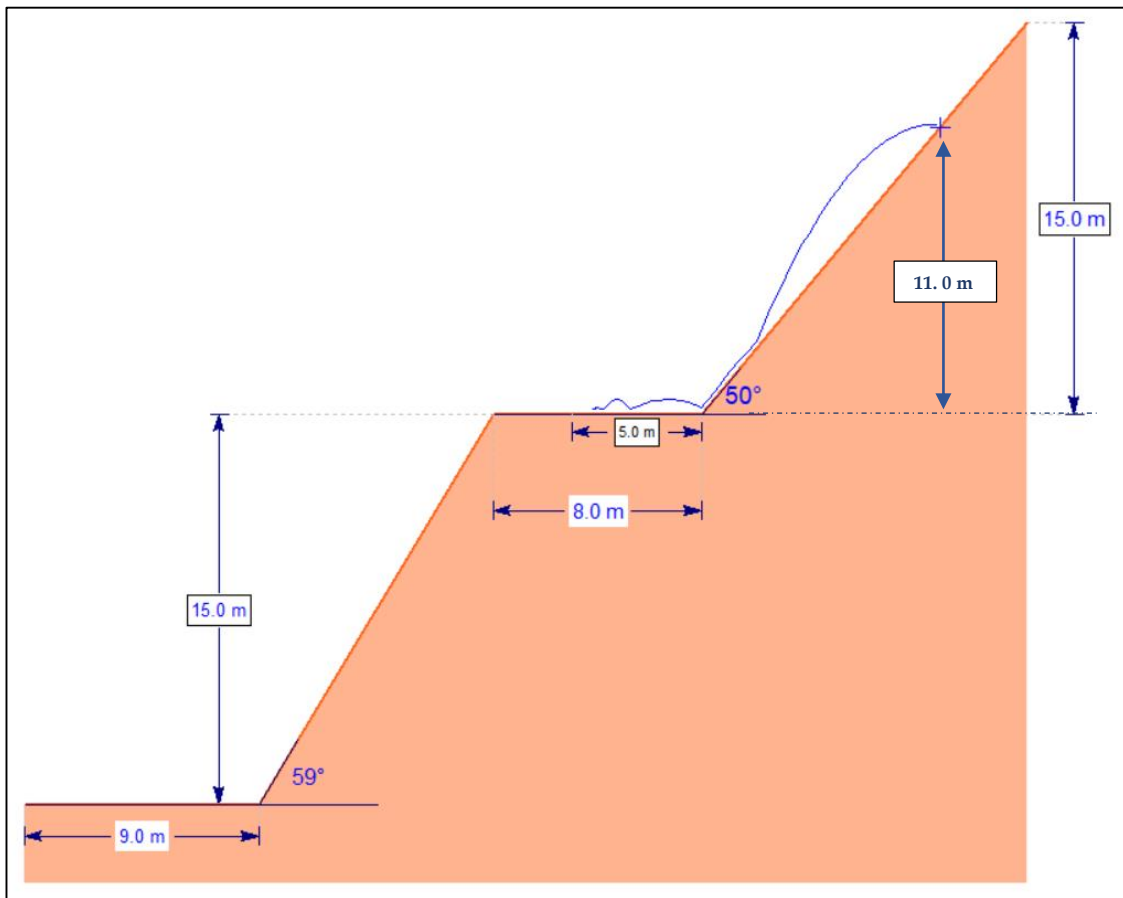


Figure 4.113. Back analysis of rockfall with RocFall 2019



4.4. Earth Structures

4.4.1. Hydraulic Dams

In the vicinity of Elazığ-Malatya region, there exist 6 dams: Dedeyolu, Karakaya, Cip, Kapıkaya (Turgut Özal), Keban and Boztepe (Recai Kutan) Dams. It was reported by personal communication that a group of engineers from General Directorate of State Hydraulics Works (DSİ) have performed reconnaissance studies immediate upon Sivrice Earthquake. Some characteristics regarding these dams are summarized in Table 4-2 as provided by DSİ.

Table 4-2. Inspected dams by DSİ reconnaissance team after Sivrice Earthquake

Inspected dams	Height (m)	Dam type	Distance to zone of energy release (km)
Dedeyolu Dam	35.7	Homogenous earthfill	15.5
Karakaya Dam	173	Concrete arch	17.0
Cip Dam	24	Center clay core earthfill	33.6
Kapıkaya Turgut Özal Dam	89.5	Center clay core rockfill	43.3
Keban Dam	207	Combined rockfill and concrete gravity	56.5
Boztepe Recai Kutan Dam	82	Clay core sand+gravel+rockfill	90.0

General layouts and typical cross sections of the Karakaya, Dedeyolu, Karakaya, Cip, Kapıkaya Turgut Özal, Keban and Boztepe Recai Kutan Dams are shown in Figures 4.114 to 4.118.



Amacı : Sulama		Purpose : Irrigation	
Baraj ve gölü		Dam and reservoir	
Tipi	: Toprak dolgu	Type	: Earthfill
Gövde hacmi	: 446 000 m ³	Dam volume	: 446 000 m ³
Kret kotu	: 1 008,00 m	Crest elevation	: 1 008,00 m
Kret uzunluğu	: 1 024,40 m	Crest length	: 1 024,40 m
Temelden yükseklik	: 24,00 m	Height from foundation	: 24,00 m
Talvegden yükseklik	: 23,00 m	Height from river bed	: 23,00 m
Temel jeolojik yapısı	: Kilitaşı, pliosen	Geological formation of foundation	: Claystone, pliosen
Maksimum su kotu	: 1 006,50 m	Maximum water surface elevation	: 1 006,50 m
Normal su kotu	: 1 004,50 m	Normal water surface elevation	: 1 004,50 m
Normal su kotunda göl hacmi	: 7,00 hm ³	Reservoir volume at normal water surface elevation	: 7,00 hm ³
Normal su kotunda göl alanı	: 1,10 km ²	Reservoir area at normal water surface elevation	: 1,10 km ²
Dolusovak		Spillway	
Tipi	: Karşıdan alışı, kapaksız	Type	: Frontal type, ungated
Kret kotu	: 1 004,50 m	Crest elevation	: 1 004,50 m
Kret uzunluğu	: 110,00 m	Crest length	: 110,00 m
Proje taşkın piki	: 690 m ³ /s	Design flood peak flow	: 690 m ³ /s
Maksimum deşarj	:	Maximum discharge	:
Santral		Power Plant	
Ünite adedi	: —	Number of units	: —
Ünite gücü	: —	Unit capacity	: —
Kurulu güç	: —	Installed capacity	: —
Yıllık enerji üretimi	: —	Annual energy generation	: —
Sulama alanı	: 1 100 ha	Irrigation area	: 1 100 ha
Taşkın kontrol alanı	: —	Flood control area	: —
Yıllık içmesuyu	: —	Annual domestic water	: —
İnşaat : İnşaatına 1965 yılında başlanılmış ve 1965 yılında tamamlanmıştır.		Construction : The construction was started in 1965 and completed in 1965	

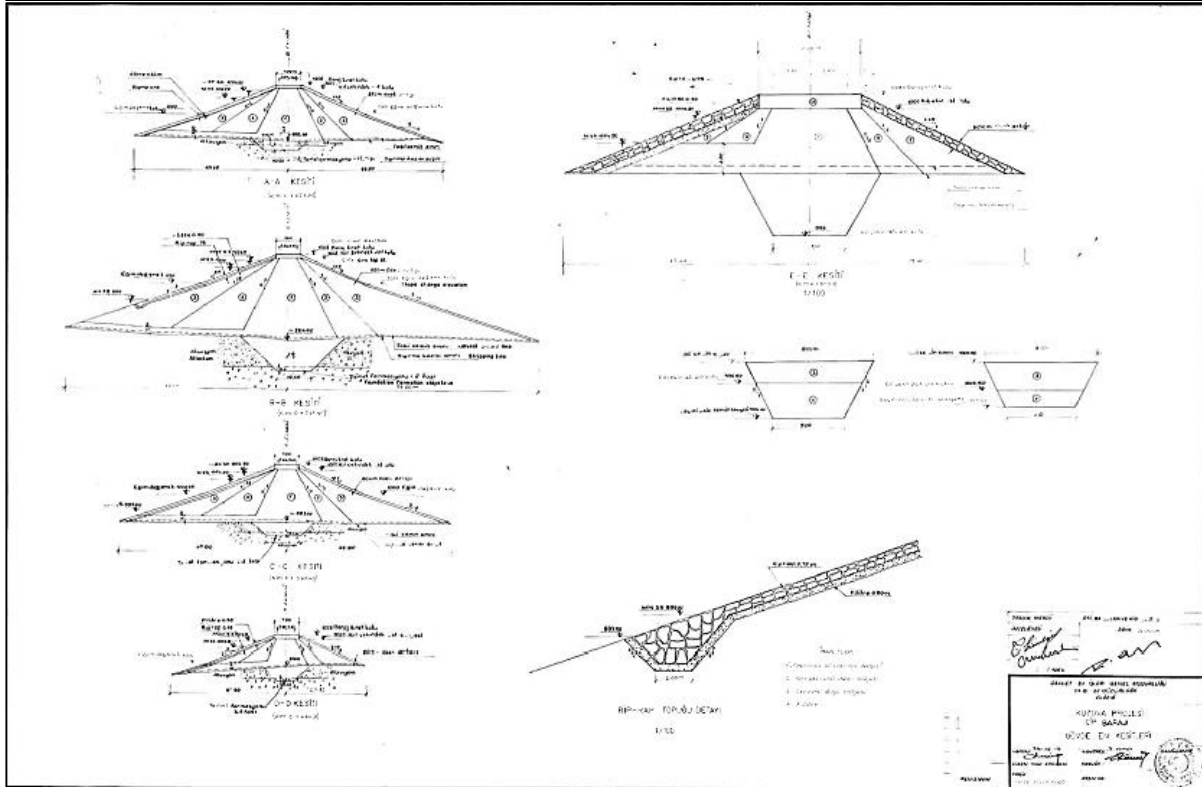


Figure 4.115. Cip Dam (DSİ)

As briefly discussed earlier, Kapıkaya Dam was visited during the 2nd day of reconnaissance studies. The upstream and downstream slopes of the dam, as well as abutments, inlet, spillway, dam body and crest were investigated in detail. No damage was observed at Kapıkaya Dam. Picture taken at Kapıkaya dam site were presented in Chapter 4.2.2, and will not be repeated again.

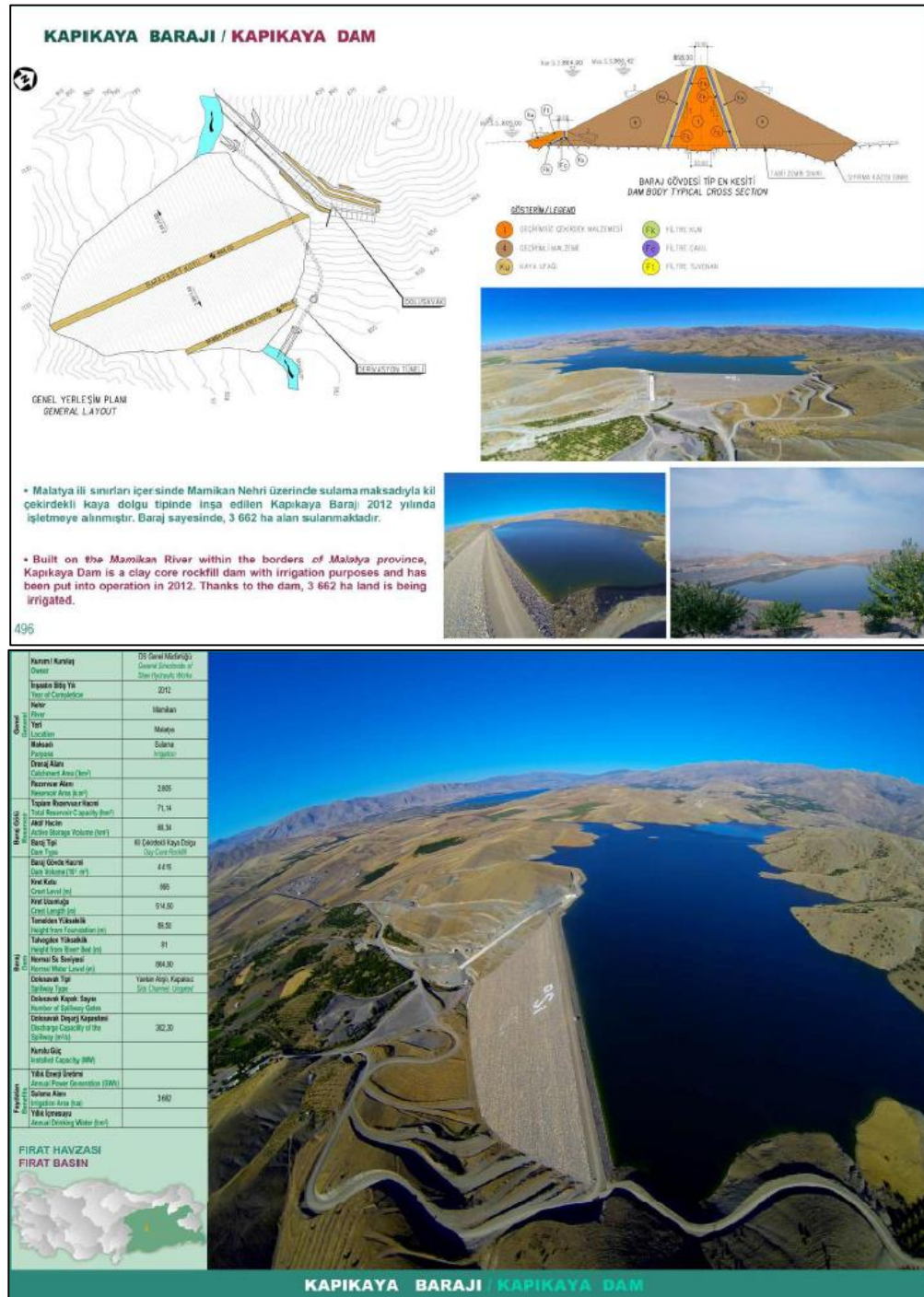
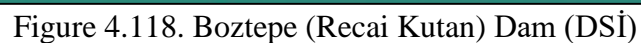


Figure 4.116. Kapıkaya Dam (DSİ)





On the basis of reconnaissance studies performed by Dam Agency, no significant damage was reported to be observed at these dams after Sivrice Earthquake, except a limited extent longitudinal < 8 mm crack, as shown in Figure 4.119, observed on the crest of Dedeyolu Dam.



Figure 4.119. Longitudinal cracks on Dedeyolu Dam crest (DSİ)



4.5. Railways

Based on Turkish Railway Authority (TCDD) database, two main railways passing through the East Anatolian Fault Zone were identified: i) Malatya-Elazığ (Van-Gölü) and ii) Malatya-Diyarbakır (Güney Kurtalan) Express Trains. Their routes are shown in Figure 4.120.

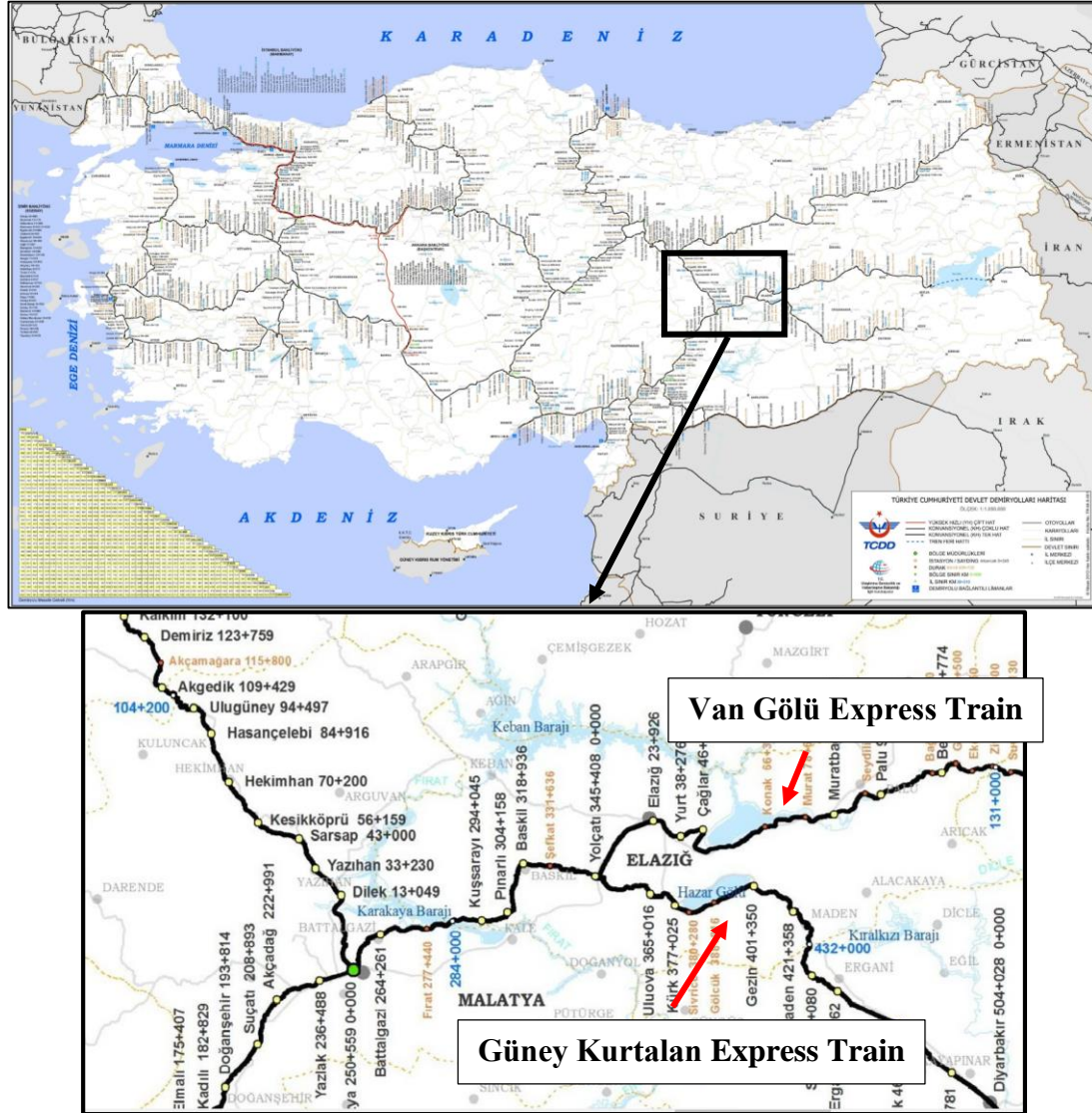


Figure 4.120. Turkish railway route map and the routes of Van Gölü and Güney Kurtalan Express Trains

As also briefly discussed earlier in Sections 4.2.1 and 4.2.2, no signs of track deformations or displacements were observed. As confirmed by the local railway authority, the railway system is in immediate service after the earthquake. A press news regarding a continuously monitored railway tunnel which cuts Eastern Anatolian Fault is shared below:

“Approximately three years ago, researchers from Yıldız Technical University discovered a railway tunnel built in the 1950s, located 50 m below the historical city in Palu, Elazığ. The tunnel was directly cut by the Eastern Anatolian Fault so the tunnel is used as a monitoring station for EAF. Two creepmeters are placed on this tunnel to monitor the fault rupture and creep behavior of the EAF. 25 GPS stations were placed on the tunnel to retrieve the satellite information of the area and the tunnel was modeled in 3D with the help of laser scanner. According to the researchers’ observation, there were no heavy damage on the Palu tunnel after the mainshock, however minor cracks were observed at the location of the East Anatolian Fault. It is advised that the tunnel should be monitored regularly, and some precautions should be taken for future events.”

4.6. Seismic Soil Liquefaction and Lateral Spreading Cases Observed in Hazar Lake and Karakaya Dam Reservoir Shores

As discussed earlier, surface manifestations of seismic soil liquefaction triggering were observed in the form of lateral spreading and sand boils along the shoreline of Hazar Lake, Fırat River and Karakaya Dam Reservoir shores. Research team investigated the Hazar Lake shores during day 1 and Fırat River during day 2 of the reconnaissance studies.

By the natural shores of Hazar Lake, seismically-induced lateral spreading, sand boils and excessive volumetric settlements were observed. A map, summarizing consolidated field observations along the shores of Hazar Lake is shown in Figure 4.121. In Figure 4.121, green pins indicate non-liquefied sites, red pins indicate sites with surface deformations along with abbreviations of type of ground failure; RF: Rock fall, LS: Lateral spread, VS: Volumetric settlement, SB: Sand Boil.



Figure 4.121. A summary of ground failure observations along the shores of Hazar Lake (Green pins indicate Non-Liquefied sites, Red pins indicate sites with surface deformations, RF: Rock fall, LS: Lateral spread, VS: Volumetric settlement, SB: Sand Boil)

By Kale Village, at the shores of Fırat River, surface manifestations of seismic soil liquefaction in the form of sand boils were observed. A map, summarizing consolidated field observations along the shores of Fırat River is shown in Figure 4.122.



Figure 4.122. A summary of ground failure observations along the shores of Fırat River and Malatya-Elazığ Route

(Green pins indicate Non-Liquefied sites, Red pins indicate sites with surface deformations, RF: Rock fall, LS: Lateral spread, VS: Volumetric settlement, SB: Sand Boil)

In day 1, surface manifestation of soil liquefaction in the form of sand boils and lateral spreading were mapped. The extent of lateral deformations was mapped as 3-5 cm along a 90 m long and 23 m wide zone at the second stop in the vicinity of Sivrice Dock, as shown in Figure 4.123. Figures 4.124 and 4.125 present the photos of lateral spreading site taken during field investigations.

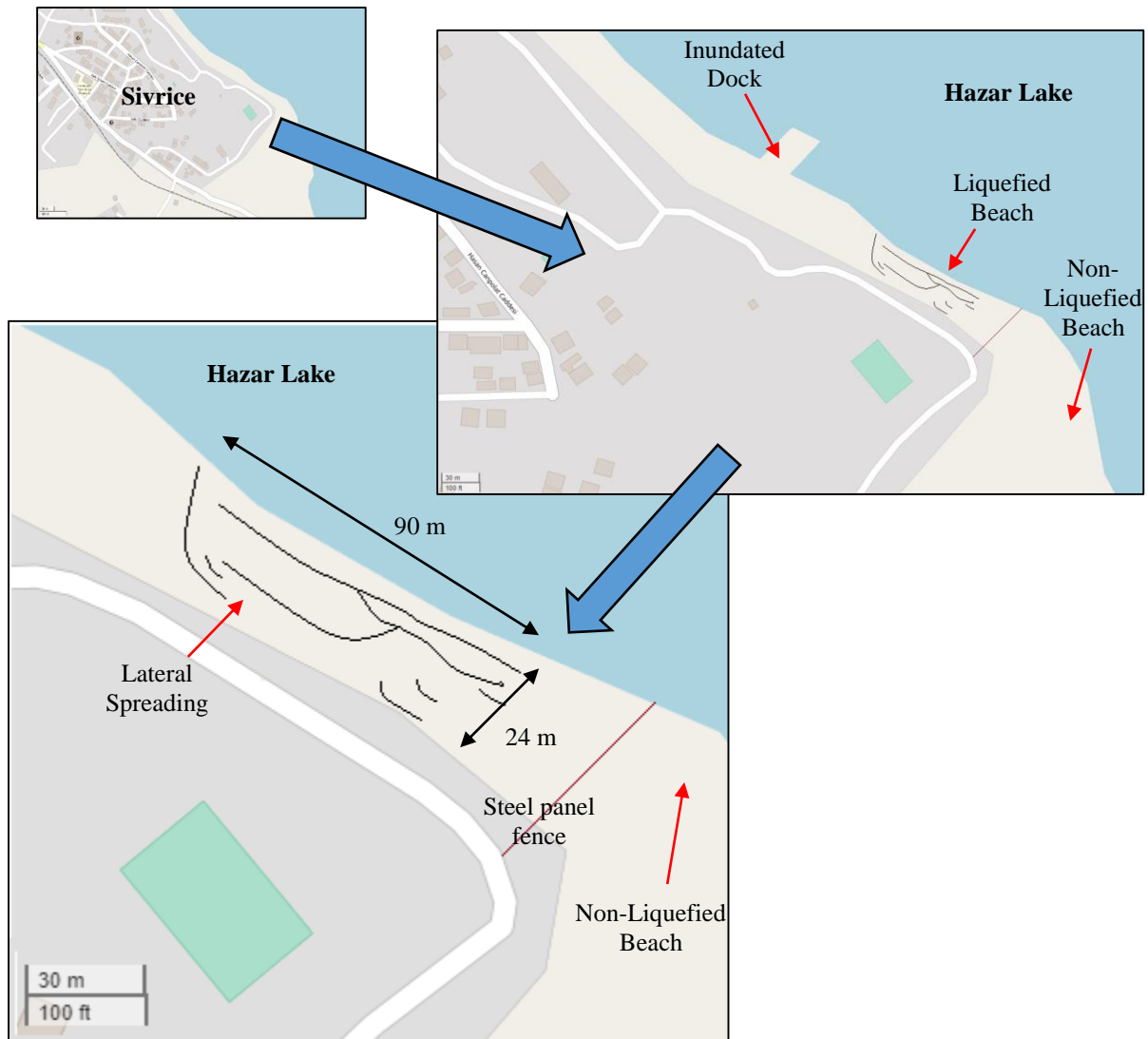


Figure 4.123. A sketch of lateral spread deformations at 2nd stop
(Sivrice Dock-38°28'10.0"N 39°17'03.6"E / 31.01.2020 / 12:11)



Figure 4.124. Deformations and cracks due to lateral spreading observed along
Hazar Lake (2nd stop)
($38^{\circ}26'50.7''N$ $39^{\circ}18'56.9''E$ / 31.01.2020 / 12:21 & $38^{\circ}26'50.5''N$ $39^{\circ}18'56.9''E$ / 31.01.2020 / 12:28)



Figure 4.125. Deformations and cracks due to lateral spreading observed along
Hazar Lake (2nd stop)
($38^{\circ}26'50.8''N$ $39^{\circ}18'55.6''E$ / 31.01.2020 / 12:34 & $38^{\circ}26'50.3''N$ $39^{\circ}18'57.1''E$ / 31.01.2020 / 12:27)

No signs of liquefaction were observed at a natural beach neighboring the lateral spreading site as shown in Figure 4.126. This beach was observed to have a milder slope when compared to the lateral spreading site shown in Figures 4.123-4.125.



Figure 4.126. No ground failure at the natural beach neighboring the lateral spreading
(2nd stop)
(338°26'48.9"N 39°18'59.4"E / 31.01.2020 / 13:08 & 38°27'58.0"N 39°20'42.4"E / 31.01.2020 / 13:08)

Ground deformations were observed due to liquefaction at 8th and 15th stops along Hazar Lake as shown in Figures 4.127 and 4.128. Sand boils were mapped and soil samples were retrieved from these locations. A series of sieve analysis tests has been performed at METU Soil Mechanics Laboratory. Based on the results of these tests, samples were reported to be potentially liquefiable as also will be discussed in the next section.



Figure 4.127. Surface manifestations of soil liquefaction in Hazar Lake (8th stop)
(38°27'49.7"N 39°24'03.3"E / 31.01.2020 / 14:16 & 38°27'50.0"N 39°24'02.5"E / 31.01.2020 / 14:20)



Figure 4.128. Surface manifestations of soil liquefaction in Hazar Lake (15th stop)
(38°29'34.6"N 39°21'03.7"E / 31.01.2020 / 17:11 & 38°29'30.6"N 39°20'57.7"E / 31.01.2020 / 17:01)

In day 2, surface manifestation of soil liquefaction in the form of sand boils were mapped along Kale shores. Figures 4.129 and 4.130 present the photos of the sand boils taken at the shores of Kale Village.



Figure 4.129. Surface manifestation of soil liquefaction at Kale Village shores (26th stop)
(38°25'23.6"N 38°45'39.0"E / 01.02.2020 / 12:18)



Figure 4.130. Surface manifestation of soil liquefaction at Kale Village shores
(26th stop)
(38°25'20.2"N 38°45'33.2"E / 01.02.2020 / 12:25)

Disturbed samples were taken from the surface of the liquefied areas. The locations of sites from where 6 samples (Hazar Lake) and 4 samples (Kale Village) were taken, are shown in Figure 4.131 and 4.132. A map showing these locations are also presented in Figure 4.133. These samples were tested at METU Soil Mechanics Laboratory to determine the soil-type, grain size and consistency characteristics. The results are comparatively presented with the particle size distribution ranges common for potentially liquefiable soils (Tsuchida, 1970), as given in Figure 4.134. Sieve analysis test results are summarized in Table 4-3. Based on USCS, most of the samples retrieved from sand boils were classified as SP (poorly graded sand) and SM (silty sand).

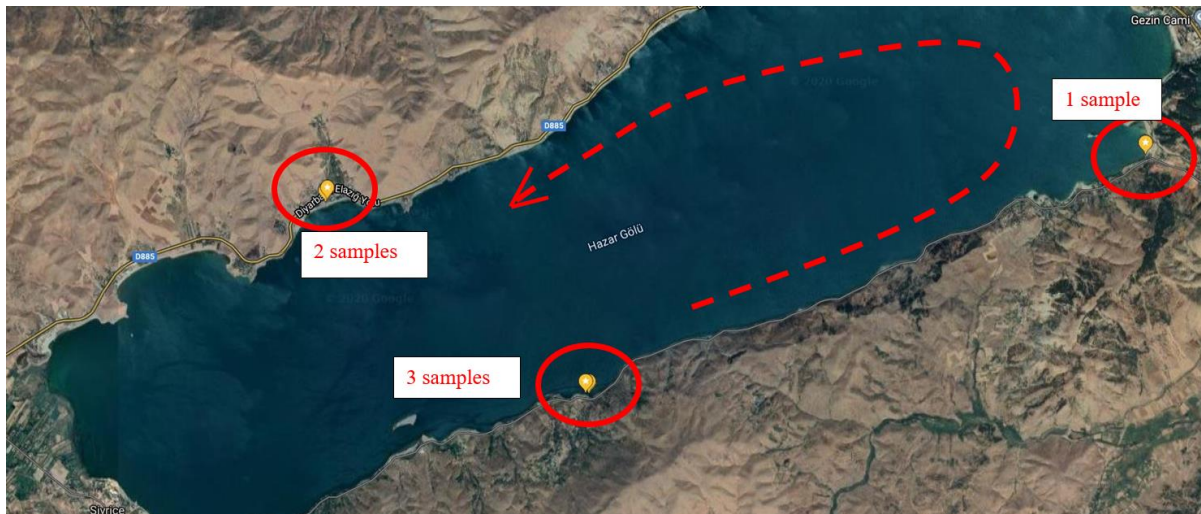


Figure 4.131. Location of sand boil samples taken from Hazar Lake shores



Figure 4.132. Location of sand boil samples taken from Kale Village shores



Figure 4.133. Location of the samples taken during site investigation (general view)

Table 4-3. Grain size distribution of sand ejecta

Region	Coordinates	Gravel %	Sand %	Fines %	Silt %	Clay %	D ₁₀ (mm)	D ₃₀ (mm)	D ₆₀ (mm)	C _u *	C _c *	Soil Type
Hazar Lake	38.463-39.4009	11.0	87.6	1.4			0.33	0.42	0.53	1.61	1.01	SP
	38.463-39.4007	28.8	41.1	30.1	27.6	2.5	0.02	0.075	0.6	30.0	0.47	SM
	38.499-39.506	4.2	80.9	14.9	11.1	3.8	0.02	0.24	0.42	21.0	6.86	SM
	38.492-39.35	10.0	87.0	3.0			0.32	0.65	1.7	5.31	0.78	SP
	38.492-39.351	4.1	83.5	12.5	10.6	1.9	0.06	0.16	0.25	4.17	1.71	SM
	38.463-39.4002	4.2	72.7	23.1	19.6	3.5	0.03	0.09	0.17	5.67	1.59	SM
Kale Village Lake side	38.424-38.762	36.4	57.5	6.2			0.09	0.2	2.9	32.2	0.15	SP-SM
	38.421-38.759	3.4	95.4	1.3			0.23	0.36	0.49	2.13	1.15	SP
	38.421-38.757	4.4	90.4	5.2			0.25	0.47	0.91	3.64	0.97	SP-SM
	38.424-38.762	26.2	70.8	3.0			0.32	0.5	1.44	4.50	0.54	SP

* $C_u = D_{60}/D_{10}$, $C_c = D_{30}^2/(D_{10} \cdot D_{60})$

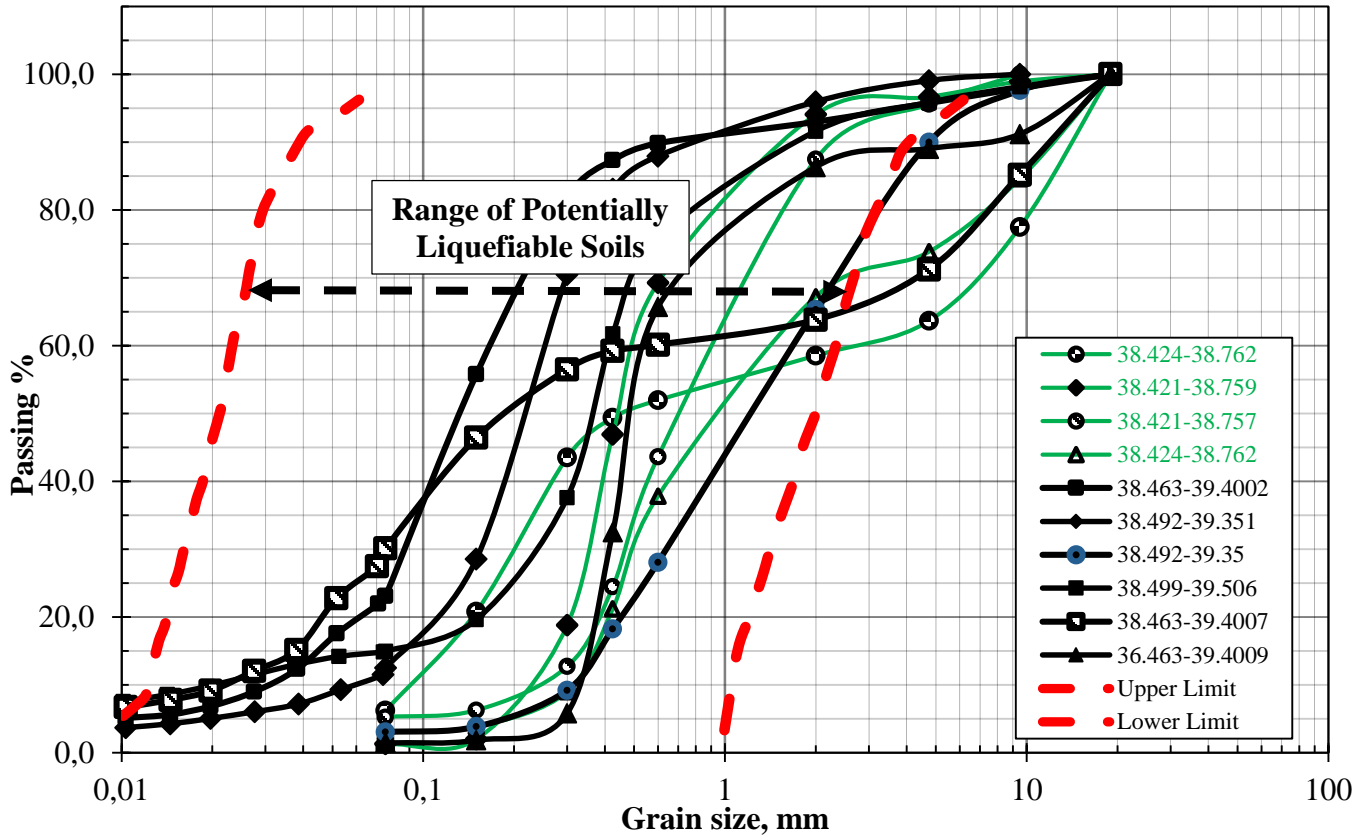


Figure 4.134. Particles size distribution curves of the sand ejecta taken from liquefied sites. (Black lines are obtained from Hazar Lake region and green lines from Kale Village side, respectively)

Although there exist free field soil sites with highly potential for liquefaction triggering around the shores of Hazar Lake and Fırat River, due to lack of urbanization in these areas, the contribution of liquefaction triggering to observed structural damage is judged to be none, except Sivrice Dock failure.



References

Tsuchida, H. (1970). “Prediction and countermeasure against the liquefaction in sand deposits. Abstract of the Seminar in the Port and Harbor Research Institute (in Japanese)